NASA CR-174923

LIGHTWEIGHT TWO-STROKE CYCLE AIRCRAFT DIESEL ENGINE TECHNOLOGY ENABLEMENT PROGRAM

VOLUME II
FINAL REPORT

(NASA-CR-174923-Vol-2) LIGHTWEIGHT TWO-STROKE CYCLE AIRCRAFT DIESEL ENGINE TECHNOLOGY ENABLEMENT PROGRAM, VOLUME 2 Final Report, Dec. 1979 - Aug. 1985 (Teledyne Continental Motors, Muskegon, N86-13329
Unclas
G3/07 04792

TELEDYNE CONTINENTAL MOTORS
General Products Division

P.D. FREEN, S.G. BERENYI, A.P. BROUWERS
M.E. MOYNIHAN

PREPARED FOR
NATIONAL AERONAUTICS AND SPACE ADMINISTRATION
NASA LEWIS RESEARCH CENTER

CONTRACT NAS3-22218

NASA

NASA CR-174923

VOLUME II

LIGHTWEIGHT TWO-STROKE CYCLE AIRCRAFT DIESEL ENGINE TECHNOLOGY ENABLEMENT PROGRAM

FINAL REPORT

TELEDYNE CONTINENTAL MOTORS
General Products Division

P.D. FREEN, S.G. BERENYI, A.P. BROUWERS
M.E. MOYNIHAN

PREPARED FOR

NATIONAL AERONAUTICS AND SPACE ADMINISTRATION
NASA LEWIS RESEARCH CENTER

CONTRACT NAS3-22215

NASA
National Aeronautics
and Space Administration

Scientific and Technical
Information Office

1. Report No.	2. Government Accession No.	3. Recipient's Catalog No.
NASA CR-174923		

4. Title and Subtitle	5. Report Date
LIGHTWEIGHT TWO-STROKE CYCLE AIRCRAFT DIESEL ENGINE TECHNOLOGY ENABLEMENT PROGRAM	August, 1985
	6. Performing Organization Code: 505-40-62

7. Author(s)	8. Performing Organization Report No.
P. D. FREEN, S. G. BERENYI, and A. P. BROUWERS, M. E. MOYNIHAN	
	10. Work Unit No.

9. Performing Organization Name and Address	11. Contract or Grant No.
TELEDYNE CONTINENTAL MOTORS 76 GETTY STREET MUSKEGON, MICHIGAN 49442	NAS3-22218
	13. Type of Report and Period Covered: Contract Report 12/79 - 8/85

12. Sponsoring Agency Name and Address	14. Sponsoring Agency Code
NATIONAL AERONAUTICS AND SPACE ADMINISTRATION WASHINGTON D.C. 20546	NASA LEWIS RESEACH CENTER

15. Supplementary Notes

FINAL REPORT. PROJECT MANAGER, JOHN J. MCFADDEN, SMALL ENGINE PROPULSION BRANCH, NASA-LEWIS RESEARCH CENTER, CLEVELAND, OHIO

16. Abstract

An experimental Single Cylinder Test Engine Program was conducted to confirm the analytically projected performance of a two-stroke cycle diesel engine for aircraft applications. The test engine delivered 78kW indicated power from 1007cc displacement, operating at 3500 RPM on Schnuerle loop scavenged two-stroke cycle. Testing confirmed the ability of a proposed 4-cylinder version of such an engine to reach the target power at altitude, in a highly turbocharged configuration. The experimental program defined all necessary parameters to permit a detailed design of a multicylinder engine for eventual flight applications; including injection system requirement, turbocharging, heat rejection, breathing, scavenging, and structural requirements.

The multicylinder engine concept is configured to operate with an augmented turbocharger, but with no primary scavenge blower. The test program was oriented to provide a balanced turbocharger compressor to turbine power balance without an auxiliary scavenging system. Engine cylinder heat rejection to the ambient air has been significantly reduced and the minimum overall turbocharger efficiency required is within the range of commercially available turbochargers.

Analytical studies and finite element modeling was made of insulated configurations of the engine - including both ceramic and metallic versions. A second generation test engine was designed based on current test results.

17. Key Words (Suggested by Author(s))	18. Distribution Statement
Diesel Aircraft Engine; Advanced Engines; Adiabatic Diesel Engine; Diesel with independent turbocharger loop; Two-Stroke Cycle Aircraft Diesel; Radial Diesel Engine; High Pressure Fuel Injection	UNCLASSIFIED - UNLIMITED STAR CATEGORY 07 AND GENERAL RELEASE

19. Security Classif. (of this report)	20. Security Classif. (of this page)	21. No. of pages	22. Price*
UNCLASSIFIED	UNCLASSIFIED		

*For sale by the National Technical Information Service, Springfield, Virginia 22161

VOLUME II

This final report is subdivided into three specific volumes.

Volume I contains the following material:

- Lists of Figures, Tables, and Appendicies; and Metric System Conversion Table.
- Section 1.0 Summary
- Section 2.0 Introduction
- Section 3.0 Engine Design and Cycle Analysis

Volume II of the report covers:

- Lists of Figures, Tables, and Appendicies; and Metric System Conversion Table.
- Section 4.0 Development Testing
- Section 5.0 Multicylinder Performance Projections
- Section 6.0 Conclusions
- Section 7.0 Recommendations
- Section 8.0 References

Volume III of the report covers:

- Lists of Figures, Tables, and Appendicies; and Metric System Conversion Table.
- Section 9.0 Appendicies

TABLE OF CONTENTS

PAGE NUMBER

VOLUME I

1.0 SUMMARY..... 1

2.0 INTRODUCTION..... 2
2.1 BACKGROUND..... 2
2.2 PREVIOUS AIRCRAFT DIESEL ENGINES..... 3
2.3 SCOPE OF WORK & PROGRAM PLAN..... 3
2.4 SIGNIFICANCE OF THIS PROJECT..... 7

3.0 ENGINE DESIGN & CYCLE ANALYSIS..... 9
3.1 PRELIMINARY DESIGN & CYCLE ANALYSIS..... 9
3.2 MULTICYLINDER CYCLE SIMULATION AND..... 11
SINGLE CYLINDER TEST ENGINE DESIGN
3.2.1 CYCLE SIMULATION..... 11
3.2.1.1 PERFORMANCE ANALYSIS..... 12
3.2.1.1.1 PORT DESIGN..... 12
3.2.1.1.2 CYCLE CALCULATIONS..... 12
3.2.1.2 DISCUSSION OF CYCLE SIMULATION RESULTS..... 14
3.2.1.3 CYCLE CALCULATIONS..... 15
3.2.2 FIRST GENERATION SCTE DESIGN..... 18
3.2.2.1 CYLINDER ASSEMBLY..... 18
3.2.2.2 COMBUSTION CHAMBER INSERT..... 19
3.2.2.3 MANIFOLD MUFF..... 20
3.2.2.4 CYLINDER TO CRANKCASE ADAPTER..... 20
3.2.2.5 FUEL INJECTION SYSTEM..... 20
3.2.2.6 PISTON AND PISTON RINGS..... 21
3.2.2.7 CONNECTING ROD..... 21
3.2.2.8 CRANKSHAFT..... 21
3.2.2.9 LABECO TEST BASE..... 22

PAGE NUMBER

VOLUME I (CONTINUED)

3.3	CYCLE SIMULATION COMPUTER PROGRAM.....	22
3.3.1	UMIST CYCLE ANALYSIS DESCRIPTION.....	22
3.3.2	INSULATION EFFECTS.....	22
3.3.3	COMBUSTION EFFECTS.....	25
3.3.4	MANIFOLD EFFECTS.....	26
3.3.5	PORT TIMING OPTIMIZATION.....	29
3.3.6	REED VALVE EVALUATION.....	30
3.3.7	CONCLUSIONS OF CYCLE ANALYSIS STUDIES.....	31
3.4	FUEL INJECTION.....	32
3.4.1	INJECTION REQUIREMENTS.....	32
3.4.2	BOSCH APF INJECTION SYSTEM.....	33
3.4.3	CAE-X INJECTION SYSTEM.....	34
3.4.4	BENDIX INJECTION SYSTEM.....	34
3.5	FINITE ELEMENT THERMAL AND STRUCTURAL ANALYSIS	36
3.6	SECOND GENERATION SINGLE CYLINDER TEST ENGINE.....	37
3.6.1	DESIGN GOALS.....	37
3.6.2	FINITE ELEMENT THERMAL AND STRUCTURAL ANALYSIS OF SECOND GENERATION ENGINE.....	38
3.6.3	SUMMARY OF CERAMIC INSULATED DESIGNS.....	39

VOLUME II

4.0	DEVELOPMENT TESTING.....	1
4.1	TEST FACILITIES.....	1
4.1.1	TEST CELL DESCRIPTION.....	1
4.1.2	INSTRUMENTATION.....	1
4.1.3	MEASUREMENT PRECISION.....	7
4.1.4	DATA REDUCTION PROGRAM.....	7
4.2	POWER COMPONENT DEVELOPMENT.....	7
4.2.1	CONFIGURATIONS 1, 2, AND 3 (ALULMINUM PISTON, ORIGINAL MANIFOLD, BOSCH APF INJECTION PUMP).....	7

PAGE NUMBER

VOLUME II (CONTINUED)

4.2.2	CONFIGURATION 4..... (ALUMINUM PISTON, ORIGINAL MANIFOLD, CAE-X INJECTION PUMP)	8
4.2.3	CONFIGURATION 5 AND 6..... (STEEL CAPPED ALUMINUM PISTON, CAE-X INJECTION PUMP, ORIGINAL MANIFOLD)	12
4.2.4	CONFIGURATION 7, 8 AND 9..... (CAST IRON PISTON, CAE-X INJECTION PUMP, NEW INTAKE MANIFOLD)	13
4.2.5	CONFIGURATION 10..... (BIG PORT CYLINDER, CLOSE COUPLED CAE-X INJECTION PUMP, STAINLESS CAPPED, CAST IRON PISTON, NEW INTAKE MANIFOLD)	15
4.2.6	CONFIGURATION 11 AND 12..... (OPTIMUM PORTED CYLINDER CLOSE COUPLED CAE-X PUMP, STAINLESS CAPPED, CAST IRON PISTON, NEW INTAKE MANIFOLD)	16
4.2.7	OPTIMUM HARDWARE CONFIGURATIONS.....	18
4.3	INJECTION SYSTEM PERFORMANCE.....	19
4.3.1	BOSCH APF PUMP.....	19
4.3.2	CAE-X INJECTION SYSTEM.....	20
4.3.3	ELECTRONICALLY CONTROLLED HIGH..... PRESSURE FUEL INJECTION SYSTEM	21
4.3.4	FUEL INJECTION SYSTEMS..... SELECTION SUMMARY	21
4.4	ENGINE PERFORMANCE.....	22
4.4.1	ENGINE PERFORMANCE TESTING..... WITH CONFIGURATIONS 1, 2, AND 3.	22
4.4.2	CONFIGURATIONS 4 THROUGH 9.....	25
4.4.3	CONFIGURATIONS 10.....	26
4.4.4	CONFIGURATIONS 11 AND 12.....	27
4.4.5	ENGINE PERFORMANCE SUMMARY.....	28

PAGE NUMBER

VOLUME II (CONTINUED)

4.4.5.1 REQUIRED OVERALL TURBOCHARGER EFFICIENCY 29

4.4.5.2 MASS FRACTION BURN RATE 29

4.4.5.3 PERFORMANCE MAPS 31

5.0 MULTICYLINDER PERFORMANCE PROJECTIONS 32

5.1 MULTICYLINDER ENGINE FUEL CONSUMPTION PROJECTION 32

5.2 TURBOCHARGING 33

5.3 PISTON SPEEDS AND BMEP LEVELS 34

5.4 HEAT LOSS 34

5.5 ENGINE SPECIFICATIONS 34

6.0 CONCLUSIONS 37

7.0 RECOMMENDATIONS 39

8.0 REFERENCES 40

VOLUME III

9.0 APPENDICES

LIST OF FIGURES

		PAGE NUMBER
VOLUME I		
3.1.1	186 KW AIRCRAFT DIESEL	42
3.1.2	SCHEMATIC 2-STROKE ENGINE WITH INDEPENDENT TURBO LOOP	43
3.1.3	COMPARISON OF SCHNUERLE AND CURTIS LOOP SCAVENGE SYSTEMS	44
3.2.1	GEOMETRICAL PORT AREAS VERSUS CRANK ANGLE	45
3.2.2	FLOW COEFFICIENTS VERSUS CRANK ENGINE	46
3.2.3	EFFECT OF A/F ON η_{tc}, TURBOCHARGER INLET TEMPERATURE, AND ISFC	47
3.2.4	EFFECT OF SCAVENGE RATIO ON SCAVENGE EFFICIENCY FOR LOOP SCAVENGED ENGINE	48
3.2.5	HIGH PRESSURE DIAGRAM FOR TAKE-OFF POWER	49
3.2.6	LOW PRESSURE DIAGRAM FOR TAKE-OFF POWER	50
3.2.7	HIGH PRESSURE DIAGRAM FOR FULL POWER CRUISE	51
3.2.8	LOW PRESSURE DIAGRAM FOR FULL POWER CRUISE	52
3.2.9	HIGH PRESSURE DIAGRAM FOR ECONOMY CRUISE POWER	53
3.2.10	LOW PRESSURE DIAGRAM FOR ECONOMY CRUISE POWER	54
3.2.11	FIRST GENERATION SINGLE CYLINDER - TEST ENGINE (SCTE)	55
3.2.12	LAYOUT OF SCTE CYLINDER COMPONENTS	56
3.2.13	LABECO SCTE TEST BASE	57
3.2.14	CYLINDER	58
3.2.15	CYLINDER PORTING ARRANGEMENT	59
3.2.16	COMBUSTION BOWL INSERT	60
3.3.1	TEMPERTURE ZONES USED FOR THERMAL MODEL	61

LIST OF FIGURES (2)

PAGE NUMBER

VOLUME I (CONTINUED)

3.3.2 HEAT RELEASE CURVE ASSUMED IN INITIAL CYCLE ANALYSIS 62

3.3.3 COMPUTER PREDICTED EFFECT OF COMPONENT INSULATION AT POWER CRUISE 63

3.3.4 COMPUTER PREDICTED EFFECTS OF ENGINE INSULATION - TAKE-OFF POWER 64

3.3.5 COMPUTER PREDICTED ENGINE PERFORMANCE VERSUS AVERAGE CHAMBER WALL TEMPERATURE 65

3.3.6 HEAT REJECTION AS A FUNCTION OF AVERAGE CHAMBER WALL TEMPERATURE FOR FOUR LOAD POINTS AT 3500 RPM 66

3.3.7 ABSOLUTE HEAT REJECTION AS A FUNCTION OF AVERAGE CHAMBER WALL TEMPERATURE AT FOUR LOAD POINTS AT 3500 RPM 67

3.3.8 COMPUTER PREDICTED TURBOCHARGER POWER BALANCE COMPARISON VERSUS HEAT LOSS AT TAKE-OFF POWER - SEA LEVEL 68

3.3.9 COMPUTER PREDICTED TURBOCHARGER POWER BALANCE COMPARISON VERSUS HEAT LOSS AT POWER CRUISE AT 7800 METERS ALTITUDE 69

3.3.10 COMPUTER PREDICTED TURBOCHARGER POWER BALANCE COMPARISON VERSUS HEAT LOSS AT 50% POWER AT 7800 METERS ALTITUDE 70

3.3.11 COMPUTER PREDICTED TURBOCHARGER POWER BALANCE COMPARISON VERSUS HEAT LOSS AT 25% POWER AT 7800 METERS ALTITUDE 71

3.3.12 COMPUTER PREDICTED EFFECT OF COMBUSTION DURATION ON THERMAL EFFICIENCY AND PEAK CYLINDER PRESSURE 3500 RPM TAKE-OFF POWER 72

3.3.13 COMPUTER PREDICTED EFFECT OF COMBUSTION TIMING ON THERMAL EFFICIENCY AND PEAK CYLINDER PRESSURE 3500 RPM TAKE-OFF POWER 73

3.3.14 COMPUTER PREDICTED EFFECT OF EFFECTIVE COMPRESSION RATIO ON THERMAL EFFICIENCY AND PEAK CYLINDER PRESSURE 3500 RPM TAKE-OFF POWER 74

3.3.15 MASS FLOW RATE/CYLINDER PRESSURE RATIO VERSUS MANIFOLD AREA 75

LIST OF FIGURES (3)

PAGE NUMBER

VOLUME I (CONTINUED)

3.3.16 TRAPPED MASS/CYLINDER PRESSURE RATIO..... 76
VERSUS MANIFOLD AREA

3.3.17 AIR-FUEL RATIO VERSUS CYLINDER PRESSURE..... 77
RATIO FOR THE OPTIMIZED MANIFOLDING
CONFIGURATION

3.3.18 EXPERIMENTAL VERSUS PREDICTED INLET..... 78
MANIFOLD PRESSURE AT PRESSURE TRANSDUCER
LOCATION

3.3.19 EXPERIMENTAL VERSUS PREDICTED EXHAUST..... 79
MANIFOLD PRESSURE AT PRESSURE TRANSDUCER
LOCATION

3.3.20 PORT TIMING OPTIMIZATION AT TAKE-OFF..... 80
POWER CONDITION

3.3.21 PORT TIMING OPTIMIZATION AT POWER..... 81
CRUISE CONDITION

3.3.22 PORT TIMING VERSUS 82

3.3.23 AIR FUEL RATIO VERSUS CYLINDER PRESSURE..... 83
RATIO FOR THE OPTIMIZED PORTING AND
MANIFOLDING CONFIGURATION

3.3.24 EFFECT OF REED VALVES ON CYLINDER..... 84
AIRFLOW AT TAKE-OFF POWER (SAME TIMING
FOR INTAKE AND EXHAUST PORTS)

3.3.25 PREDICTED PERFORMANCE FOR OPTIMIZED..... 85
CONFIGURATION

3.3.26 TEMPERATURE INPUTS AND PREDICTED HEAT..... 87
LOSS THROUGH CYLINDER ZONES AT TAKE-OFF POWER

3.4.1 FUEL INJECTION CAMSHAFT PROFILE..... 88

3.4.2 CAE-X PUMP CROSS SECTION..... 89

3.4.3 CAMSHAFT PROFILE, VELOCITY, AND..... 90
ACCELERATION FOR AVCR-1360 TYPE CAM

3.4.4 ADVANCE MECHANISM FOR CAE-X PUMP..... 91
(SCTE-CONFIGURATION)

3.4.5 COOLED INJECTION NOZZLE HOLDER AND ADAPTER..... 92

3.4.6 BENDIX DCX-3-28 FUEL INJECTOR..... 93

LIST OF FIGURES (4)

PAGE NUMBER

VOLUME I (CONTINUED)

3.4.7 FUEL INJECTOR EVENTS WITH A BENDIX DCX-3-28 INJECTOR 94

3.4.8 FUEL INJECTION CONTROLLER BLOCK DIAGRAM FOR BENDIX DCX-3-28 SYSTEM 95

3.6. SECOND GENERATION SINGLE CYLINDER TEST ENGINE -COOLED CONFIGURATION 96

3.6.2 SECOND GENERATION SINGLE CYLINDER TEST ENGINE -INSULATED CONFIGURATION 97

VOLUME II

4.1.1 ENGINE TEST CELL LAYOUT 41

4.1.2 SCTE TEST CELL CONTROL ROOM 42

4.1.3 TEST CELL OIL SUPPLY SYSTEM 43

4.1.4 TEST CELL FUEL SYSTEM 44

4.1.5 TEST CELL COMBUSTION AIR SUPPLY SYSTEM 45

4.1.6 CYLINDER THERMOCOUPLE LOCATION 46

4.1.7 INJECTOR ASSEMBLY AND PRESSURE TRANSDUCER INSTALLATION 47

4.1.8 INJECTOR NOZZLE HOLDER ASSEMBLY AND COMBUSTION BOWL INSERT 48

4.1.9 IMPACT SAMPLING VALVE INSTALLATION 49

4.1.10 COMPOSITION OF EXHAUST GASES FROM DIESEL AND SPARK IGNITION ENGINES 49

4.1.11 CHECK VALVE IN EXHAUST SAMPLING ASSEMBLY 50

4.1.12 EXHAUST SAMPLING VALVE INSTALLED IN INTAKE/EXHAUST MUFF 51

4.1.13 SAMPLE INPUT DATA FOR DATA REDUCTION PROGRAM 52

4.1.14 SAMPLE OUTPUT DATA FROM DATA REDUCTION PROGRAM 53

4.2.1 POWER COMPONENTS FOR AIRCRAFT ENGINE (SCTE) 54

4.2.2 LABECO ENGINE TEST BASE FOR AIRCRAFT ENGINE (SCTE) 55

LIST OF FIGURES (5)

		PAGE NUMBER
VOLUME II (CONTINUED)		
4.2.3	CYLINDER ASSEMBLY FOR AIRCRAFT ENGINE (SCTE).....	56
4.2.4	INITIAL INTAKE MANIFOLD MUFF CONFIGURATION..... FOR AIRCRAFT ENGINE (SCTE)	57
4.2.5	ASSEMBLED FIRST GENERATION SINGLE CYLINDER..... TEST ENGINE (SCTE)	58
4.2.6	ENGINE CONFIGURATION WITH CAE-X PUMP.....	59
4.2.7	INTAKE MANIFOLD MODIFICATION FOR..... CONFIGURATION 4	60
4.2.8	CONNECTING ROD FOR CONFIGURATION 4.....	61
4.2.9	PISTON SKIRT WITH KNURLING FOR..... LUBRICANT RETENTION	62
4.2.10	PISTON PROFILE DEVELOPED FOR ALUMINUM..... PISTON	63
4.2.11	SCUFFED PISTON REMOVED FROM CONFIGURATION 4.....	64
4.2.12	CONNECTING ROD REMOVED FROM CONFIGURATION 4.....	65
4.2.13	STEEL CAPPED ALUMINUM PISTON ASSEMBLY.....	66
4.2.14	ALUMINUM PISTON AND SCREWED ON STEEL CAP.....	67
4.2.15	COMBUSTION CHAMBER AND INJECTION NOZZLE..... COMPONENTS	68
4.2.16	ASSEMBLED COMBUSTION CHAMBER AND..... INJECTION NOZZLE	69
4.2.17	EFFECT OF IMPROPER GROOVE ANGLE ON..... RING POSITION	70
4.2.18	DUCTILE IRON PISTONS..... FOR CONFIGURATIONS 6, 7 AND 8	71
4.2.19	COMBUSTION CHAMBER FOR USE WITH..... DOMED PISTON - CONFIGURATIONS 7, 8 AND 9	72
4.2.20	"BOKOR" FINISH OF PISTON SKIRT..... FOR OIL RETENTION	73
4.2.21	PISTON PROFILE DEVELOPED FOR CAST..... IRON PISTON	74
4.2.22	MANIFOLD CONFIGURATION FOR CONFIGURATION..... 10 THROUGH 12	75

LIST OF FIGURES (6)

PAGE NUMBER

VOLUME II (CONTINUED)

4.2.23 NEW CONNECTING ROD WITH "V" DRILLED..... 76
OIL SUPPLY

4.2.24 INTERIOR VIEW OF CYLINDER AFTER 60 HOURS..... 77
OF RUNNING ON CONFIGURATION 10

4.2.25 AIR GAP INSULATED PISTON AND COMBUSTION..... 78
BOWL ASSEMBLED IN CYLINDER

4.2.26 AIR GAP INSULATED PISTON CAP..... 79

4.2.27 INSIDE DIAMETER PROFILE TRACE OF CYLINDER,..... 80
6.35 MM ABOVE PORTS

4.2.28 INSIDE DIAMETER PROFILE TRACE OF..... 81
CYLINDER NO. 3, 6.35 MM BELOW PORTS

4.3.1 INJECTION CHARACTERISTICS FOR CAE-X..... 82
PUMP AT 1325 PUMP RPM

4.3.2 INJECTION CHARACTERISTICS FOR CAE-X..... 83
PUMP AT 1750 PUMP RPM

4.3.3 CAE-X PUMP WITH A 71.1 CM INJECTION..... 84
LINE AS INSTALLED ON THE SCTE

4.3.4 CAE-X PUMP WITH A 17.8 CM INJECTION..... 85
LINE AS INSTALLED ON THE SCTE

4.3.5 INJECTION DURATION VERSUS INJECTED..... 86
VOLUME FOR THREE INJECTION PUMP
CONFIGURATIONS TESTED AT 3500 RPM

4.3.6 IGNITION DELAY VERSUS INJECT VOLUME..... 87
FOR THREE PUMP CONFIGURATION AT 3500 RPM

4.3.7 DYNAMIC PRESSURE AND NEEDLE LIFT..... 88
CHARACTERISTICS

4.4.1 COMPARISON OF OVERALL FLOW COEFFICIENTS..... 91
USING ORIGINAL MANIFOLD AT 3500 RPM

4.4.2 COMPARISON OF OVERALL FLOW COEFFICIENTS..... 92
USING ORIGINAL MANIFOLD AT 2650 RPM

4.4.3 ENGINE PERFORMANCE VERSUS ENGINE SPEED..... 93
FOR CYLINDER NO. 1 FOR CONFIGURATIONS
1, 2 AND 3

4.4.4 ENGINE PERFORMANCE VERSUS ENGINE SPEED..... 94
FOR CYLINDER NO. 3 FOR CONFIGURATIONS
1, 2 AND 3

LIST OF FIGURES (7)

PAGE NUMBER

VOLUME II (CONTINUED)

4.4.5 ENGINE PERFORMANCE VERSUS IMEP FOR..... 95
CYLINDER 3 AT 3500 RPM FOR CONFIGURATION 4

4.4.6 PISTON TOP CONFIGURATIONS EVALUATED..... 97
FOR PORT FLOW COEFFICIENTS

4.4.7 INTAKE PORT FLOW COEFFICIENT..... 98

4.4.8 EXHAUST PORT FLOW COEFFICIENT..... 99

4.4.9 AVERAGE OVERALL PORT FLOW COEFFICIENT.....100
WITH OPTIMIZED MANIFOLDING AT 3500 RPM

4.4.10 AVERAGE OVERALL PORT FLOW COEFFICIENT.....100
WITH OPTIMIZED MANIFOLDING AT 2650 RPM

4.4.11 DYNAMIC INTAKE MANIFOLD PRESSURE..... 101
AT 3500 RPM.

4.4.12 DYNAMIC EXHAUST MANIFOLD PRESSURE..... 102
AT 3500 RPM

4.4.13 ENGINE PERFORMANCE FOR CONFIGURATION..... 103
10 AT 3500 RPM

4.4.14 ENGINE PERFORMANCE COMPARISONS AT..... 105
3500 RPM FOR CONFIGURATIONS 10 AND 12

4.4.15 CYLINDER TEMPERATURE DISTRIBUTION FOR..... 107
CONFIGURATION 10 AT 3500 RPM AND
9.6 BAR IMEP

4.4.16 CYLINDER TEMPERATURE DISTRIBUTIONS..... 108
FOR CONFIGURATION 12 AT 3500 RPM AND
9.6 BAR IMEP

4.4.17 ENGINE PERFORMANCE COMPARISON FOR..... 109
CONFIGURATIONS 11 AND 12 AT 3500 RPM

4.4.18 CALCULATED TRAPPING EFFICIENCIES. 111

4.4.19 REQUIRED OVERALL TURBOCHARGER EFFICIENCY..... 112
AT 6.90 BAR IMEP AND 3500 RPM FOR FIVE
ENGINE CONFIGURATIONS

4.4.20 ENGINE HEAT BALANCE AT 6.9 BAR IMEP..... 113
AND 3500 RPM FOR FIVE ENGINE CONFIGURATIONS

4.4.21 REQUIRED OVERALL TURBOCHARGER EFFICIENCY..... 114
AT 9.0 BAR IMEP AND 3500 RPM FOR FOUR
ENGINE CONFIGURATIONS

LIST OF FIGURES (8)

PAGE NUMBER

VOLUME II (CONTINUED)

4.4.22 ENGINE HEAT BALANCE AT 9.0 BAR IMEP..... 115
AND 3500 RPM

4.4.23 MASS FRACTION BURN RATES FOR THREE..... 116
SELECTED POINTS FOR CONFIGURATION 12

4.4.24 SINGLE CYLINDER AIRCRAFT DIESEL..... 118
PERFORMANCE OF CONFIGURATION 12A,
3/4 LOAD PROPELLER CURVE

4.4.25 SINGLE CYLINDER AIRCRAFT DIESEL..... 120
PERFORMANCE OF CONFIGURATION 12A,
FULL LOAD PROPELLER CURVE

4.4.26 AIRFLOW PARAMETERS FOR CONFIGURATION 12A..... 122

4.4.27 FMEP VERSUS RPM AND PISTON SPEED FOR SCTE..... 123

5.1.1 FMEP VERSUS PISTON SPEED FOR GTDR 246..... 124
AND OTHER SIMILAR ENGINES

5.1.2 PREDICTED GTDR 246 FUEL MAP..... 125

5.1.3 PREDICTED ALTITUDE PERFORMANCE OF..... 126
MULTICYLINDER ENGINE

5.2.1 COMPRESSOR FLOW REQUIREMENT PLOTTED ON..... 127
AN ADVANCED COMPRESSOR MAP GENERATED FOR
NASA UNDER CONTRACT NAS3-22750

5.3.1 PISTON SPEED OF ELEVEN SELECTED AIRCRAFT..... 128
ENGINES

5.3.2 BMEP OF ELEVEN SELECTED AIRCRAFT ENGINES..... 129

5.4.1 GTDR-246 DIESEL AIRCRAFT ENGINE (WITH..... 130
VERTICAL CYLINDERS) FULL SCALE MOCKUP

5.4.2 GTDR-246 DIESEL AIRCRAFT ENGINE (WITH..... 131
HORIZONTAL CYLINDERS) FULL SCALE MOCKUP

LIST OF TABLES

		PAGE NUMBER
VOLUME I		
I	PREVIOUS AIRCRAFT ENGINES	4
II	SPECIFIC DATA OF PREVIOUS AIRCRAFT DIESEL ENGINES	4
III	PORT DATA	13
IV	OPERATING PARAMETERS	16
V	COMPARISON OF SCAVENGING RATIOS	17
VI	SCTE FUEL INJECTION SYSTEM REQUIREMENTS	33
VII	COMPARISON OF ALTERNATE INSULATIVE CONCEPTS	40
VOLUME II		
VIII	ESTIMATED TOLERANCE OF PRIMARY VARIABLES	5
IX	RECOMMENDED PISTON RINGS	11
X	AVAILABLE CYLINDER PORT CONFIGURATIONS	23
XI	PROJECTED MAXIMUM HEAT REJECTION RATE FOR GTDR-246	34
XII	GTDR-246 ENGINE SPECIFICATIONS	36

LIST OF APPENDICES

VOLUME III

I. ENGINE CYCLE SIMULATION AND DETAILED HEAT TRANSFER ANALYSIS OF THE SINGLE CYLINDER TEST ENGINE WITH CORRELATION TO TEST MEASUREMENTS.

II. STRUCTURAL ANALYSIS OF THE SINGLE CYLINDER TEST ENGINE

III. SECOND GENERATION SINGLE CYLINDER TEST ENGINE PARTS LIST

IV. FEASIBILITY ASSESSMENT OF LOW HEAT REJECTION CONFIGURATION OF THE TELEDYNE LIGHTWEIGHT DIESEL ENGINE.

V. PROJECT SUMMARY REPORT ON ELECTRONICALLY CONTROLLED FUEL INJECTION SYSTEM FOR GENERAL AVIATION DIESEL ENGINE.

VI. EVALUATION OF K-1000F PISTON RING SET FROM TWO CYCLE AIRCRAFT ENGINE.

VII. EVALUATION OF TELEDYNE RINGS AND PISTON WITH STEEL CROWN AND ALUMINUM SKIRT

VIII. FUEL AND OIL SPECIFICATIONS

Metric Conversion Factors

FROM:	MULTIPLY BY:	TO:	FROM:	MULTIPLY BY:	TO:
km	0.6214	mi	bar	100	kPa
km	3281	ft	bar	1.01972	kg/cm^2
m	3.281	ft	bar	14.50377	psi
m	39.37	in	MPa	1000	kPa
dm	3.937	in	MPa	10.1972	kg/cm^2
mm	0.03937	in	MPa	145.0377	psi
m^3	35.31	ft^3	kPa	0.14504	psi
m^3	61,023	in^3	kg/cm^2	9.812	N/cm^2
m^3	264.2	gallons	kg/cm^2	14.223	psi
ℓ	0.0353	ft^3	N-m	0.10197	kgm
ℓ	61.02	in^3	N-m	0.73759	ft-lb
ℓ	0.264	g	kgm	7.2333	ft-lb
m^2	10.76	ft^2	m^3/kW	26.331	ft^3/HP
metric ton	2.205	lb	m^3/kg	16.0165	ft^3/lb
kg	2.2046	lb	kW/ℓ	0.02198	HP/in^3
MN	224,810	lb	kg/kW	1.644	lb/HP
kN	224.81	lb	kg/ℓ	0.03613	ib/in^3
N	0.102	kg	kcal	3.9683	BTU
N	0.22481	lb	kcal/kg	1.8	BTU/lb
°K	1.8	°R	kcal/kg-°C	1	BTU/lb-°F
°C	1.8°C + 32	°F	g/kWh	0.00164	lb/HP-hr
kW	1.341	HP			

4.0 DEVELOPMENT TESTING

Previous sections in Volume I of this three volume report have discussed the analysis, design, and hardware configuration of the single cylinder test engine (SCTE). Section 4 provides a detailed discussion of the actual development testing that was conducted, and the experimental results that were obtained during this test program. The test facilities used are described first, followed by discussions of:

- o Power component development (detailed by engine configurations)
- o Injection system development
- o Engine performance description (detailed by engine configurations)

4.1 Test Facilities

All engine testing was conducted at TCM`s facilities in Muskegon, Michigan. Special test equipment was provided to the project on an "as required" basis. The facilities used, their configuration, their limitations, and projected accuracies are described in this Section 4.1. The fuel and lube oil specifications used in this program are tabulated in Appendix VIII.

4.1.1 Test Cell Description. The engine test cell facilities are shown in Figures 4.1.1 through 4.1.5. The engine output power is absorbed by a 45kW motoring electric dynamometer in series with a 75 kW water brake dynamometer. Speed and torque are controllable from the control room. An engine overspeed safety is provided which shuts off the fuel for an engine overspeed condition or in the event of an electrical power failure.

Pressurized engine oil is supplied to the engine by a separate oil system. Figure 4.1.3 shows a diagram of the oil system. The oil pressure and temperature is feedback controlled so that constant controlled conditions can be maintained. An oil weigh scale is used to measure the engine oil consumption. The oil is filtered by three, full flow filters.

The fuel system is shown in Figure 4.1.4. Fuel temperature is feedback controlled from the control room and fuel pressure is open loop controlled.

4.1.2 Instrumentation. The torque absorbed by the trunnion bearing mounted electric dynamometer was measured by a precision balance scale. The force that the scale measured was converted to torque by multiplying it by the torque arm length. The torque absorbed by the water brake was measured by a strain gage load cell and was read out digitally on an electronic display.

Temperatures were measured by a forty channel digital data logger. This data logger scanned the forty channels every second and decided which channels were in an alarm situtation.

An alarm situation existed when a channel temperature was above a preset high limit or below a preset lower limit. When an alarm situation existed, a light alerted the operator of the situation. The temperatures that were measured are shown in Table VIII and Figure 4.1.6. These included: fourteen cylinder temperatures, all oil inlet and outlet temperatures, four air intake temperatures, three exhaust temperatures, cooling air inlet and outlet temperatures, fuel temperatures, and cell ambient temperature.

Steady state pressures were measured by three different means. Very low pressure and differential pressures were measured by water filled manometers. Accurate measurement of low pressures were recorded by precision bourdon - tube pressure gages. Oil, water, and fuel pressures were measured by bourdon - tube pressures gages.

Fuel flow was measured by a volumetric fuel flow meter. This unit accurately measured (by quartz timer) the amount of time it took for the engine to consume a specified volume of fuel from a precision calibrated burrette. The timer was actuated by light sensitive sensors located at the calibration points on the fuel burrette. Various fuel volumes could be selected from the meter's control box located in the control room in order to select the time frame desired for the fuel flow measurement.

The measured volumetric flow rate was converted to mass flow rate by a density correcting factor which is a function of fuel temperature in the burrette. Fuel density was measured every time fuel tank delivery was made so that variances in fuel density were accounted for.

Combustion air flow was measured by either a 25.4mm or a 76.2mm subsonic nozzle. The small nozzle was used to measure air flows between .40kg/hr and 200 kg/hr. The large nozzle measured air flows between 136kg/hr and 820kg/hr. The temperatures and pressure before the nozzles were recorded so that density effects could be accounted for. The pressure differential across each nozzle was measured by water filled manometers. Oil flows were measured using turbine meters. These meters provide output electrical frequency proportional to volume flow rate. The frequency was measured by a precision frequency counter with a one second gate time. The frequency was then converted to volume flow rate by the calibration curves. These curves required oil viscosity as a gage factor. The oil viscosity versus temperature curve and the oil density versus oil temperature curve were supplied by the oil supplier. Oil density was required to calculate the oil mass flow rate.

The cooling air flow was measured by a calibrated bell mouth flow meter. This flowmeter required the measurement of pressure differential across the meter and temperature at the flowmeter entrance to evaluate air mass flow rate from the calibration curve. Pressure differential was measured by a water filled manometer and temperature by a thermocouple.

Cylinder pressure was measured by a water cooled piezoelectric pressure transducer screwed into the removable combustion chamber, and sealed against a flat bronze washer. The passage from the transducer to the combustion chamber was four millimeters in diameter and four and one-half millimeters long. This short passage minimized phasing and ringing problems which hinder dynamic pressure measurements. The reasonant frequency of the transducer was 250 kilohertz.

Dynamic intake and exhaust pressures were also measured by water cooled piezoelectric transducers. Their natural frequency was 250 kilohertz. The intake pressure transducer was flush mounted to the inside diameter of the left intake manifold, fifty millimeters from the intake ports. The exhaust transducer was similarly mounted fifty millimeters from the exhaust ports. These transducers were very reliable and no problems were encountered with them.

Injection pressure was measured by a piezoelectric transducer capable of measuring pressures up to 2070 bar. Figure 4.1.7 shows a photograph of the transducer as it was installed in the injection holder. Its natural frequency was 250 kilohertz.

This transducer was a new product and reliability problems were encountered with it. Consequently, much engine running was done without injection pressure data. Problems encountered with the transducers included the housing cracking and the microelectronics failing. Toward the end of the program, the manufacturer had repaired the sensors and they appeared to work reliably.

The injector needle lift was measured by a miniture 1.5mm diameter Hall effect sensor installed in the nozzle holder. This sensor required attaching a cobalt samarian magnet to the spring seat. The sensor is shown along with the entire nozzle and combustion bowl assembly in Figure 4.1.8.

The dynamic variables of cylinder pressure, intake and exhaust pressure, injection pressure, and needle lift were displayed on two, six channel oscilloscopes. Timing marks every 10^{o}CA and top dead center marks were indented on the engine flywheel. These timing marks were sensed by two variable reluctance transducers and displayed on the two

oscilloscopes. A camera was available for photographing the oscilliscope traces. Later in the development program, a high speed digital acquisition system was used for data acquisition and reduction of these high speed dynamic parameters.

Exhaust smoke was measured by a smoke intensity meter. This unit measures the intensity of black smoke in Bosch units. The exhaust sample is drawn from the exhaust pipe after the back pressure butterfly valve. Unfortunately the system was not very reliable and therefore, not much usable smoke data was obtained in the program.

Many attempts were made to measure cylinder trapping efficiency. The method that was used had been done successfully by Taylor and Kannappan. This method determines the trapped mass in the cylinder of a two stroke engine by using an impact sampling valve. It uses a sampling valve which samples only the first exhaust blowdown gases before the intake ports open. The sample consists only of combusted air and fuel which was trapped in the cylinder. Chemical analysis of the CO_2 and O_2 content in this sample will reveal the trapped air-fuel ratio. Since the mass flow rate of fuel is known, the trapped air mass flow rate can be calculated. From this, trapping efficiency can be evaluated.

Figure 4.1.9 shows the layout of the sampling valve. The sample valve consists of a flat check valve and seat. A back pressure is maintained on the check valve approximately 130 Kpa higher than the intake pressure. When the exhaust ports are first uncovered by the piston, the high pressure exhaust gases impinge on the sampling valve. These gases at higher pressure than the back pressure cause the check valve to open, allowing the gases to enter the sample valve. This continues until the blowdown pressure falls below the back pressure. The check valve then closes preventing the sample from escaping.

The back pressure is maintained by a presssure relief valve installed at the receiving tank. As exhaust sample flows into the tank, the relief valve bleeds off an equal amount, maintaining a constant back pressure. The bled off sample flows into an emissions analyzing cart and the content of CO_2 and O_2 are determined. The CO_2 and O_2 concentrations in the sample determined the air-fuel ratio of the trapped mass when the mixture is lean as shown in Figure 4.1.10.

Figures 4.1.11 and 4.1.12 show details of the sampling valve and its installation.

The problems encountered with the impact sampling valve were primarily with the sealing of the flat check valve. The seat would get exhaust carbon and dirt on it and the seal was lost. This would make the analyzed sample useless.

TABLE VIII

ESTIMATED TOLERANCE OF PRIMARY MEASURED VARIABLES

PERFORMANCE		
RPM	± 1	count
BRAKE TORQUE	± 1	%
MOTORING TORQUE	± 1	%
FUEL TIME	± 10	ppm
FUEL VOLUME	± .05	%
AIR FLOW Δ P	± .25	%
JOURNAL OIL FLOW	± 1.5	%
PORT OIL FLOW	± 1.5	%
TRANSDUCER OIL FLOW	± 1.5	%
SMOKE (Bosch)	± 30	%
POINT OF IGNITION	± .5	C.A.
PEAK CYLINDER PRESSURE	± 1.5	%
INJECTION PRESSURE	± 1.0	%
INJECTION BEGINS	± .5	C.A.
INJECTION DURATION	± .5	C.A.

HEISE GAGES		
LA SHOP AIR	± .5	%
LB INTAKE PLEN.	± .5	%
LC INTAKE LEFT	± .5	%
LD INTAKE RIGHT	± .5	%
RA EXHAUST PORT	± .5	%
RB EXHAUST PLEN.	± .5	%

PRESSURE GAGES		
1) OIL	± 2	%
2) OIL SQUIRT	± 2	%
3) FUEL	± 2	%
4) WATER	± 2	%
5) INJECTION PUMP OUT	± 2	%

TEMPERATURES		
INTAKE RIGHT	± 1.0	°C
INTAKE LEFT	± 1.0	°C
OIL IN	± 1.0	°C
OIL OUT	± 1.0	°C
EXHAUST PLEN.	± 2	%
EXHAUST PORT	± 2	%
FUEL METER	± 1.0	°C
FUEL FILTER	± 1.0	°C
HEAD	± 8.0	°C
AMBIENT	± 1.0	°C
SHOP AIR	± 1.0	°C
CYLINDER OIL IN	± 1.0	°C
CYLINDER OIL OUT	± 1.0	°C
INTAKE PLENUM TOP	± 1.0	°C
INTAKE PLENUM BOTTOM	± 1.0	°C
COOL AIR IN	± 1.0	°C
COOL AIR OUT	± 1.0	°C
TRANSMISSION OIL OUT	± 1.0	°C
EXHAUST PLENUM	± 2	%

MANOMETERS		
PAN PRESSURE	± .25	%
CYLINDER COOL AIR	± .25	%
COOL AIR Δ P	± .25	%
CYLINDER TEMPERATURES	± 4	%
DYNAMIC INTAKE PRESSURE	± 1	%
DYNAMIC EXHAUST PRESSURE	± 1.5	%

TABLE VIII

ESTIMATED TOLERANCE OF CALCULATED DATA

ENGINE DATA

RPM	± 1	count
BRAKE TORQUE	± 1	%
FRICTION TORQUE	± 1	%
INTAKE PRESSURE	± .5	%
INTAKE TEMPERATURE	± 1.0	^{o}C
EXHAUST PRESSURE	± .5	%
EXHAUST TEMPERATURE	± 2	%
OIL INLET TEMPERATURE	± 1.0	^{o}C
FUEL TEMPERATURE	± 1.0	^{o}C
CASE PRESSURE	± .25	%
AIR FLOW	± .52	%
FUEL FLOW	± .19	%
COOLING AIR FLOW	± .75	%
OIL SQUIRT FLOW	± 1.5	%
OIL JOURNAL FLOW	± 1.5	%
PORT OIL FLOW	± 1.5	%
X-DUCER FLOW	± 1.5	%

TRAPPED AIR DATA

SCAVENGE RATIO (AVL)	± .93	%
SCAVENGE RATIO (TAYLOR)	± .93	%

PERFORMANCE DATA

IHP	± .83	%
IMEP	± .824	%
BHP	± .67	%
BMEP	± 1.0	%
FHP	± .67	%
MECH. EFF. (%)	± 1.0	%
A/F RATIO	± .56	%
P_i/P_e	± .709	%
Δ P	± .707	%
Δ P/P_i	± 1.0	%
ISFC	± .85	%
BSFC	± .69	%
SMOKE	± 30	%

INJECTION PUMP DATA

INJECTION PRESSURE	± 1.0	%
INJECTION (DURATION) (^{o}CA)	± .7	^{o}CA
INJECTION BEGINS (BTDL)	± .5	^{o}CA
FUEL/CYCLE (MM^3)	± .19	%

TURBOCHARGER REQUIRED EFFICIENCY (97% MECHANICAL EFFICIENCY)

SEA LEVEL	25,000Ft.
± 1.6%	± 1.6%

COMBUSTION DATA

POINT OF IGNITION	± .5	^{o}CA
PEAK CYLINDER PRESSURE	± 1.5	%
IGNITION DELAY	± .707	^{o}CA

HEAT BALANCE DATA (% OF FUEL ENERGY)

OIL	TRANS.	EXH. PORTS	COOL AIR	EXHAUST	BHP	UNACCOUNTED TOTAL
±12.6 % of %	± 1.5% of %	± 6.26 % of %	± 1.67 % of %	± 3.42 % of %	± .67% of %	100

Several different configurations were tried in order to resolve this problem, but no reliable solution was found within the time frame of the development program. As a result, measured trapping efficiencies were not recorded.

4.1.3 Measurement Precision. The primary variables that were measured by each engine run are shown in Table VII. Also shown in this table are the estimated primary variables accuracy. The tabluated basic accuracies were used to estimate the uncertainty of the calculated results.

4.1.4 Data Reduction Program. For each engine run, a computer program was used to reduce the measured data to give the useful calculated data. This computer program contained all calibration curves and fluid properties in memory. Figures 4.1.13 and 4.1.14 show the measured input and calculated output, respectively. The trapped air data shown should be ignored because of the sampling valve problems discussed before. This input data was not used.

The heat balance data is calculated from the oil and air flows along with their respective temperature changes as they flow through the engine.

4.2. Power Components Development

This Section 4.2 gives a chronological description of the mechanical development activity throughout the program. Performance parameters are not covered here and are discussed in detail in Sections 4.3 and 4.4.

4.2.1 Configuration One, Two, and Three. Configurations 1, 2 and 3 featured the engine hardware as initially designed. Power component development centered around initial shakedown tests and durability evaluation.

The hardware shown in Figures 4.2.1 thru 4.2.5 was assembled with few problems. Initial motoring and firing tests however, revealed several problems. The piston-to-cylinder bore clearances, as well as the piston cam grind side contour and ring land diameters were not correct and caused scuffing problems. Also, the top piston ring experienced excessive wear in a very short time due to an incompatibility between the "Nikasil" cylinder coating and the chrome top ring. The three compression rings, which were pinned to prevent rotation sheared off their respective pins in their ring groove. Severe wear of the two wrist pin bushings in the piston and the one bushing in the connecting rod was experienced. The two piston bushings, which were

initially installed with an interference fit, rotated in their bores and pushed out past the piston outside diameter and caused severe cylinder scuffing. The connecting rod bushing overheated because of lack of lubrication. The splash oiling system, for this bushing was not adequate. The cylinder hold down nut experienced fretting between the nut and the cylinder flange. Finally, the combustion chamber insert was difficult to seal, as was the intake manifold muff.

The piston cam grind and side contour were revised by trial and error. The engine was run a short time and where the piston showed heavy wear, material was removed from this area. The piston profile optimization process was not quite complete at the end of Configuration 3. The chrome top ring was replaced with a plasma coated molybdenum and chromium-carbide faced ring to reduce ring wear. The second, third, and fourth rings were replaced with straight faced rings instead of taper faced rings to increase oil lubrication to the upper portion of the cylinder.

No material changes were made for these rings or to the oil control ring. The engine was run with this ring pack with the rings unpinned. The ring gaps were radiused slightly to prevent ring clipping. This ring pack resulted in a significant improvement in ring wear; but the wear was still too high. The rings did not experience ring tip clipping.

Various attempts were made at developing a 'Mae West' profile for the cylinder port area. Mae West reliefs were tried ranging from .025mm to .070mm, on the diameter. No conclusive evidence was found to identify which, if any, of the Mae West profiles was the optimium. Honing of the Mae West profile proved to be most difficult.

The original connecting rod was modified by attaching an external oil feed line to supply pressurized oil to the pin bushing. This significantly reduced the bushing wear rate and overheating, but still not to an acceptable level. This connecting rod eventually failed. This failed connecting rod was replaced with a forged rod that was rifle drilled to supply pressurized oil to the wrist pin bushing. A spiral grooved bushing was used in this rod. This connecting rod proved durable but wear rates of the pin bushing were still not acceptable.

The two piston pin bushings were pinned in place to prevent rotation. Wear rates for these bushings were at an acceptable level, although still higher than desired. No further problems were encountered with these bushings. Provisions were made for aluminum caps to be held in place by the wrist pin snap rings. These caps prevented the intake air pressure from the ports leaking through the bushings to the crankcase, and thus carrying with it the oil film.

The fretting of the cylinder hold down nut was reduced by increasing the installation torque to 1085 Newton meters.

A total of seventy hours of running time was accumulated on Configurations 1, 2 and 3. The engine was successfully run up to a power of 9 bar IMEP at 3500 RPM. Problem areas that still remained were: Cylinder scuffing, high ring wear, combustion chamber leaking, and piston pushing. Progress had been made in these areas, but the problems were not completely solved. The Nikasil coating on the cylinder I.D. could not be easily refurbished after a scuff incident since there were no United States vendors for this coating process. Hard chrome plating was selected as the process for future refurbishing the cylinder.

4.2.2 Configuration Four. The following modfications and/or additions were made prior to the testing of Configuration 4 hardware:

- CAE-X injection pump with 71cm X 1.6mm injection line was installed
- Hard chrome plated cylinder honed to .635 to .762 μm rms finish
- Modified intake manifold
- New connecting rod with L/R of 4 and foot valve.
- Knurled piston skirt
- Kopper's company recommended ring pack

Figure 4.2.6 shows a photograph of this engine configuration. The CAE X pump was directly driven off the camshaft through a flexible coupling. The injection line was 71cm long.

The intake manifold shown in Figure 4.2.7 was modified by welding two angled tubes to the intake area of the aluminum casting. This allowed easier plumbing of the manifold to the intake plenum.

A new connecting rod was installed in the engine for Configuration 4. This connecting rod, shown in Figure 4.2.8 was longer than the rod used previously. The connecting rod was rifle drilled and included a foot valve so that an adequate oil supply could be provided to the wrist pin bushing.

The piston skirt was knurled as shown in Figure 4.2.9. This knurling acts as a vehicle for transferring oil from the bottom half of the cylinder over the ports and to the top half of the cylinder.

The cylinder was hard chrome plated, ground, and then honed to size. A .07mm "Mae West" was provided.

The CAE-X pump was installed and driven at half engine speed. The rings used for this configuration were as recommended by the Koppper's company and shown below:

Top Ring, P/N B7792A
106 X 2.921mm rect. K1000F plasma coated keystone twist, K28, .254/.584 end gap

Second Ring, P/N B7794
108 X 2.4892mm Crown K1000F plasma rectangular twist, K28, .25/.51 end gap.

Third Ring and Fourth Rings
108 X 2.892 Crown rectangular twist K iron, .25/.51 end gap

Oil Ring
108 x 4.5 conformable close rail oil ring assembly, (225 psi spring) .25/.64 end gap.

The engine was assembled and a ten hour test schedule was conducted. Upon inspection, all parts appeared to be in good condition. A minor piston machining of the top ring land was required because there were signs of contact there with the cylinder wall. The final piston profile, as installed, is shown in Figure 4.2.10.

The engine was again reassembled and the power level gradually increased to the takeoff power level (78.3kW). The engine had run a total of 35 hours up to this point. Upon inspection of the cylinder after running, it was evident that scuffing had occurred. The engine was disassembled for a complete inspection.

There were two reasons for the scuff. The thermal limits of the aluminum piston had been exceeded and the Ni-resist insert for the top ring had become debonded from the aluminum as shown in Figure 4.2.11 The standing oil jet pipe rotated due to vibration, causing it to miss the piston oil cooling gallery. This resulted in piston overheating. This debonding has been noted in previous runs but to a much lesser degree. The piston ring inspection also revealed that severe ring butting has occurred. Details of this inspection are shown in Appendix VI. Koppers then recommended the following ring end clearances:

TABLE IX

RECOMMENDED PISTON RINGS

	PART NUMBER	END CLEARANCES (mm)
Top Ring	B7792	1.016 - 1.27
Second Ring	B7794	.762 - 1.016
Third Ring	B7793	.762 - 1.016
Fourth Ring	B7793	.762 - 1.016
Oil Ring	B7796	.635 - .889

They also recommended increasing the amount of negative point protrusion on the second and third rings to eliminate any port clipping and decreasing the oil ring pressure to 1200 kPa.

The two piston wrist pin bushings showed metal wear and the connecting rod bushing shown in Figure 4.2.12 also experienced extreme overheating.

This configuration confirmed that full power could be accomplished with this hardware; however, additional developmental refinements would be required. The aluminum piston's contour and cam grind were established.

Knurling the piston made it possible to run full power. The thermal limits of the aluminum piston, however, were exceeded. For this reason, the all aluminum piston was not run again. The CAE-X pump worked out very well. The wrist pin bushings in both the piston and especially the connecting rod still remained a problem. Elimination of ring butting should improve reliability from here on.

Problems that still remained to be solved at the end of testing of Configuration 4 were:

- Sealing of the combustion chamber
- Need to reduce thermal loading on aluminum piston
- Reduce wear and overheating of wrist pin bushings in piston and connecting rod.

4.2.3 Configurations Five and Six. The following modifications or additions were made for Configurations 5 and 6:

- Steel capped aluminum piston with knurled skirt
- New combustion chamber sealing system
- Fuel injection nozzle cooler
- Hardened injection nozzle
- Silver plated connecting rod bushing with a revised oil flow
- Koppers rings with recommended ring end clearances

The steel capped piston used, is shown in Figures 4.2.13 and 4.2.14. The aluminum piston skirt was used to support a steel cap which carried the top ring. The cap was screwed onto the aluminum base, radially pinned in three locations (120^{o} apart) and pinned through the center of the cap so that concentricity could be maintained between the cap and the piston skirt. A thermal barrier between the top of the aluminum skirt and the back of the steel cap was provided via air gaps.

The two bronze piston pin bushings were silver plated for improved wear resistance. An oil passage was drilled from the top side of both bushings into the piston oil cooling gallery so that the oil flow to these bushings would be increased. The connecting rod bushing was also silver plated. The top half of the oil annulus in the bushing was blocked off. Now all of the oil delivered to the bushing had to flow out of the bottom half load bearing area, thus providing maximum lubrication and cooling.

Figure 4.2.15 shows the new combustion chamber insert assembly along with the nozzle cooler and injection assemblies. These components are shown assembled in Figure 4.2.16. This combustion chamber required a steel ring to be pressed into the cylinder to provide a shoulder for the sealing gasket. The injection nozzle cooler was sealed against the top of the combustion chamber via a spark plug gasket.

Configuration 5 scuffed the cylinder after only four hours of running time. The aluminum skirt was in fine condition indicating no piston cam grind or profile problems. The scuffing was caused by an incorrectly machined top keystone ring groove. Figure 4.2.17 shows a schematic of this problem.

The excessive keystone angle allowed the piston ring to be back edge supported. Cylinder pressure caused the ring to droop which resulted in line contact between the ring and the cylinder wall. This resulted in ring scuffing.

Configuration 6 included a new piston cap which was correctly machined to tolerance. This build scuffed after eight hours of running at half load. The Kopper's company report shown in Appendix VII analyzes the ring problems. Essentially, the steel cap configuration, as designed would not provide a stable enough top ring groove. The keystone groove would close up and pinch in on the ring due to thermal distortion. This caused the ring to stick, and eventually stand proud in the groove resulting in scuffing.

At the conclusion of Configuration 6 testing, it became apparent that:

- The steel capped aluminum piston was a promising concept but more development was required.
- The new combustion chamber seating system showed promise. The design needed to be modified to accept commercially available sealing gaskets.
- The injection nozzle cooling assembly worked flawlessly and eliminated injection nozzle tip overheating.
- The increased ring end clearances eliminated ring butting.
- The silver plated connecting rod bushing with the revised oil flow scheme eliminated the bushing wear problems.
- The silver plated piston pin bushings showed no signs of wear.

4.2.4 Configurations Seven, Eight, and Nine. Configurations 7, 8, and 9 primarily involved developing the ring groove configuration, cam profile, and skirt contours for a thin walled, ductile iron piston. Figure 4.2.18 shows a photograph of the two piston configurations delivered. These pistons have no cast-in oil flow passages like the aluminum piston did. They did however, rely on a standing oil jet squirting the underside of the piston crown for cooling. Cooling oil supply per piston of 5.7 liters per minute was recommended for these pistons. The dome top piston was used for these three configurations. A combustion chamber was designed and fabricated to fit the domed contour of this piston crown. It is shown in Figure 4.2.19.

This combustion chamber utilized a different sealing gasket than was used in Configurations 5 and 6. This commercially avialable sealing gasket was a ring 99.4mm in diameter made of a .79mm diameter stainless steel wire.

Configuration 7 was run for four hours at light load before scuffing occurred. The new pistons and the piston manufacturer's recommended cylinder-to-piston clearances were used. The scuffing was caused by both the piston rings and the piston itself. The ring grooves were not correctly specified to allow for sufficient side clearance. Therefore, ring sticking occurred.

Also every ring land showed contact with the cylinder which was a very undesirable condition.

The combustion chamber and sealing method for Configuration 7 proved to be leak-tight and very reliable.

Configuration 8 consisted of a modified cast iron piston with increased ring land-to-cylinder-bore clearances, as well as, a "Bokor" finish on the piston skirt. This finish shown in Figure 4.2.20 was to accomplish the same oil retention function as the knurling did for the aluminum piston. Knurling the piston skirt was not a practical, reliable method for finishing the piston.

As an additional precaution, oil was misted into the induction air in the ratio of one part oil to forty parts air to provide a sufficient oil supply to the upper half of the cylinder.

This configuration scuffed after only ten hours of running at medium load. Inspection revealed that ring scuffing had occurred. The cause was insufficient lubrication to the piston rings. The honing profile of the cylinder bore was almost nonexistent after a short amount of running time. Careful inspection of this cylinder and another cylinder which was honed by the same vendor, revealed the surface finish consisted of much torn and folded metal instead of a clean cut honing pattern. The measured surface finish of .60 to .90 μm rms was not actually cut into the cylinder bore.

This raised metal was rapidly worn away leaving no honing pattern in which to retain oil. The lack of lubrication was appararently caused by an insufficient cylinder honing pattern.

Configuration 9 consisted of a newly chrome-plated cylinder and honed with a rigid type 120 grit diamond hone. This hone put the recommended .76 to 1.0 μm rms surface finish in the cylinder with torn or folded metal. The engine was assembled with the desired optimized iron piston with the cut back ring lands and "Bokor" skirt finish. Oil was still

added to the intake air in the ratio of one to forty. The engine was run for eighteen hours at up to half load, with no apparent problems. Further testing at higher loads resulted in another scuffing incident. This time piston scuffing, and not ring scuffing, was caused by too tight a fit between the piston ring lands and the cylinder. This scuff was not too severe and the cylinder was reground and honed.

Now the only problem that remained with the hardware after the end of the testing of Configuration 9 was optimization of piston and ring lands dimensions.

4.2.5 Configuration Ten. Configuration 10 included the following components:

- Cylinder #3, chrome plated and honed to a bore diameter 108 mm with a .76 to 1.0 μm rms.
- Cast iron, dome topped piston with modified cam ground profile, ring, grooves and ring land dimensions.
- A new crankshaft and connecting rod.
- New intake manifold
- Close coupled CAE-X pump with a 15 cm injection line.
- Koppers ring pack with large ring and gaps and increased negative point protrusions.

The cylinder was ground to a bore diameter 107.95mm and then honed with a rigid type diamond hone to 108 mm with a surface finish of .76 to 1.0 μm rms. The piston's diametral clearance profile and ring lands as installed, are shown in Figure 4.2.21.

A radial side clearance of .53mm was provided for the top ring, .127mm for the second, third and fourth rings, and .051mm for the oil ring. The larger end clearances were provided for the ring as recommended by the ring supplier. A new intake manifold shown in Figure 4.2.22 was designed and installed on the cylinder for this configuration. The manifold relies on a light press fit for air sealing around the ports.

A new crankshaft along with the corresponding connecting rod was also installed in the test engine for this configuration. This crankshaft had a 76.2mm crankpin for additional strength instead of a 57.15mm crankpin that the old crankshaft had.

This new crankshaft also features a larger fillet radius. The main bearing diameters were kept the same. The crankpin was rifle drilled for oil from both main bearing journals.

The connecting rod shown in Figure 4.2.23 was "V" drilled configuration for good oil supply pressure to the wrist pin bushing. A foot valve was also fitted for dependable oil flow. The wrist pin bushings were silver plated and were wider than the old connecting rod bushings, thus providing greater bearing support area. Oil supply to the top half of the bushings was restricted to force the oil out of the loaded area of the bushings.

The injection pump was belt driven through a cogged belt and installed with a short injection line (15mm).

This configuration was run for sixty hours between three quarter and full load at 3500 RPM. Polishing and some scuffing of the ports areas limited further testing. The piston, in general, was in excellent condition as were the piston rings. Very little wear was measured in any of the power components except the cylinder inside diameter. Figure 4.2.24 shows a photograph of the cylinder's port areas after sixty hours of running. Some scuffing was evident as is extensive polishing. This problem had not been evident previously. In previous cases, major scuffing occurred so early in development testing that much of the evidence used to form a hypothesis was masked. It was believed that the polishing was a result of agressive behavior between the cast iron pistons and the chrome bore and bore distortion in the port areas.

The only development problem remaining at the end of Configuration 10, therefore, was the problem of bore polishing. The new components added to the engine for this configuration caused no problems. The piston's contour, ring groove, and ring land dimensions were developed to the point where no further design modification was necessary.

4.2.6 Configurations Eleven and Twelve. Configurations 11 and 12 had the same features as Configurations 10 except for the addition of a stainless steel piston cap on the flat top cast iron piston and a tin plated piston skirt to resolve the polishing noted above. Also, some cooling fins were removed from the cylinder to reduce heat loss.

Figure 4.2.25 shows a diagram of the piston, combustion chamber, injector and cylinder. Figure 4.2.26 shows the stainless steel piston cap . The piston cap was made of 321 stainless steel which maintains sufficient strength and corrosion resistance up to 875°C, for this application. Air gaps were used to reduce the heat flow from the cap to the piston body. A stainless steel wire seal ring was used

to prevent gas leakage from the combustion chamber to the air gaps. The cap was secured to the piston by a belleville washer and a stainless steel 19.05mm nut which was tack-welded to ensure it did not come loose. The threaded portion of the piston cap was drilled to reduce weight and heat flow. The drilled portion was capped with a stainless steel plug to prevent cooling oil from entering this hole.

The .05mm thick tin plating on the piston skirt was used to eliminate the cylinder polishing. The same piston profile shape was used as before, but the piston was machined round instead of cam shaped. No cam grinding equipment was available to machine the pistons after they were tin plated. The "Bokor" finish was machined into the tin plating.

A total of fifty hours of running time at between one half and full load was accumulated on Configurations 11 and 12. No major scuff incidents occurred during that time, but the port polishing remained. No problems were encountered with the piston. The accelerated rate of the polishing was a direct result of the increased exhaust temperature due to the insulated piston configuration.

An inside diameter profile trace of the cylinder revealed tne cause of the polishing as was the honing process prior to assembly.

A rigid hone with synthetic diamond stones was used to put the desired surface finish (.76 - 1.0 μm rms) on the cylinder wall. Unfortunately, the hone also removed material unevenly from the port area. Figures 4.2.27 and 4.2.28 are cylinder profile traces above and below the ports, respectively. This uneven removal of stock during honing was caused by the uneven pressure that the honing stones applied to the cylinder inside diameter while traversing over the ports. When the stones traversed a port, about 4 cm of the 10 cm of stone length was unsupported. Since the pressure on the stones was essentially constant, the unit loading on the cylinder wall above and below the port was sixty percent higher than was the case when the stones were fully supported on a port bridge.

This caused the uneven cutting action. The uneven cylinder bore caused the piston and piston rings to load the high points (i.e., port bridges) in the cylinder. The rings and piston then wore away the honed surface finish on the port bridges. Once this happened, the bridges could not retain an oil film and scuffing occurred.

Configurations 11 and 12 demonstrated the feasibility of the air barrier stainless steel capped piston. No problems were encountered with the cap, the piston or the piston rings. The only problem which still remained at the end of the development program was the port bridge polishing.

4.2.7 Optimum Hardware Configuration. The following list of recommended hardware result from the testing done to date. This configuration has a good chance of obtaining durability, as well as achieving low heat loss:

- Nitrided steel liner, brush honed to .76 to 1.0 μm rms finish. Initially no "Mae West" port area relief.

- Stainless steel capped piston with tin plated skirt. "Bokor"finish on piston skirt machined as shown in Figure 4.2.20, piston profile shown in Figure 4.2.21, .165mm top ring side clearance, .114mm side clearnace for 2nd, 3rd and 4th ring, and .050mm for the oil control ring.

- Air barrier insulated stainless steel combustion chamber as shown in Figure 4.2.19.

- Ring pack and ring clearance, shown in Table IX.

- Connecting rod with tin plated, grooved, bronzed wrist pin bushing. Connecting rod must be drilled for bushing oil supply and have a foot valve. The bushing should only allow oil to flow out of the loaded, bottom half of the bearing.

- The piston's wrist pin bushings should also be tin plated, grooved, and made of bronze with caps over the ends to prevent induction air leakage.

- Nozzle cooler assembly as shown in Figure 3.4.5 should be used.

Nitrided steel liner would be superior to the chrome plated liners. The nitrided steel liner has superior hot hardness over hard chrome to increase scuff resistance. Also, ring manufacturers have extensive experience with rings running on nitrided steel which also has superior oil wetting capability. Hard chrome has very poor wetability characteristics.

The liner must be honed with a brush-type of hone. This type of hone consists of many round abrasive balls attached to stiff nylon bristles which are attached to a wire shaft. This hone would remove material more evenly, and has been used commercially in the honing of two-stroke cycle engines. This hone was used on the SCTE cylinder. However, the correct hone abrasive was not available for the hard chrome bore so that an acceptable surface finish was not obtained. Selection of the correct abrasive for this hone will be required.

The piston and rings worked satisfactorily and no future modifications are foreseen.

4.3 Injection System Performance. A number of variations on the injection system were evaluated throughout this program. This section 4.3 describes the combinations of injection hardware tested in this program.

4.3.1 Bosch APF-1B Injection System. Four, eight-hole nozzles were tested with the Bosch APF-1B during this program (.20, .225, .25, and .30mm). The .25mm diameter nozzle tip resulted in the best engine performance. The smaller hole diameters resulted in excessive injection durations at higher fuel flows. The 0.30mm hole diameter resulted in the same or slightly longer durations, and had the disadvantage of low injection pressure due to the larger nozzle area. The larger nozzle configuration also resulted in reduced engine performance compared to the .25mm diameter tip.

Of the two nozzle spray angles tested (165^{o} and 155^{o}), the 155^{o} nozzle gave the best engine performance. The 165^{o} angle plume inpinged on the upper surface of the combustion insert.

Erratic nozzle needle lift was also observed during testing, particularly at the rated speed of 3500 RPM. This problem was eliminated by decreasing the injection line volume and increasing the fuel supply pressure to the pump.

Prior to these changes, the 9mm plunger pump was replaced with a 10mm of the same type. This change was made to raise injection pressure. Erratic injection occurred and the cause of the problem was never fully defined. The 10mm pump was then removed and never used again.

The APF-1B pump itself worked quite well, particularly considering the fact that it was driven at engine speed when originally designed for half speed. However, because of the low profile cam used, the plunger velocity, even at 3500 RPM, was not sufficient to deliver the desired pressures. This cam shape did allow the high speed operation of the pump at the required speed which would not have been possible with a "faster" cam without modifications to the pump assembly.

This pump was used for preliminary performance evaluation and it served this purpose well. Its flow capability at higher engine loads was sufficient, but resulted in excessive injection duration (24^{o} CA at 66 mm^{3}/injection). This limited the power potential of the engine.

4.3.2 CAE-X Injection System. The single cylinder version of the CAE-X pump was evaluated on a bench. The injection line length, delivery valve size, fuel flow, and pump speed were varied and their effect on injection pressure, injection duration, and injection delay was monitored. The injection nozzle used for this study had eight holes at 0.24mm diameter.

The data shown in Figure 4.3.1 and 4.3.2 revealed that reducing the injection line length from 71 to 40cm at a constant fuel rate had a significant, positive effect on injection pressure and duration.

The effect was diminished by reducing the injection line length even further. The injection pressure was limited for these tests to 1300 bar since the pump's durability at higher pressures was questionable.

The bench test results indicated that the CAE-X injection system could deliver the system performance required for the aircraft diesel SCTE. This injection pump was initially installed on the SCTE as shown in Figure 4.3.3. The injection line length was 71.1cm.

All engine runs with this pump configuration included a $50mm^3$ retraction volume delivery valve and used a 1.6mm inside diameter injection line. The injection nozzle was drilled for eight holes at 0.24mm diameter with 157° included angle. The valve opening pressure was set at 260 bar. The pump timing was varied from the control room by adjusting the pump timing mechanism via a hydraulic actuator.

The CAE-X pump was later repositioned and the injection line length was reduced to 17.8cm. The delivery valve retraction volume was reduced to $30mm^3$ for stable pump operation. This set-up is shown in Figure 4.3.4. It proved to be a very reliable system.

Figure 4.3.5 shows a comparison of the injection duration versus injected volume for the three injection pump systems tested on the SCTE.

Where the APF-1B injection system was load limited, the close coupled CAE-X system produced the full load fuel requirement of $95mm^3$ per injection with a 22° duration of injection.

The injection characteristics of the three systems are also reflected in Figure 4.3.6. This figure displays ignition delay versus injected volume and demonstrates that the close coupled CAE-X system gives shorter ignition delay than the other two systems.

This shorter ignition delay was a direct result of better fuel to air mixing caused by the higher injection pressure and injection pressure rise rate obtained from the close coupled CAE-X pump system.

Figure 4.3.7 shows the dynamic injection pressure and needle lift at three fuel flow points for the close coupled and the longer injection line CAE-X pump systems. The close coupled system showed much better injection characteristics. The injection pumps were identical except for the delivery valves.

The CAE-X pump showed no wear and gave no major problems for the duration of this program. Its performance was excellent. The ADB injection nozzles showed some fretting at the nozzle to injector body seal caused by over pressurization. The nozzle and holder assemblies were designed for 950 bar. A higher pressure capacity holder and nozzle is needed for future development work. The injection nozzle cooler worked effectively after the initial development stage and no further needle seat overheating was encountered.

4.3.3 Electronically Controlled High Pressure Fuel Injection System (HPFIS). As part of this program, an electronically controlled, hydraulically amplified fuel injection system was fabricated and bench tested by Bendix Engine Products Division. Features of this system are described in Section 3.4.4 of this report. However, due to the numerous operational and durability problems encountered in the bench testing and operation on Jet "A" fuel, the system was never installed on the engine for full evaluation. Therefore, no engine data are presented for comparison with the other two systems evaluated. The Bendix final report is included as Appendix V and describes the details of this development testing and problems encountered.

4.3.4 Fuel Injection Systems Selection Summary. Of the three separate injection systems evaluated during this SCTE test program, the CAE-X pump, close coupled with a short injection line, and operating with a 14mm plunger, gave the best results. A variable timing mechanism was used and an automatic timing advance feature would be required for multicylinder applications. Given further development time, the electronically controlled system may ultimately prove out to be more suitable due to the additional flexibility it offers in terms of timing and also the potential high pressures regardless of engine speed and load. This, however, remains to be proven on an operating engine.

Whichever system is chosen for the ultimate application, additional development work would be required with pump operation on jet fuels.

4.4 Engine Performance. Previous sections have primarily discussed the hardware aspects of the test program. This Section 4.4 discusses the performance aspects, and is arranged in chronological order (similar to the hardware descriptions).

4.4.1 Engine Performance Testing With Configurations One, Two & Three. The performance testing for Configurations 1, 2 and 3 was primarily concerned with cylinder air flow characteristics for three porting configurations shown in Table X.

Figure 4.4.1 and 4.4.2 show the average overall port coefficients versus cylinder pressure ratio for the three cylinders at 3500 RPM and 2650 RPM. Average overall port flow coefficients are defined as follows:

$$C = \frac{Rs}{2}\left(\frac{r}{r-1}\right)\left(\frac{s}{A_i}\right)\left(\frac{P_i}{P_e}\right)\phi_1$$

Where:

C = Overall Port Flow Coefficient

R_s = Scavenge Ratio

r = Overall Compression Ratio

A_i = Speed of Sound in Intake Manifold

S = Average Piston Speed

P_i = Intake Manifold Pressure

P_e = Exhaust Manifold Pressure

k = Specific Heat Ratio

ϕ_1 =

$$\sqrt{\frac{2}{k-1}\left(\frac{P_e}{P_i}\right)^{2k} - \left(\frac{P_e}{P_i}\right)^{\frac{k+1}{k}}}$$

TABLE X

AVAILABLE CYLINDER PORT CONFIGURATIONS

CYLINDER	INTAKE PORT HEIGHT (mm)	TOTAL INTAKE PORT AREA (mm^2)	EXHAUST PORT HEIGHT (mm)	TOTAL EXHAUST PORT AREA (mm^2)	$A_{exhaust}$ / A_{intake}
1	29	3084.1	41	2432	.788
2	26	2764.7	35	2076	.751
3	31	3296.7	43	2550	.774

The average overall port flow coefficient is a convenient parameter for evaluation of engine air flow characteristics. These two figures show that cylinder 3 with the larger intake and exhaust ports had the highest average overall port flow coefficients. The flow coefficients predicted by AVL at 3500 RPM were very close to the measured value for both cylinders 2 and 3. Cylinder 1 with the second largest ports actually had the lowest flow coefficients. At 2650 RPM the port flow coefficient for cylinder 1 is considerably higher than those for cylinder 2. This apparent contradiction indicated that an engine speed dependent manifold tuning effect may have caused this phenomenon.

Figure 4.4.3 shows engine performance versus RPM for lines of constant cylinder pressure ratio at constant IMEP and intake manifold pressure for cylinder 1. There was a significant adverse tuning effect which caused a decrease in air fuel ratio at higher speeds. This resulted in poor fuel consumption, high exhaust pressure and high heat loss.

Generally, scavenge ratio and air-fuel ratio decreased with higher RPM. This caused the required overall turbocharger efficiency to decrease due to the greater exhaust temperature. For the most part, ISFC followed air-fuel ratio.

The required overall turbocharger efficiency is high except at those points where the fuel consumption is excessive. These points were beyond the smoke limit. Smoke was not plotted on this curve because of the high experimental error associated with the measurement system. Fuel economy and required overall turbocharger efficiency are a tradeoff. Increasing one decreases the other.

Figure 4.4.4 shows the same parameters for cylinder 3, which had the largest ports. This cylinder also showed an adverse tuning affect at 3000 RPM but was much less significant than that encountered with cylinder 1.

Fuel consumption for Configuration 3 was equal to or better than with cylinder 1. Required overall turbocharger efficiency improved compared to cylinder 1 for a given RPM and air-fuel ratio. This was a result of the reduced cylinder pressure ratio required to give the same air-fuel ratio.

Not enough data was collected from tests of cylinder 2 to plot a similar curve. However, the data that was collected indicated the same trends.

In summation, cylinder 3 with its large ports, required the least amount of cylinder pressure ratio to flow an equal amount

of air, with no penalty in fuel consumption. The required cylinder pressure ratio for a given air-fuel ratio resulted in lower required overall turbocharger efficiency. Therefore, cylinder 3 was used for nearly all the remaining devel pment and testing work.

4.4.2 Configurations Four Through Nine. Configuration 4 featured cylinder 3, the cone top aluminum piston, .63 squish ratio open combustion chamber, CAE-X injection system with the 71.1cm injection line, and the modified original manifold. The goal of testing Configuration 4 was to demonstrate takeoff power. This goal was attained.

Figures 4.4.5 shows engine performance versus IMEP at 3500 RPM. The predicted performance at both full power and power cruise are shown. The data points at 10.6 and 13.1 bar IMEP were run at leaner air-fuel ratios than necessary to reduce the risk of scuffing. This caused the data curves to appear inconsistent.

The fuel consumption was actually lower than predicted; but indicated heat loss, cylinder pressure ratio, $\Delta P/P$, and required turbocharger efficiency were all higher than predicted. This indicated that heat loss had to be reduced, as did cylinder pressure ratio for a given air-fuel ratio.

Previous testing of Configurations 1, 2 and 3 indicated that manifold tuning could be the problem. To address this, the port flow coefficients were measured and this data put into the cycle simulation program. The program was then used to optimize manifolding configuration based on air flow.

Port flow coefficients were also evaluated with several different piston cap configurations shown in Figure 4.4.6. The intake port flow coefficients are shown in Figure 4.4.7 and the exhaust port flow coefficients in Figure 4.4.8. The cone top piston gave the highest flow coefficient for both the intake and exhaust ports. The radiused piston top configurations all showed better flow coefficients than the corresponding sharp edge piston top configurations. These data also confirmed that AVL's original assumption for port flow coefficients were very good.

The testing of Configuration 4 demonstrated that full takeoff power could be attained with the CAE-X pump configuration. Fuel consumption was acceptable, but the required cylinder pressure ratio and heat loss needed to be reduced. Since the radiused edge piston gave superior flow over sharp edged piston, all further testing was conducted with radiused edge piston.

Configurations 5 through 9 were basically centered on resolving hardware problems and no meaningful performance data was obtained. Performance evaluations were continued with Configuration 10.

4.4.3 Configuration Ten. Configuration 10 featured cylinder 3, the dome top cast iron piston with radiused top edge, .8 squish ratio combustion chamber, close coupled CAE-X injection system, and the optimized intake and exhaust manifold. Figures 4.4.9 and 4.4.10 show the significant increase in overall average port flow coefficients for the optimized manifold compared to the original manifold. This new manifold resulted in significantly less cylinder pressure ratio requirements for a given air-fuel ratio than was originally predicted or measured.

Figures 4.4.11 and 4.4.12 show the dynamic intake and exhaust pressures respectively, for the optimized manifold and the original manifold. The absolute dynamic intake pressure for the original manifold was about thirty kPa (0.3 bar) below the mean pressure at bottom dead center which is the opposite of the desired condition. A high pressure is desired at bottom dead center because the port area is a maximum thus increasing mass flow. The optimized manifold has nearly constant pressure with much less pressure cycle fluctuations.

The original exhaust manifold also had large amplitude pressure pulses which resulted in poor air-flow characteristics. A low pressure pulse would be desired at bottom dead center where the port area is at a maximum. Both the original and the new configurations exhibit this characteristic.

Again, the optimized manifold has relatively small amplitude pressure pulses and they occur mostly during the port's open period.

The optimized manifold, cast iron piston, and improved injection characteristics obtained from the close coupled CAE-X injection system were reflected in engine performance as shown in Figure 4.4.13. Lines of constant air-fuel ratio were plotted so that the trade-off between required overall turbocharger efficiency and air-fuel ratio could be analyzed. On the average, the reduction of air-fuel ratio from 55 to 45 reduced the required overall turbocharger efficiency twelve percent and increased ISFC four percent.

The leaner air-fuel ratio points gave improved fuel consumption and lower heat loss at the expense of lower exhaust temperature and higher cylinder pressure ratio. This in turn resulted in higher required overall turbocharger efficiency. Based on these data, it is most likely that the engine would not run self-sustained at overall air-fuel ratios leaner than 45 to 1. The cost for this is a four percent increase in fuel consumption.

The measured engine performance was superior to the predicted performance in all areas except exhaust

temperature. Fuel consumption was significantly better due to improved combustion and reduction in heat loss through the piston. The cast iron pistons have a much lower conductivity than original aluminum pistons.

The required overall turbocharger efficiency (for self-sustained operation) of approximately 59 percent with this combination of hardware exceeded expectations. However, even this relatively low required efficiency would still depend on the availability of a fairly advanced turbocharger. To reduce this required efficiency still further, heat loss needed to be further reduced, and the conserved energy must be made available in the form of higher exhaust temperatures.

4.4.4 Configurations Eleven & Twelve. Configurations 11 and 12 utilized the air gap insulated, stainless steel capped, cast iron piston to reduce heat loss. Configuration 11 used cylinder 1 with modified ports machined to the optimum specifications based upon the cycle simulation work. Configuration 12 used cylinder 3 with some cooling fins removed from the cylinder head area.

Figure 4.4.14 shows a comparison of performance between Configurations 12 and 10. The only difference between the two configurations was the piston. The air gap stainless steel capped piston reduced the indicated heat loss by approximately forty percent while exhaust temperature increased by about nine percent.

The air flow characteristics and fuel consumption remained unchanged. The required overall turbocharger efficiency was reduced by about nine percent to approximately fifty-three percent.

Figure 4.4.15 and 4.4.16 show the cylinder temperature distribution for Configuration 10 and 12.

Cylinder temperatures 2 through 5, and 7 through 10 showed essentially no difference between the two configurations. However, temperatures 6 and 1 were considerably higher for Configuration 12 than Configuration 10.

This was primarily due to the reduction in cylinder head cooling fins.

The temperature at point 11, measured by a thermocouple welded to the back of the stainless steel combustion chamber was 166°C higher for Configuration 12. This also results from removal of the cooling fins and the insulating effect of the stainless steel capped piston.

Figures 4.4.17 shows engine performance for Configurations 11 and 12. Configuration 11 used a cylinder with a much higher intake port timing and slightly advanced exhaust port timing compared to cylinder 3. At A/F = 45, Configuration 11 showed a higher fuel consumption and heat rejection than did Configuration 12.

The cylinder pressure ratio, exhaust temperature, and required overall turbocharger efficiency, were relatively equal between these configurations.

Configuration 11 was runnable at fuel consumption and heat loss values equal to Configuration 12, but to do so required a fifty-five to one air-fuel ratio. This resulted in lower exhaust temperature, higher cylinder pressure ratio, and higher required overall turbocharger efficiency.

This trend was not predicted by the cycle simulation program. In essence, the large intake ports did not improve air flow. The exhaust ports became the limiting factor. They would have to be enlarged to increase air flow. The larger (i.e., advance) intake ports also caused significant short circuiting of the air from the intake to exhaust ports, resulting in a decrease in trapping efficiency. Therefore, the cylinder with the large ports required a greater overall air-fuel ratio than cylinder 3 did for an equivalent trapped air-fuel ratio. The trapped air-fuel ratio is the basic governing variable affecting indicated specific fuel consumption.

This dependency between ISFC and trapped air-fuel ratio was used to quantify trapping efficiency. Figure 4.4.18 shows the trapping efficiency versus scavenge ratio for Configurations 4, 11 and 12 (also in Reference 6 data). The error bands represent an error estimate of trapped air-fuel ratio of plus or minus two.

Configuration 11 showed trapping efficiencies between forty-seven and forty-nine percent while Configuration 12 showed trapping efficiencies between fifty-nine and sixty-five percent.

Any improvement in trapping efficiency will directly reduce the required overall turbocharger efficiency since for a given trapped air-fuel ratio, a higher trapping efficiency will require less overall air flow from the compressor. This increases the exhaust temperature, and reduces the required cylinder pressure ratio; and thus, the required overall turbocharger efficiency is reduced.

4.4.5 Engine Performance Summary. This section summarizes the most important engine performance parameters obtained during the experimental testing phases of this program.

4.4.5.1 Required Overall Turbocharger Efficiency. Figures 4.4.19 and 4.4.20 show the required overall turbocharger efficiency and the engine heat balance for Configurations 3, 4, 10 and 12, which were run at 3500 RPM and 6.9 bar IMEP. Figures 4.4.21 and 4.4.22 show similar data at 9.0 bar IMEP and 3500 RPM, the cruise power condition. Throughout the course of this program, significant reductions in the overall turbocharger efficiency required for unassisted scavenging have been attained. This was a result of increased exhaust energy and reduced cylinder pressure ratio required.

The exhaust energy was increased by reducing the heat loss insulating the piston crown, and increasing the insulating effectiveness of the combustion chamber. The cooling fin area around the cylinder head was also reduced. The cylinder's required pressure ratio for a given air-fuel ratio was also reduced by the optimized manifold used in Configuration 12.

During the development program, the indicated work was increased 9% at the 3500 RPM, 9.0 bar IMEP power level. The engine was run at approximately 46 to 1 overall air-fuel ratio for all the data shown in Figure 4.4.21.

Air-fuel ratio has a significant effect on thermal balance, and the required overall turbocharger efficiency. This effect is illustrated in Figures 4.4.19 and 4.4.20 for (C) and (D). The only difference between runs (C) and (D) was the air-fuel ratio. The richer point (D) needed a lower required overall turbocharger efficiency, but gave higher heat loss, lower exhaust energy, and lower indicated work. The lower indicated work was caused by the decrease in combustion efficiency with richer air-fuel ratios. The heat loss was higher because the increased cylinder gas temperatures which resulted from the rich air-fuel ratio produced greater cylinder gas to wall temperature gradients which are the driving force for the heat loss. The overall required turbocharger efficiency was lower for the richer air-fuel ratio point which ran at a lower cylinder pressure ratio and higher exhaust temperature.

4.4.5.2 Mass Fraction Burn Rate. Figure 4.4.23 shows the mass fraction burn rate for three points for Configuration 12. These measured results indicated that the combustion system was extremely good, as confirmed by the excellent thermal efficiency results. The fast burn rates which gave higher thermal efficiency and resulted from the improved close coupled fuel injection characteristics, low heat loss, and to some degree, combustion chamber geometry. To confirm the validity of the measured burn rates, and to provide a credible model for use in predicting operating points that were not run experimentally, a mathamatical model was generated to predict mass fraction burn

rate for the Configuration 12 combustion system configuration. This model was based upon the Marzouk-Watson Correlation (Reference 7). The following equations were used to calculate mass fraction burn rate:

$$FB = \beta f_1(t) + (1-\beta) f_2(t)$$

Where: $f_1(t)$ = premixed burning function

$f_2(t)$ = "diffusion" burning function

β = phase proportionality factor of premixed to total burning

and: $$\beta = 1 - a F^b / ID^c$$

Where: F = equivalence ratio

ID = ignition delay (ms)

and: $.80 < a < .95$

$.25 < b < .60$

$.25 < c < .50$

$$f_1(t) = 1 - (1-t^{K1})^{K2}$$

$$f_2(t) = 1 - \exp(-K_3 t^{K4})$$

$$K_1 = 2.0 + 1.25 \times 10^{-8} (ID \times N)^{2.4}$$

$$K_2 = 5000$$

$$K_3 = 14.2/F^{0.644}$$

$$K_4 = .79K_3 0.25$$

This Marzouk-Watson correlation was basesd upon experimental data. The constants a, b, and c were varied to calibrate this model with the measured results. These predicted results are shown in Figure 4.4.23. The values of the constants used are:

a = .80

b = .60

c = .25

The model requires the input of engine RPM, trapped air fuel ratio, and ignition delay to predict mass friction burn rate. This burn rate can then be used as input to the simulation program to predict engine performance for engine conditions not run in the test cell.

4.4.5.3 Performance Maps. Data points were run for cylinder 12 hardware to simulate propeller load curves. These data were then used to predict the multicylinder engine fueling maps. Multicylinder friction estimates were also used.

Figures 4.4.24 and 4.4.25 show the engine performance for the three quarter and full load propeller curves. The full power point was not run during testing of the Configuration 12 hardware. The dashed line represents an extrapolation of Configuration 12 performance. The full load point for Configuration 10 is shown.

Figure 4.4.26 shows the air-flow characteristics for Configuration 12. These air flow characteristics were used for predicting multicylinder engine performance.

Figure 4.4.27 shows the actual motoring friction mean effective pressure for the single cylinder engine with the Configuration 12 hardware. This was also used for predicting the multicylinder engines performance described in Section 5.0.

5.0 MULTICYLINDER PERFORMANCE PROJECTION

The ultimate goal of an aircraft diesel engine test program would be to confirm the initially projected multicylinder engine performance based on a limited amount of data obtainable on the single cylinder test engine. Based on the information collected during this three year program, and described in the first four sections, it is now possible to project the expected performance of the conceptual four cylinder engine originally designed for this application. This Section 5 assembles all of the experimental and analytical data collected during this program, and from it, projects the multicylinder engine perforance.

5.1 Multicylinder Engine Fuel Consumption Projection

The indicated fuel consumption measured during the testing of Configuration 12 was used to predict a multicylinder engine brake specific fuel map. This required a prediction of the multicylinder engine's friction or friction mean effective pressure (FMEP). Figure 5.1.1 shows the predicted FMEP versus piston speed for the multicylinder engine (GTDR 246) along with three other similar engines. The predicted GTDR 246 engine's FMEP was based primarily upon the SCTE motoring friction results. These data were then plotted against the other similar engines. The predicted friction appears to be consistant with the tabulated values. 88% mechanical efficiency was predicted for the GTDR246 at full load. This includes the power required to the fuel injection pump, oil pump, gear reduction, fuel pump, vacuum pump and engine mechanical friction.

This predicted friction was used in conjunction with the measured indicated fuel consumption to predict brake specific fuel consumption for the GTDR 246. This projected fuel map is shown in Figure 5.1.2. The dashed lines represent BSFC based on the SCTE ISFC trends. The solid lines are based upon actual SCTE data.

Figure 5.1.3 shows the predicted engine performance for full load, power cruise, and economy cruise. The maximum brake power is limited by the turbocharger. For this example, a maximum compressor pressure ratio of seven was assumed. This pressure would allow the engine to deliver full rated power up to 6Km altitude if rated power is set at 4000 RPM instead of the original design goal of 3500 RPM. No inlet ram affect was assumed for the turbocharger. Actual ram effects will reduce the required compressor pressure ratio to obtain the desired inlet pressure.

It is apparent from the fuel map that the fuel consumption penalty for going to 4000 RPM is negligible, ~ 3%.

For the power cruise, the engine speed would be reduced to 3500 RPM. This would give 166 kW of brake output up to an altitude of 7.8 Km with between 221 and 225 gm/kW-hr fuel consumption.

For further fuel consumption reduction, the engine speed could be reduced to 3000 RPM which would produce 149 kW up to 7.8Km at a BSFC of around 218gm/kW-hr.

The constant fuel consumption for a given load, independent of altitude, is based upon the engine's combustion air flow and inlet pressure remaining constant. This is a function of the turbocharger characteristics.

5.2 Turbocharging

The turbocharger is a key element in the operation of the aircraft diesel engine. Since it is a two-stroke cycle engine, it requires positive air pressure (induction air) for cylinder scavenging to occur. It is highly desirable for the turbocharger to supply this air pressure and flow without any agumentation. Augmentation being either an exhaust combustor augmentation, or an engine driven air pump. Both of which would significantly increase fuel consumption.

The SCTE demonstrated that required overall turbocharger efficiency is down around 52% including an assumed turbocharger mechanical efficiency of 97%. This would require a compressor and turbine adiabatic efficiency of about 72%. Further reductions in turbocharger efficiencies are possible with further engine development and the utilization of a pulse type turbocharger system instead of a constant pressure system.

A criteria for success of the aircraft diesel is that it must operate self-sustained for the cruise condition so that fuel economy benefits can be obtained.

For minimum fuel consumption, it would also be desirable to have self-sustained turbocharger operation for take-off power so that a plane could climb rapidly with good fuel economy to cruise altitude. A 7:1 compressor pressure ratio was selected to allow the engine to operate satisfactorily up to 7.8 kilometers.

The compressor requirements of this aircraft diesel shown in Figure 5.2-1 are plotted on the advanced map developed by the Garrett Turbine Engine Company for NASA under contract NAS3-22750. This compressor was conceived for an advanced general aviation rotary engine. The GTDR 246 requires more air flow at full power than this compressor can supply, but it appears that cruise power up to 7.8 Km is easily obtainable from the same compressor. A larger capacity turbocharger would be required for the aircraft diesel to reach the desired ultimate ratings shown, but in general, larger turbomachinery is more efficient.

The GTDR 246 would most likely require a variable area nozzle for the turbine section of the turbocharger to operate over such a large altitude span.

The turbine area sets the engine's pressure ratio and air-fuel ratio and this needs to be carefully controlled.

5.3. Piston Speeds and BMEP Levels

Figures 5.3.1 and 5.3.2 show piston speed and BMEP of eleven aircraft engines including this proposed aircraft diesel, (GTDR 246). These bar charts are shown to illustrate this engine's relative ranking of these parameters among other aircraft engines. The piston speed and BMEP ratings are important as far as engine dependability and life are concerned and it is evident that the selected values for this engine are conservative relative to the other similar engines.

5.4 Heat Loss

Based upon the SCTE measured heat loss and the predicted mechanical efficiency, the heat loss for the aftercooler, oil cooler, and cylinder cooling was calculated. These results are shown in Table XI.

TABLE XI
PROJECTED MAXIMUM HEAT REJECTION RATE FOR GTDR-246

	AFTERCOOLER HEAT REJECTION	OIL COOLER HEAT REJECTION	CYLINDER HEAT REJECTION
kW	61.1	22.1	66.6
% OF FUEL ENERGY	8.2	3.0	8.9

These numbers were based upon full load engine performance at 4000 RPM at 6.2 kilometers altitude with a compressor pressure ratio of seven to one. A compressor efficiency of 72% was assumed.

5.5 Engine Specifications

Based on this technology enablement program, and considering the findings and conclusions of references 1 thru 4, two potential multicylinder engine configurations have been made up. Figures 5.5.1 and 5.5.2 illustrate full scale mock-ups of such engine configurations.

Both configurations are radial engines, with Figure 5.5.1 showing a version with the cylinders in a vertical plane. Figure 5.5.2 shows the cylinders in a horizontal plane.

In a single engined airplane where the cabin width - not the engine - determines frontal area, the first version would be more advantageous.

The second configuration would be more appropriate in a twin engined application where the engine nacelle height could be significantly reduced - thus reducing frontal drag. Table XII shows engine specifications for the multicylinder engines.

TABLE XII
GTDR-246 ENGINE SPECIFICATIONS

MODEL TYPE	GTDR-246. 4 Cylinder, radial, air cooled, geared drive, turbocharged, 2 cycle diesel				
CONSTRUCTION	Aluminum alloy crankcase, cylinders with steel barrels. Schnuerle loop scavenged with oil cooled ports. Single throw crankshaft with slipper type connecting rods and dynamic counterweights.				
SUPERCHARGER	Variable geometry turbocharger with combustor augmentation system and intercooling. Turbocharger driven electrical generation system (Auxiliary Power Unit).				
FUEL INJECTION	Direct injection with individual pumps per cylinder. Electronically controlled timing. Engine capable of operation on military and commercial jet fuels.				
LUBRICATION	Pressure fed 4.9 - 6.3 Kg/cm^2 (70 - 90 psi). Dry sump. Cooler.				
BORE AND STROKE		108 x 110	mm	4.25 x 4.33	in.
DISPLACEMENT		4.03	liters	246	in^3
COMPRESSION RATIO		11.2:1	effective	11.2:1	effective
WIDTH AND HEIGHT	-1*	.66 X .66	m	26 X 26	in.
	-2*	.66 X .53	m	26 x 21	in.
LENGTH (INCL.TURBO)	-1	1.06	m	42	in.
	-2	1.27	m	50	in.
FRONTAL AREA	-1	.43	m^2	4.69	$ft.^2$
	-2	.35	m^2	3.79	$ft.^2$
FUEL		JP-5,JET-A,DF-A			
FUEL CONSUMPTION (at economy cruise)		215	gm/Kw-hr	.35	lb/hp-hr
RATING - TAKE OFF		268	kW	360	hp
POWER CRUISE		175	kW	235	hp
ECONOMY CRUISE		149	kW	200	hp

*SEE FIGURES 5.5.1 AND 5.5.2 FOR -1 AND -2 CONFIGURATION DEFINITION

6.0 CONCLUSIONS

The program demonstrated its basic objectives, which were to define and quantify the enabling technologies necessary for the operation of a high output, two-stroke cycle diesel engine, suitable for ultimate application as a general aviation aircraft propulsion system.

The design power levels, specific fuel consumption, air flow, and scavenging pressure requirements were demonstrated in a Single Cylinder Test Engine (SCTE).

The fuel injection parameters required to reach the target SFC's can be achieved with today state-of-the-art injection systems. Requirements for high pressure, variable timing, and cooled nozzles have been defined.

Airflow and scavenge pressure requirements with the Schnuerle loop scavenge system can be acheived with relatively near term advancements in turbocharging technology. The overall turbocharger efficiencies required for operating the engine in a self-sustaining mode - i.e. without auxiliary blowers, are within today's state-of-the-art. The turbocharging pressures required to deliver the desired power levels at altitude are on the order of 6 or 7:1; which are not commercially available with current turbochargers and would require further development effort.

To match the engine's airflow requirements throughout its projected operating range will require the application of variable geometry to the turbocharger. Although this technology has been successfully demonstrated in laboratory and prototype applications, it is not currently an "off-the-shelf" item, and would also need further development. If the "turbocharger only" mode of operation is adopted - without auxiliary blowers - it will be necessary to develop a system of combustor augmentation for start up and low speed, low load operations. The development of such a combustor is well within today's gas turbine engine technology.

To provide adequate energy to the turbine for self-sustained scavenging, the heat rejection from the engine cylinder had to be minimized. was provided in this hardware program by the application of "air gap" insulation technologies using all metallic components. Analytical studies were made to explore the use of ceramic insulators. Finite element thermal and structural modeling of these items indicated that with today's available ceramic materials, it would be a marginal system at best.

However, since material developments in monolithic ceramic components are advancing at a rapid rate, this approach may someday become an attractive alternative. A second generation

set of hardware using the insulating materials was designed as part of this program. Some hardware was procurred for evaluation, however, funding limitations precluded actual assembly and testing of these parts.

One area of technology that was not addressed in adequate detail is the question of tribology (or study of long term friction, wear, and lubrication) aspects of such an engine.

Some limited durability of the operating components has been demonstrated by this program, however, this aspect of the proposed engine concepts needs more detailed proof.

In conclusion, the engine concept explored in this contract (and its predecessors) is a viable alternative to today's reciprocating gasoline powered general aviation engine. The engine demonstrated in this program offers significant benefits in terms of SFC, weight, and the ability to operate on kerosine base fuels. These can be reflected directly in improved payload, speed, and range. The technology to achieve these goals is either currently available or can be made available with relatively near term developmental programs.

7.0 RECOMMENDATIONS

Based on the results of this analytical and experimental program, the technical feasibility of developing a lightweight aircraft diesel engine has been demonstrated. The enabling technologies have been defined. To bring this engine concept closer to its intended application, a follow-on program is recommended. Such a program should consist of the following elements:

1. Detailed design, procurement, and test cell evaluation of multicylinder configuration of the engine

2. Detailed design, procurement, and engine testing of a turbocharger for this engine application

3. Continued exploratory evaluations of the insulated version of the engine on a single cylinder test engine.

4. Tribology and long term durability testing on a single cylinder test engine

5. Integration of each of the above elements into a multicylinder engine for an engine demonstration.

6. Inital flight testing of the engine.

If the engine successfully demonstrates these elements, the economics of the market place, and the intangible user acceptability criteria would determine the ultimate application for such an engine.

8.0 REFERENCES

REFERENCES

1. ALEX P. BROUWERS, TELEDYNE CONTINENTAL MOTORS, 150 KW AND 300 KW LIGHTWEIGHT DIESEL AIRCRAFT ENGINE STUDY, NASA CR-3260, 1980.

2. LEON A. ZMROCZEK, BEECH AIRCRAFT CORPORATION, ADVANCED GENERAL AVIATION COMPARATIVE ENGINE/AIRFRAME INTEGRATION STUDY, NASA CR-165565, 1982.

3. GEORGE L. HUGGINS AND DAVID R. ELLIS, CESSNA AIRCRAFT COMPANY, ADVANCED GENERAL AVIATION COMPARATIVE ENGINE/AIRFRAME INTEGRATION STUDY, NASA CR-165564, 1981.

4. ALEX P. BROUWERS, TELEDYNE CONTINENTAL MOTORS, 186 NET KW ,LIGHTWEIGHT DIESEL AIRCRAFT ENGINE, NASA CR-326L, 1980.

5. R. L. MCDANIEL, T. M. DRZEWIECKI, J. MENI, SCIENCE AND TECHNOLOGY ASSOCIATES, INC., ADVANCED ENGINE TECHNOLOGY FOR ARMY AIRCRAFT, REPORT STA-007 UNDER CONTRACT NAS2-11748, 1984.

6. CHARLES F. TAYLOR, THE INTEGRAL COMBUSTION ENGINE IN THEORY AND PRACTICE, VOLUME I.

7. N. WATSON, M. MARZOUK, AND A. D. PILLEY, COMBUSTION CORRELATION FOR DIESEL ENGINE SIMULATION, SAE 800028, DIESEL COMBUSTION AND EMISSIONS SP86, 1980.

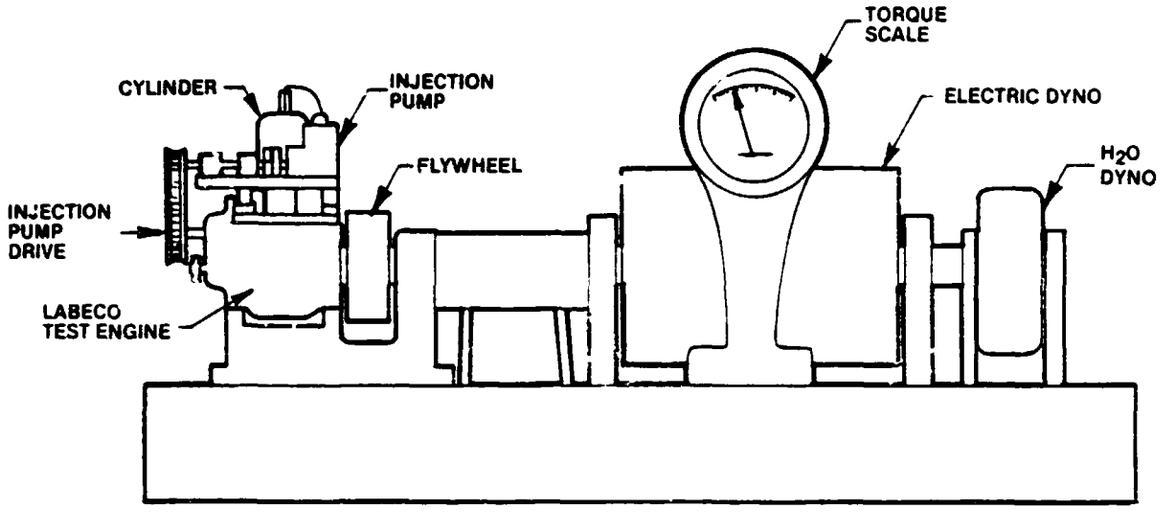

Figure 4.1-1. Engine Test Cell Layout

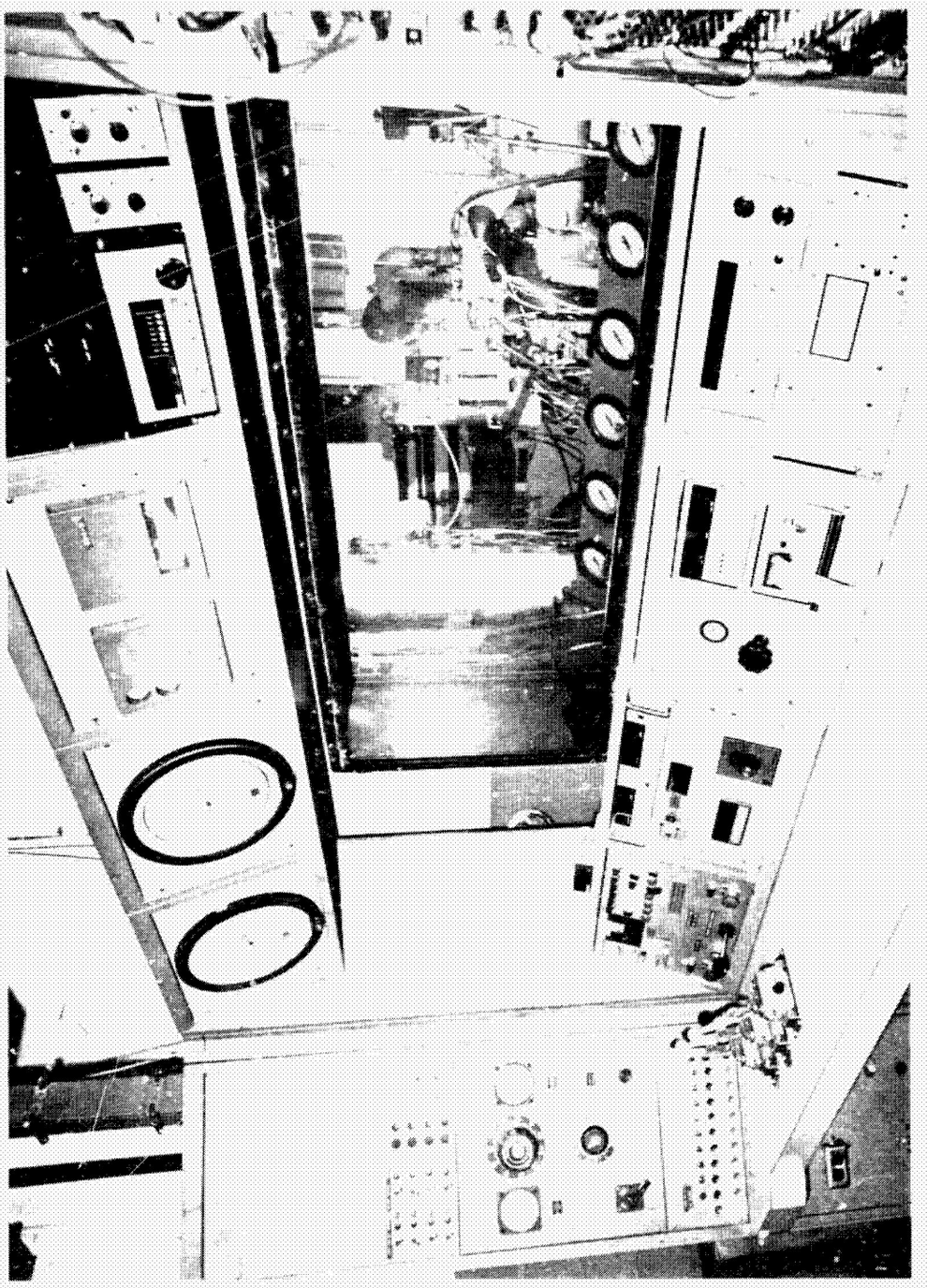

Figure 4.1-2. SCTE Test Cell Control Room

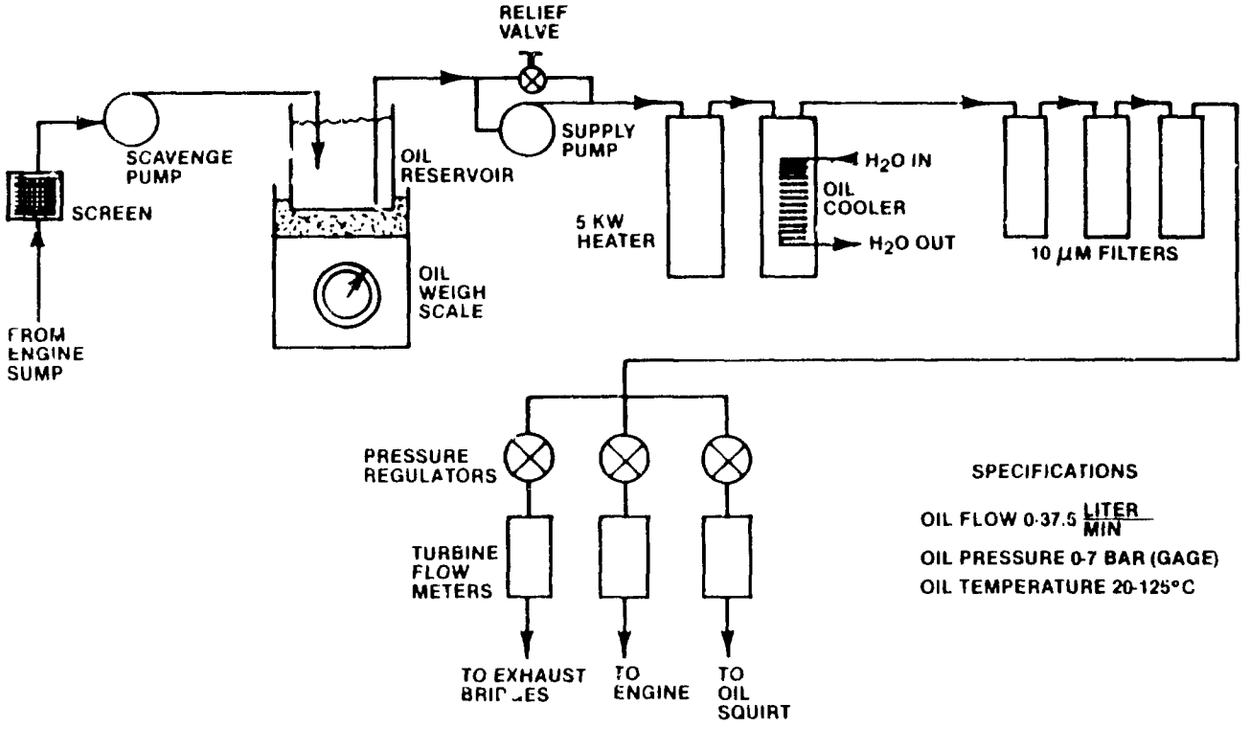

Figure 4 1-3. Test Cell Oil Supply System

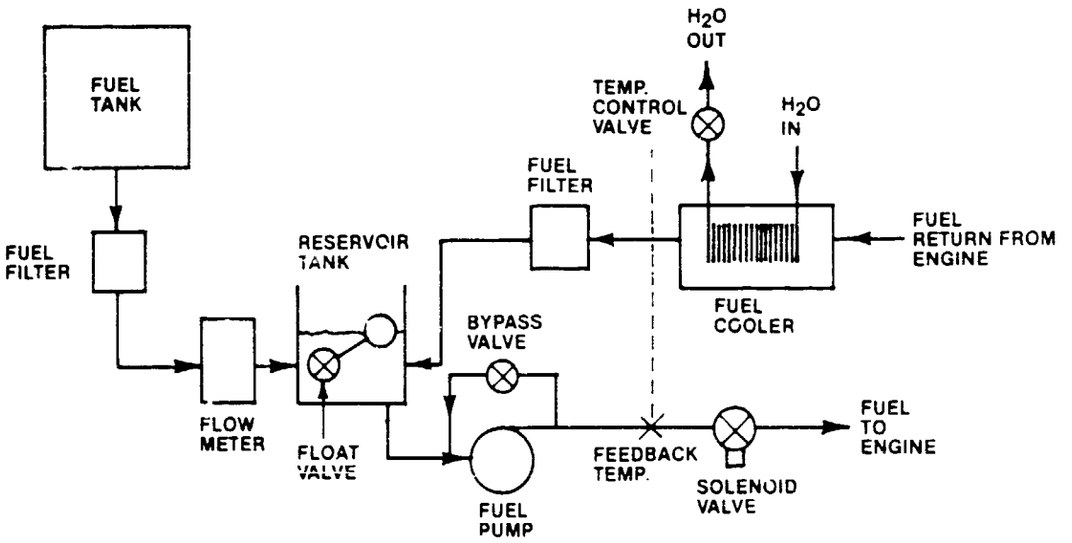

SPECIFICATIONS

FUEL FLOW 0-4000 LITER/HR.

FUEL PRESSURE 0-7 BAR

FUEL TEMP 20-40°C

Figure 4.1-4. Test Cell Fuel System

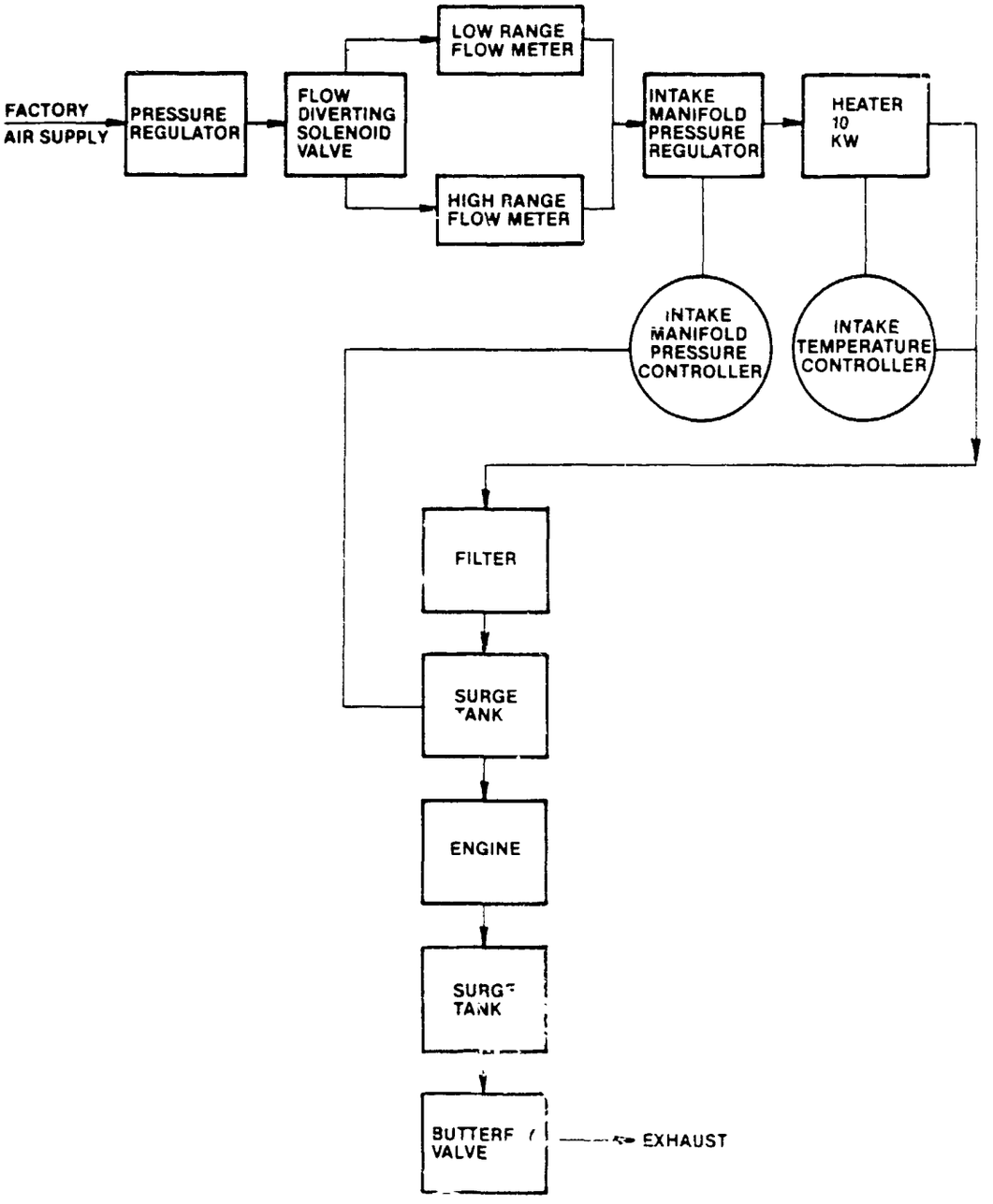

Figure 4.1-5. Test Cell Combustion Air Supply System

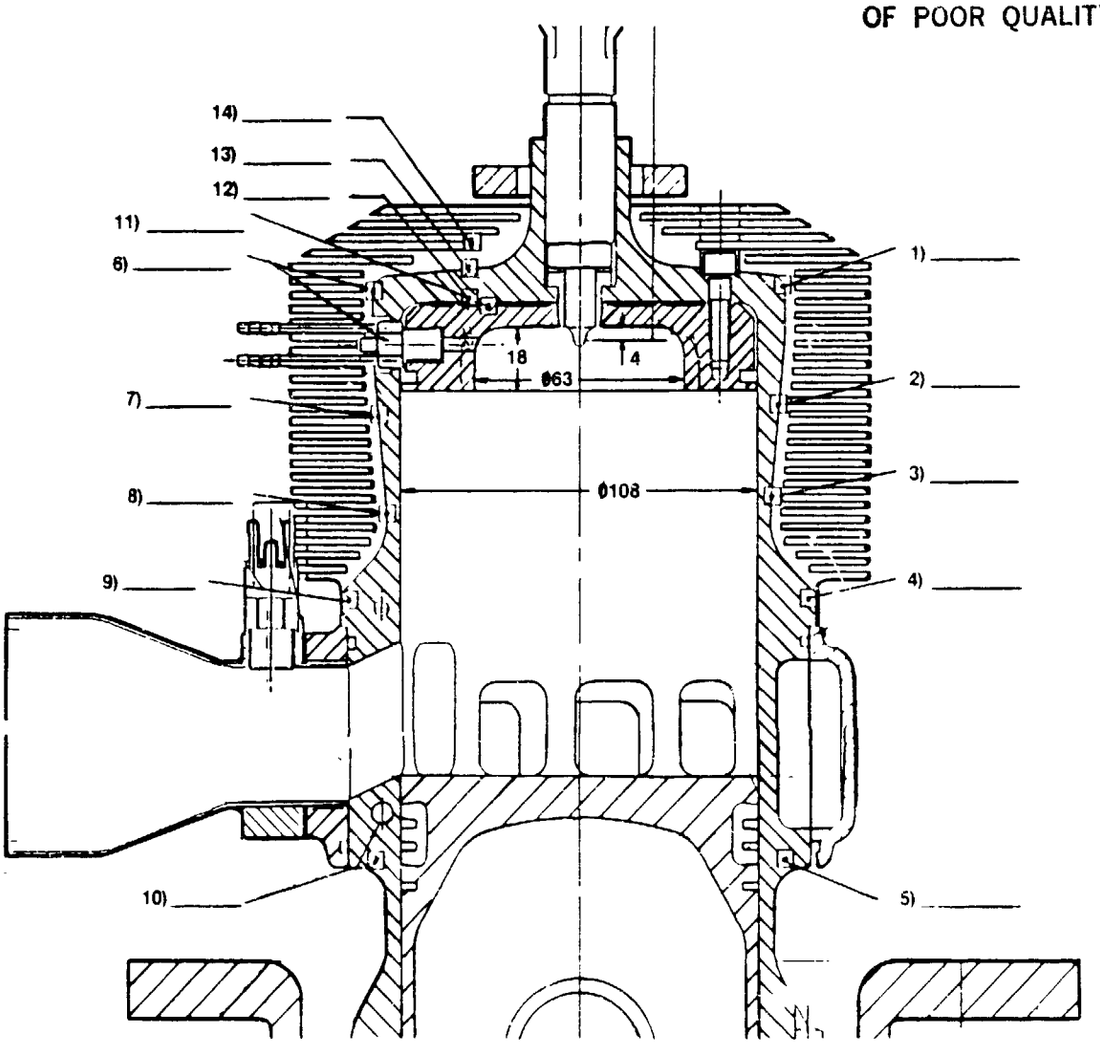

Figure 4.1-6. Cylinder Thermocouple Locations

Figure 4.1-7. Injector Assembly and Pressure Transducer Installation

Figure 4.1-8. Injection Nozzle Holder Assembly and Combustion Bowl Insert

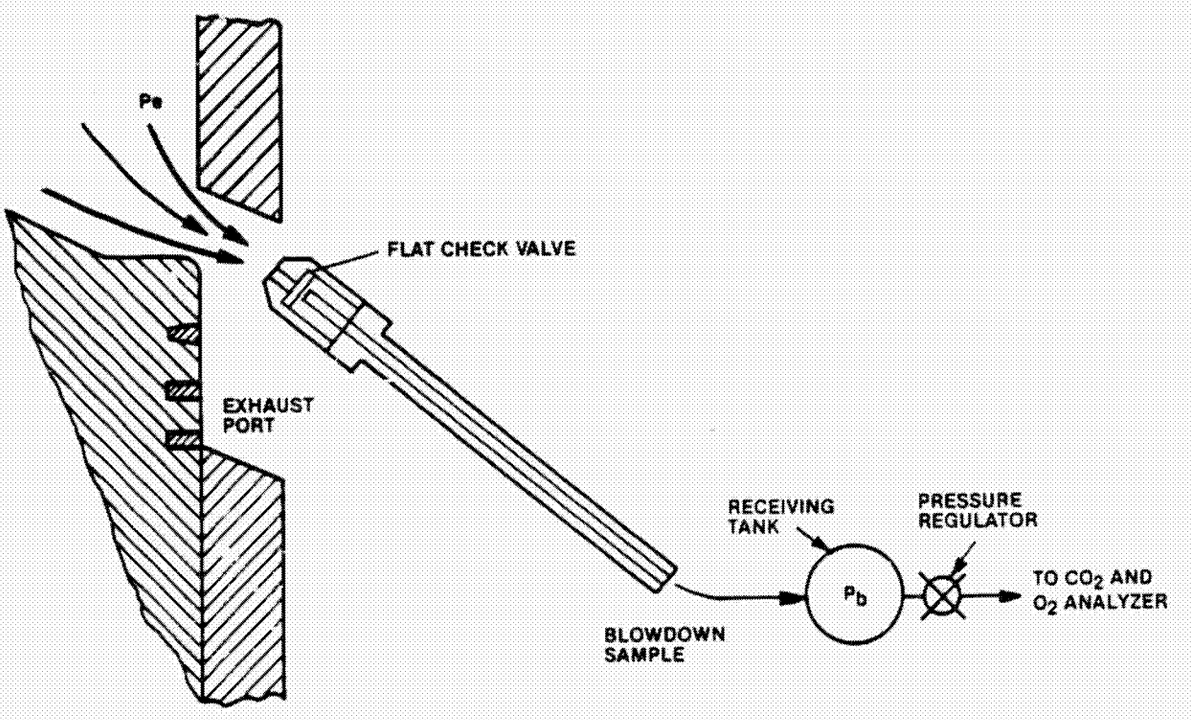

Figure 4.1-9. Impact Sampling Valve Installation

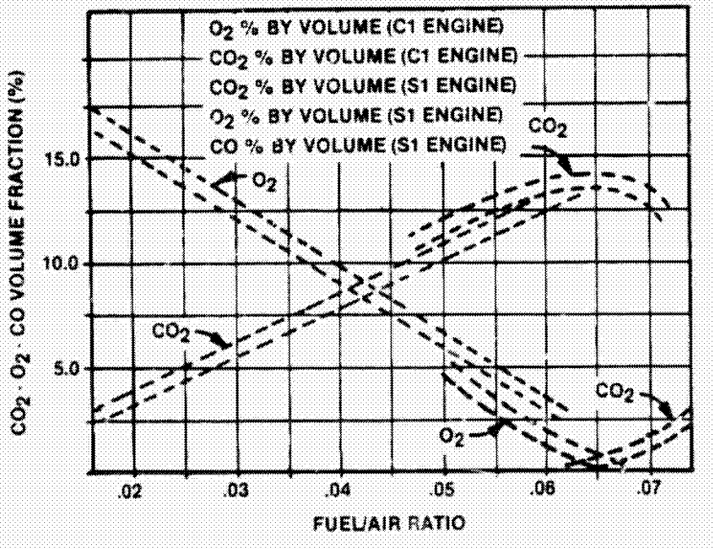

Figure 4.1-10. Composition of Exhaust Gases from Diesel and Spark Ignition Engines

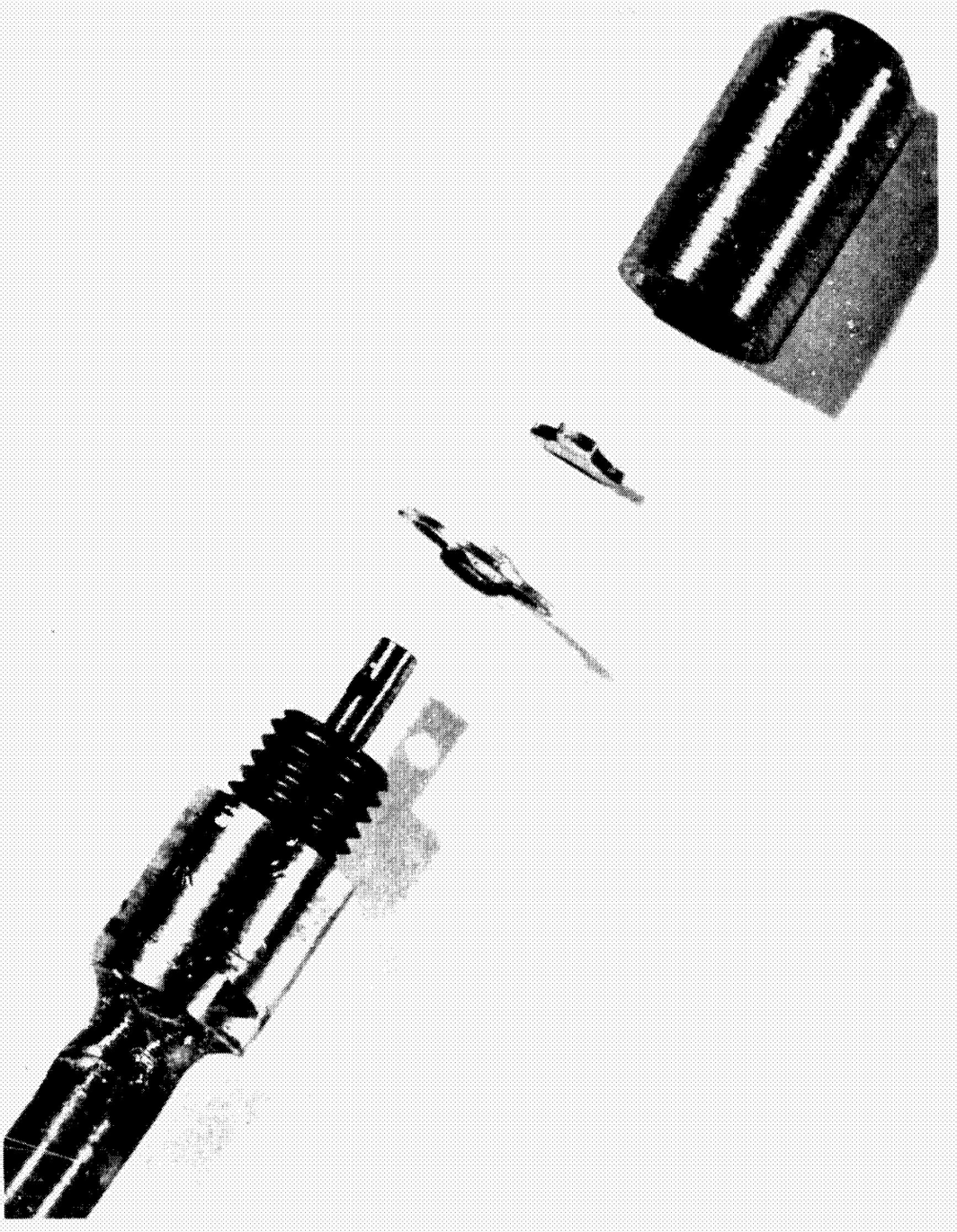

Figure 4.1-11. Check Valve in Exhaust Sampling Assembly

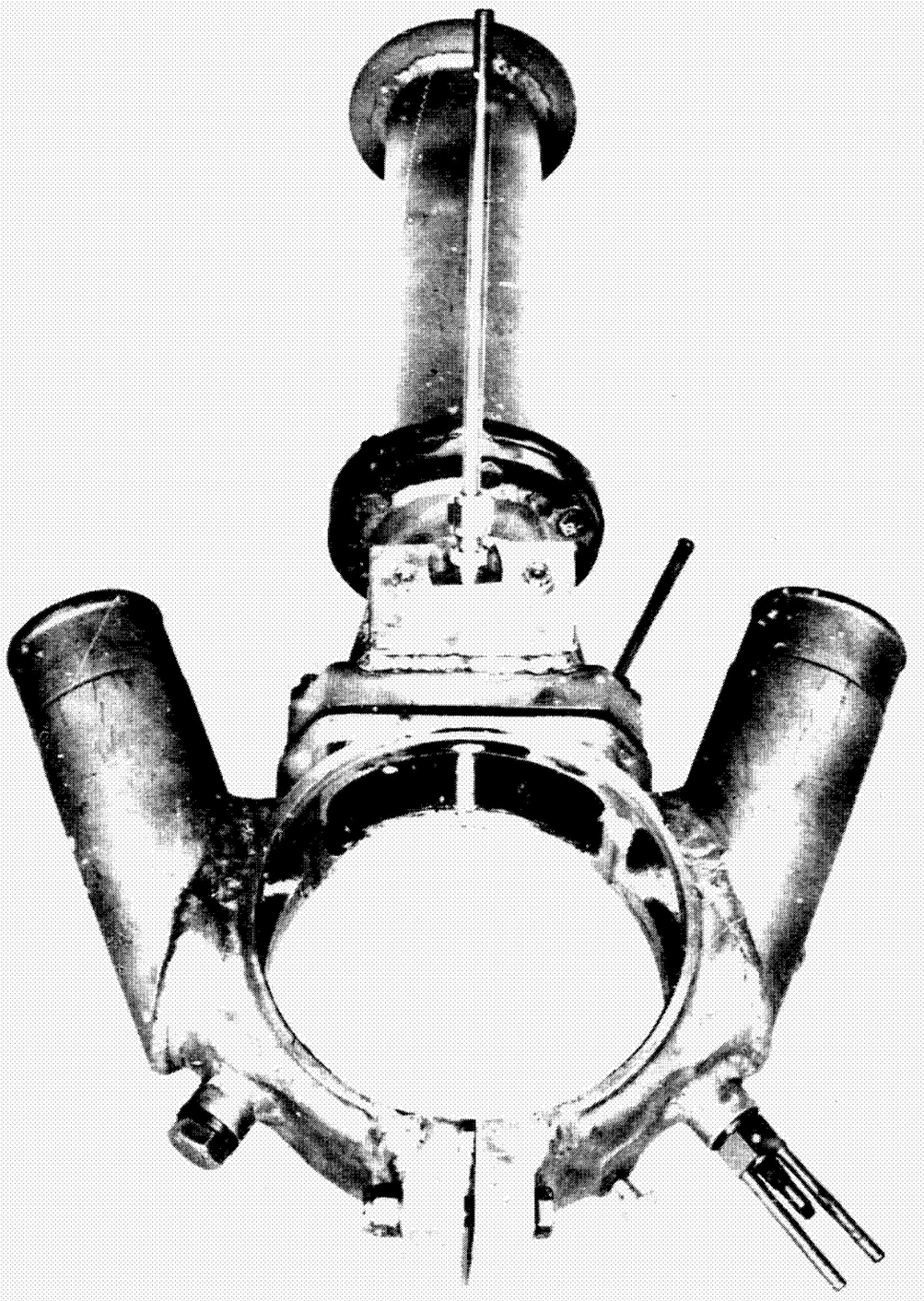

Figure 4.1-12. Exhaust Sampling Valve installed in Intake/Exhaust Muff

```
                    ECHO INPUT DATA
                    ===============

RUN NO.:668
DATE    :8/29/84
BUILD   :12-A

     PERFORMANCE                    TEMPERATURES
     ===========                    ============

RPM                    3501.   1)INT RT.          205.
BRK. TQ(SCALE)        59.80    2)INT LFT.         228.
BRK. TQ(H2O)           0.00    3)OIL IN           172.
FRIC TQ(SCALE)        27.20    4)OIL OUT          203.
FUEL FLOW              0.00    5)EXH. PLEN        942.
MI AIR DLTA P.        27.50    6)EXH. PORT        911.
FUEL TIME              56.5    7)FUEL METER        75.
FUEL VOLUME           200.0    8)FUEL FILTER       73.
JKM. OIL FLOW         294.0    9)HEAD             656.
SQUIRT OIL FLOW       798.0    10)AMBIENT          81.
PT OIL FLOW           422.0    11)SHOP AIR         75.
TRANS OIL FLOW         31.4    12)CYL OIL IN      169.
SMOKE                   4.0    13)CYL OIL OUT     197.
P.C.I.                 10.0    14)INT. PLENTOP    215.
PEAK CYL. PRESS.      1750.    15)INT. PLENBTM    215.
INJ. PRESS           12000.    16)COOL AIR IN     108.
INJ. BEGINS             18.    17)COOL AIR OUT    238.
INJ. DURATION           20.    18)TRANS OIL OUT   243.
                               19)EXH. PLEN      1006.

     EMISSIONS
     =========
CO2(TRAP)       0.0
O2(TRAP)        0.0
CO2(IP)         0.0
O2(IP)          0.0

                          PRESSURE GAGES
                          ==============
                       1)OIL              57.0
                       2)OIL SQUIRT       64.0
                       3)FUEL             80.0
                       4)H2O              48.0
                       5)INJ. OIL         24.0

      HEISE GAGES
      ===========
                          MANOMETERS
                          ==========
LA)SHOP AIR      185.0
LB)INT. PLEN      78.0   1)PAN PRESS.      1.900
LC)INT LFT.       78.0   2)CYL COOL AIR   18.300
LD)INT RT.        78.0   3)COOL AIR DELTA  6.900
RA)EXH. PORT      69.8
RB)EXH PLEN       70.0
```

Figure 4.1-13. Sample Input Data for Data Reduction Program

S.C.T.E. DATA OUTPUT

RUN : 668
BUILD: 12-A
DATE: 8/29/84

ENGINE DATA

RPM	3501.00
BRAKE TORQUE (FT-LB)	78.52
FRICT. TORQUE (FT-LB)	35.71
INTAKE PRESS.(IN-HG)	78.00
INT. TEMP.(DEG F)	215.00
EXHAUST PRESS.(IN HG)	70.00
EXHAUST TEMP.(DEG F)	1006.00
OIL INLET TEMP.(DEG F)	172.00
FUEL TEMP.(DEG F)	73.00
CASE PRESS.(IN H2O)	1.90
AIR FLOW(LB/HR)	974.48
FUEL FLOW(LB/HR)	23.62
COOLING AIR(LB/HR)	1416.06
OIL SQUIRT FLOW(LB/HR)	774.71
OIL JOURNAL FLOW(LB/HR)	1374.82
PORT OIL FLOW(LB/HR)	382.31
X-DUCER OIL FLOW(LB/HR)	31.35

PERFORMANCE DATA

IHP	76.15
IMEP(PSI)	140.06
BHP	52.34
BMEP(PSI)	96.27
FHP	23.81
MECH EFF.(%)	68.74
OVERALL A/F(CALC)	41.25
OVERALL A/F(O2)	14.60
OVERALL A/F(CO2)	2424.44
PI/PE	1.11
DELTA P(IN HG)	8.00
DELTA P/PI	0.103
ISFC(LB/IHP-HR)	0.310
BSFC(LB/BHP-HR)	0.451
SMOKE(BOSCH)	4.00

TRAPPED AIR DATA

TRAPPED A/F RATIO(O2)	14.6
TRAPPED A/F RATIO(CO2)	*****
TRAPPED A/F RATIO(AVG)	*****
TRAPPED AIR MASS(AVG LB)	0.13713
SCAVENGE RATIO (AVL)	0.850
SCAVENGE RATIO (TAYLOR)	0.896
SCAVENGE EFF. (AVL)	*****
SCAVENGE EFF. (TAYLOR)	*****
TRAPPING EFF.	*****

INJECTION PUMP DATA

INJECTION PRESS.(PSI)	12000.0
INJECTION DUR.(DEG CA)	20.0
INJECT. REGIMES(BTDC)	18.0
FUEL/CYCLE(MM3)	60.4

COMBUSTION DATA

POINT OF IGNITION (BTDC)	10.0
PEAK CYL. PRESS.(PSI)	1750.0
IGNITION DELAY (DEG CA)	8.0

HEAT BALANCE DATA(% OF FUEL ENERGY)

OIL	TRANS	EX. PORTS	COOL AIR	EXHAUST	B.H.P.	UNACCOUNTED	TOTAL
7.98	0.27	1.26	10.28	47.80	30.48	1.93	100.

TURBOCHARGER REQ'D EFFICIENCY SEALEVEL 52.4 25000 FEET 53.5
97% MECH. EFF.

Figure 4.1-14. Sample Output Data from Data Reduction Program

Figure 4.2-1. Power Components for Aircraft Engine (SCTE)

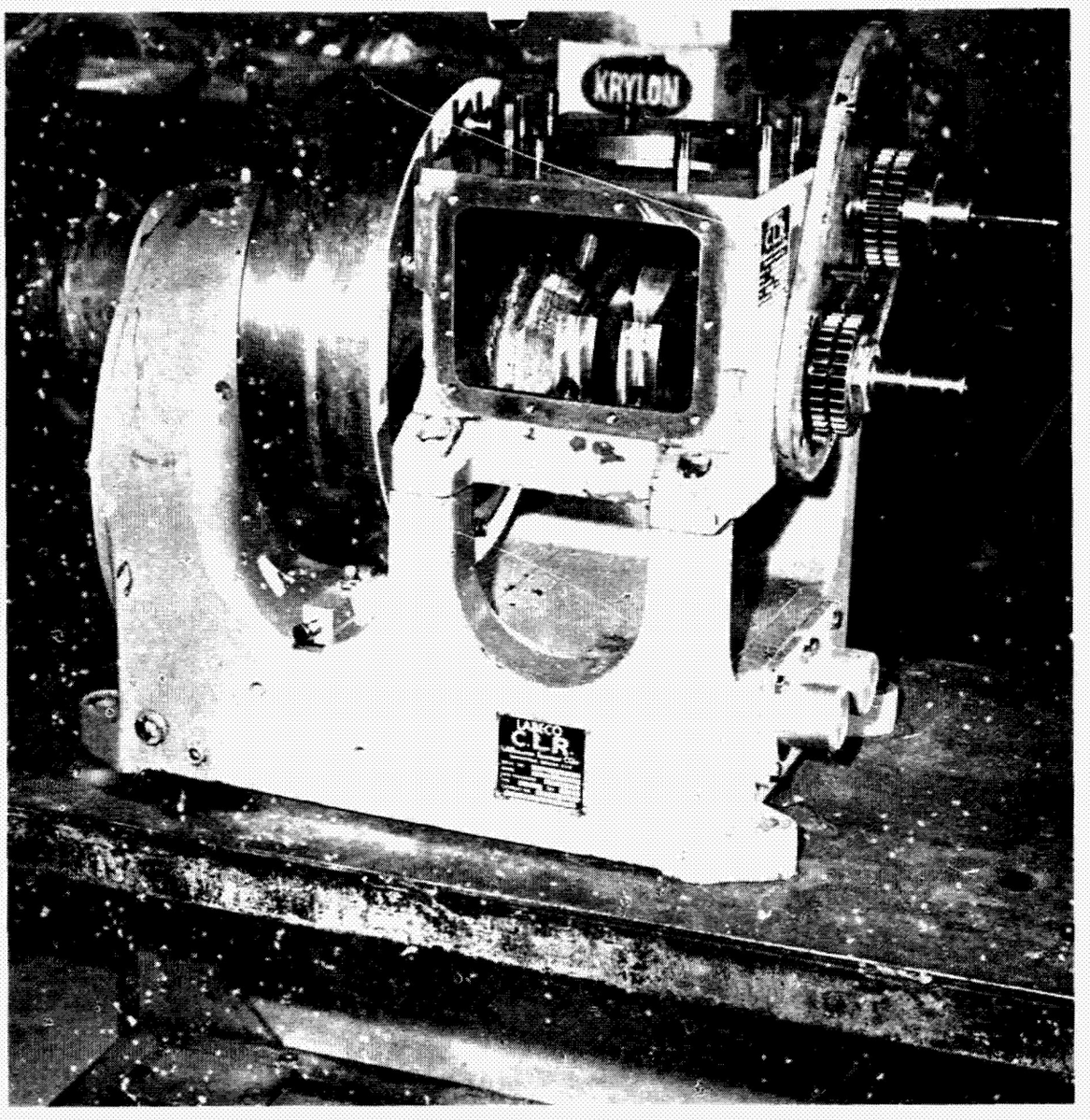

Figure 4.2-2. LABECO Engine Test Base for Aircraft Engine (SCTE)

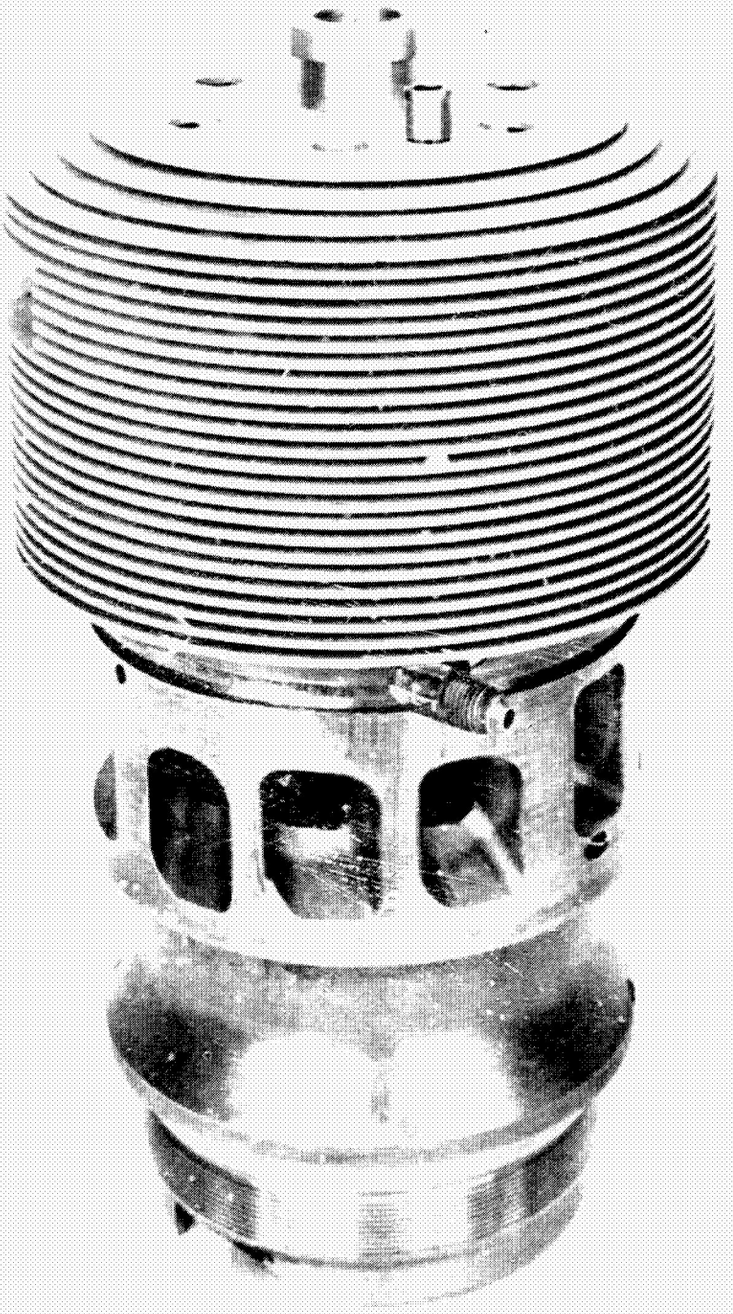

Figure 4.2-3. Cylinder Assembly for Aircraft Engine (SCTE)

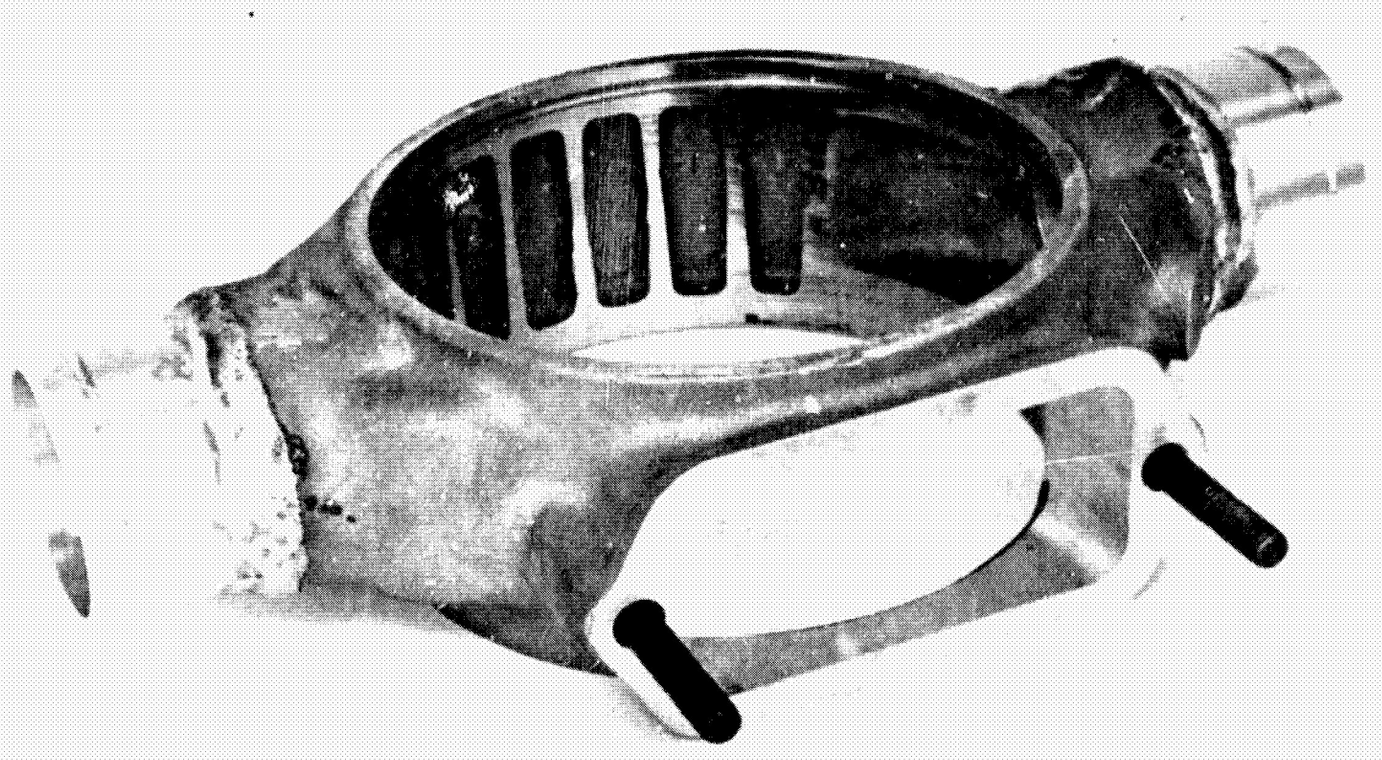

Figure 4.2-4. Initial Intake Manifold Muff Configuration for Aircraft Engine (SCTE)

Figure 4.2-5. Assembled First Generation Single Cylinder Test Engine (SCTE)

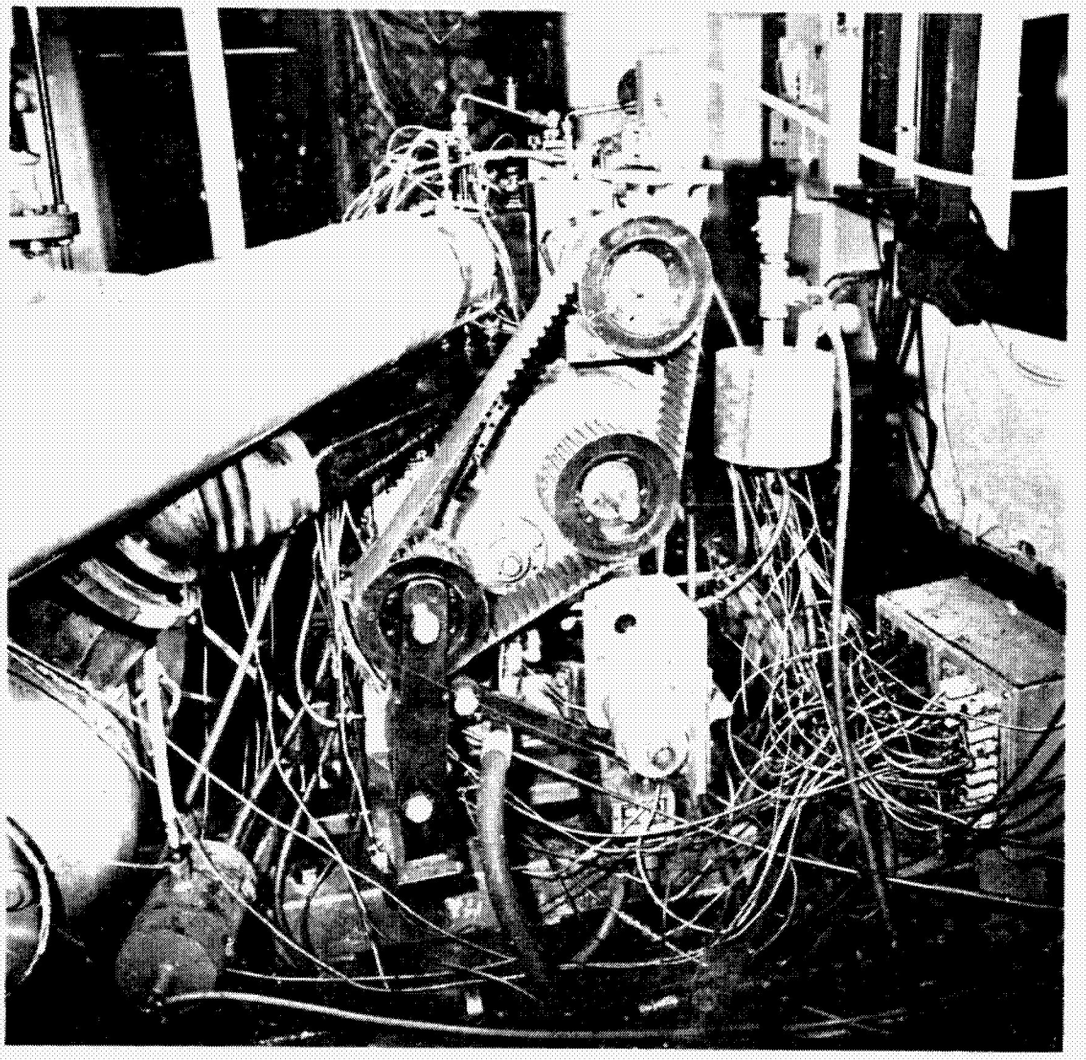

Figure 4.2-6. Engine Configuration with CAE-Y Pump

Figure 4.2-7. Intake Manifold Modification for Configuration 4

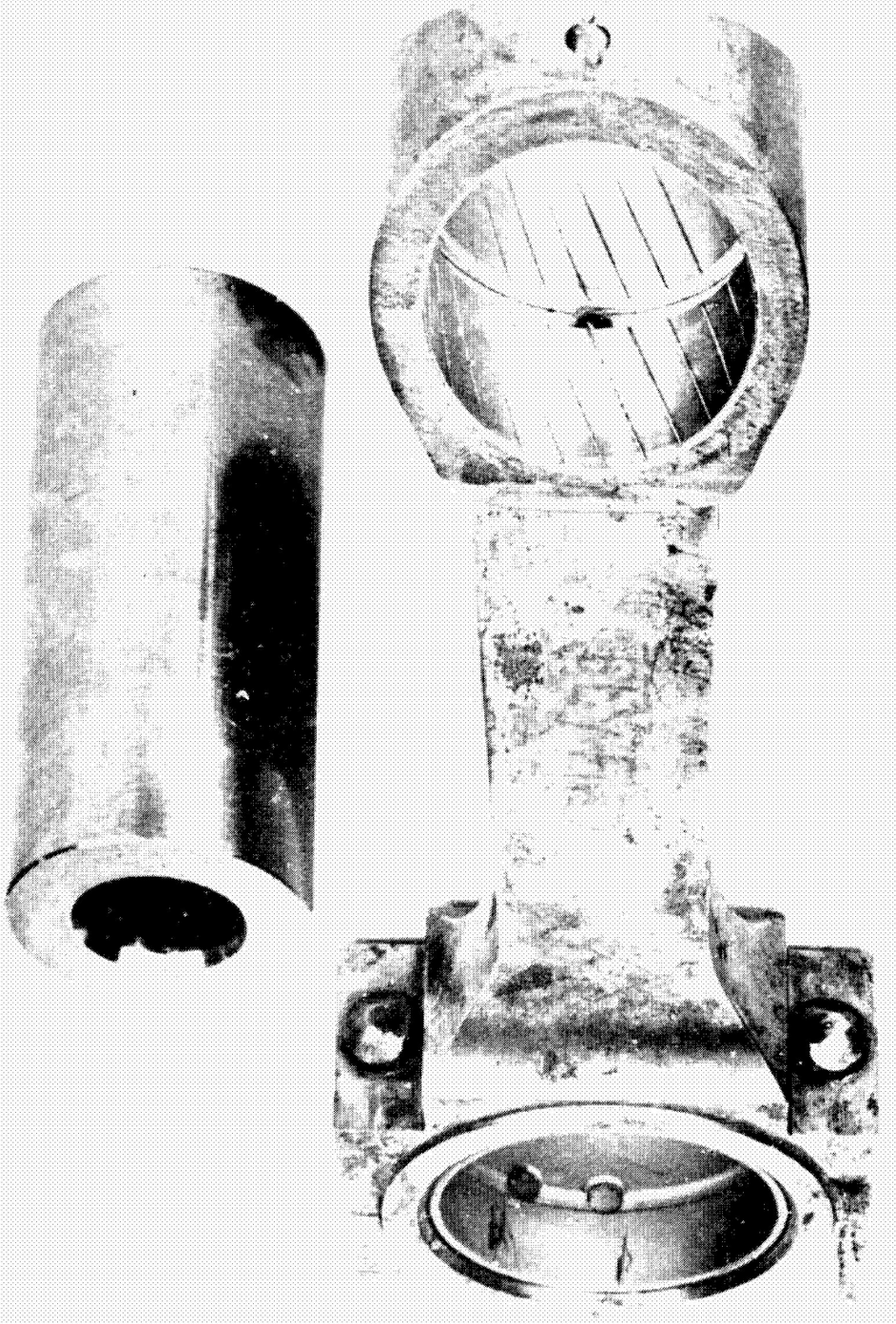

Figure 4.2-8. Connecting Rod for Configuration 4

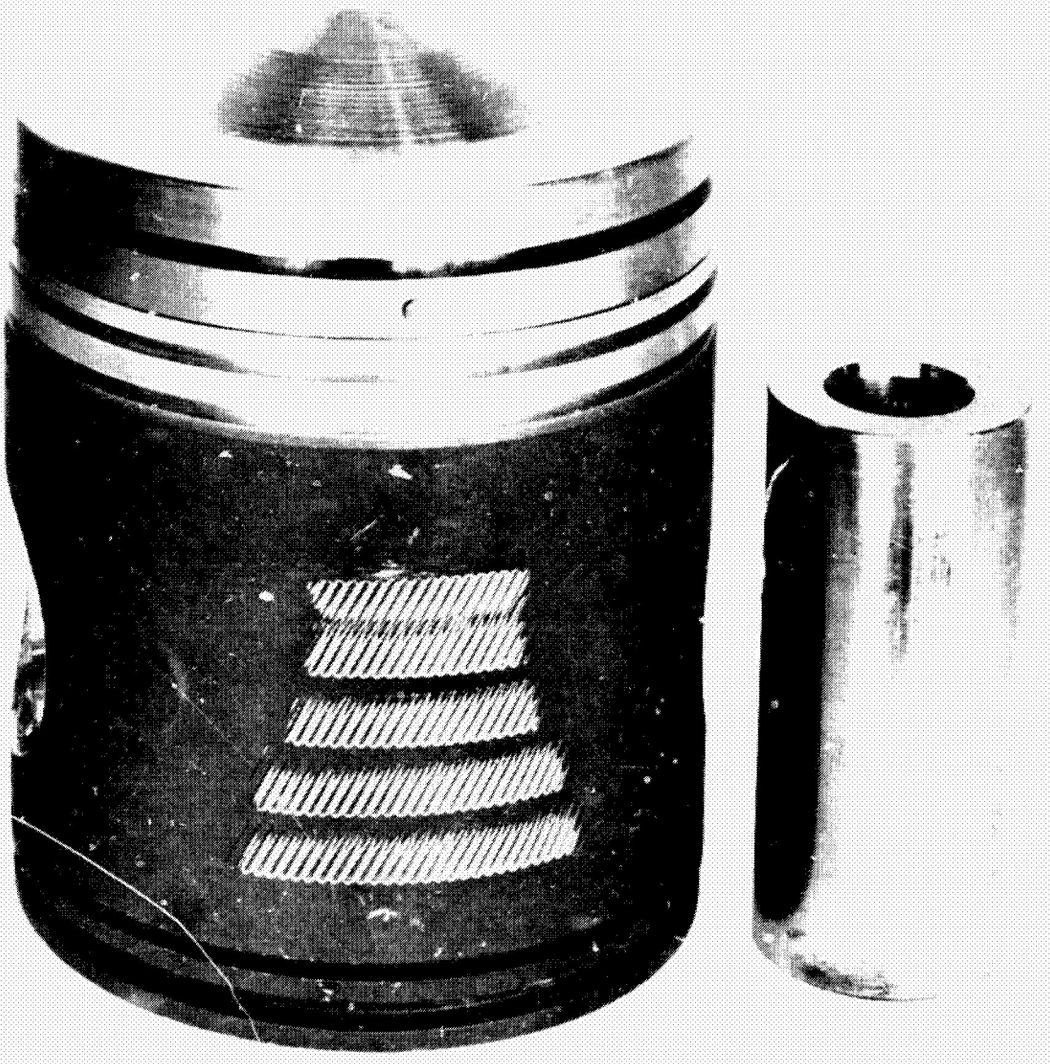

Figure 4.2-9. Piston Skirt with Knurling for Lubricant Retention

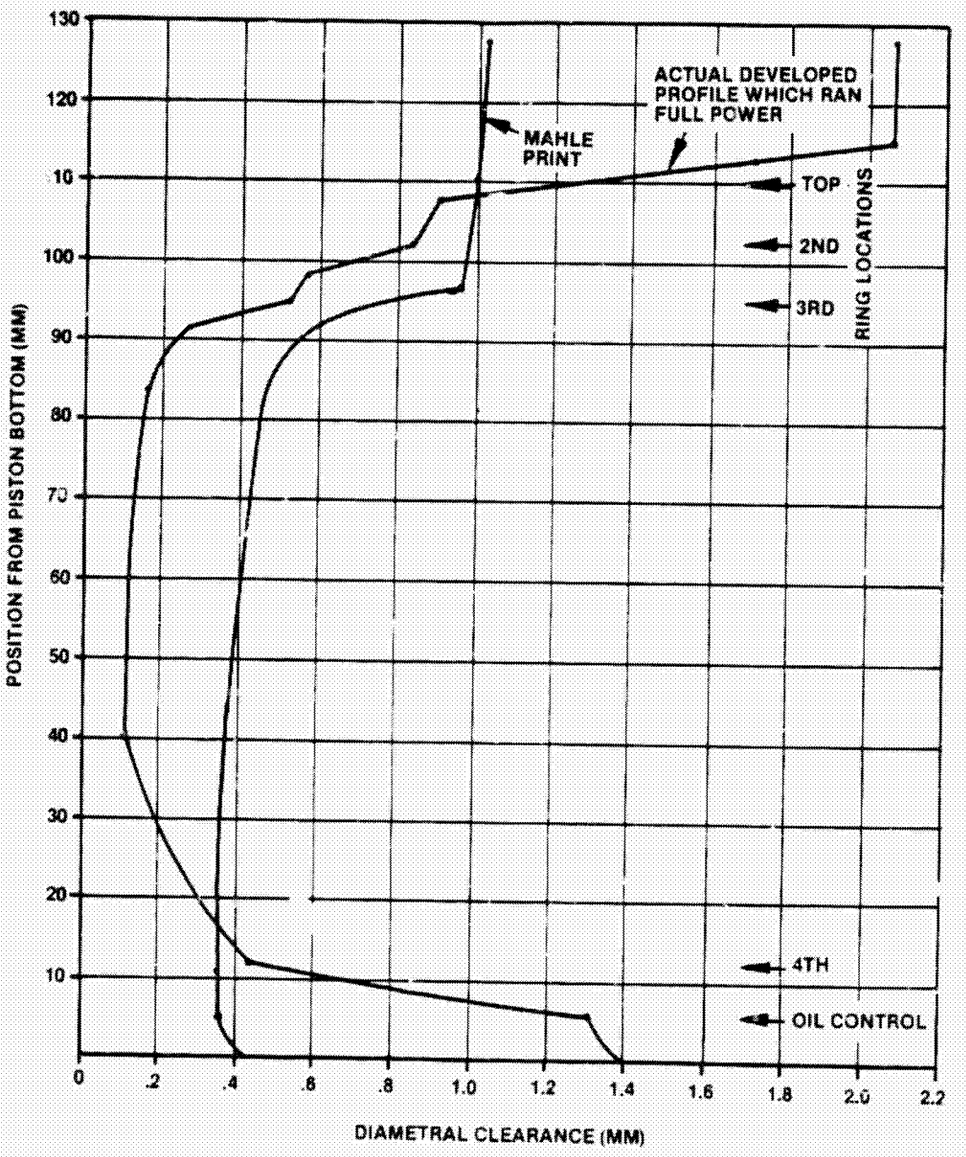

Figure 4.2-10. Piston Profile Developed for Aluminum Piston

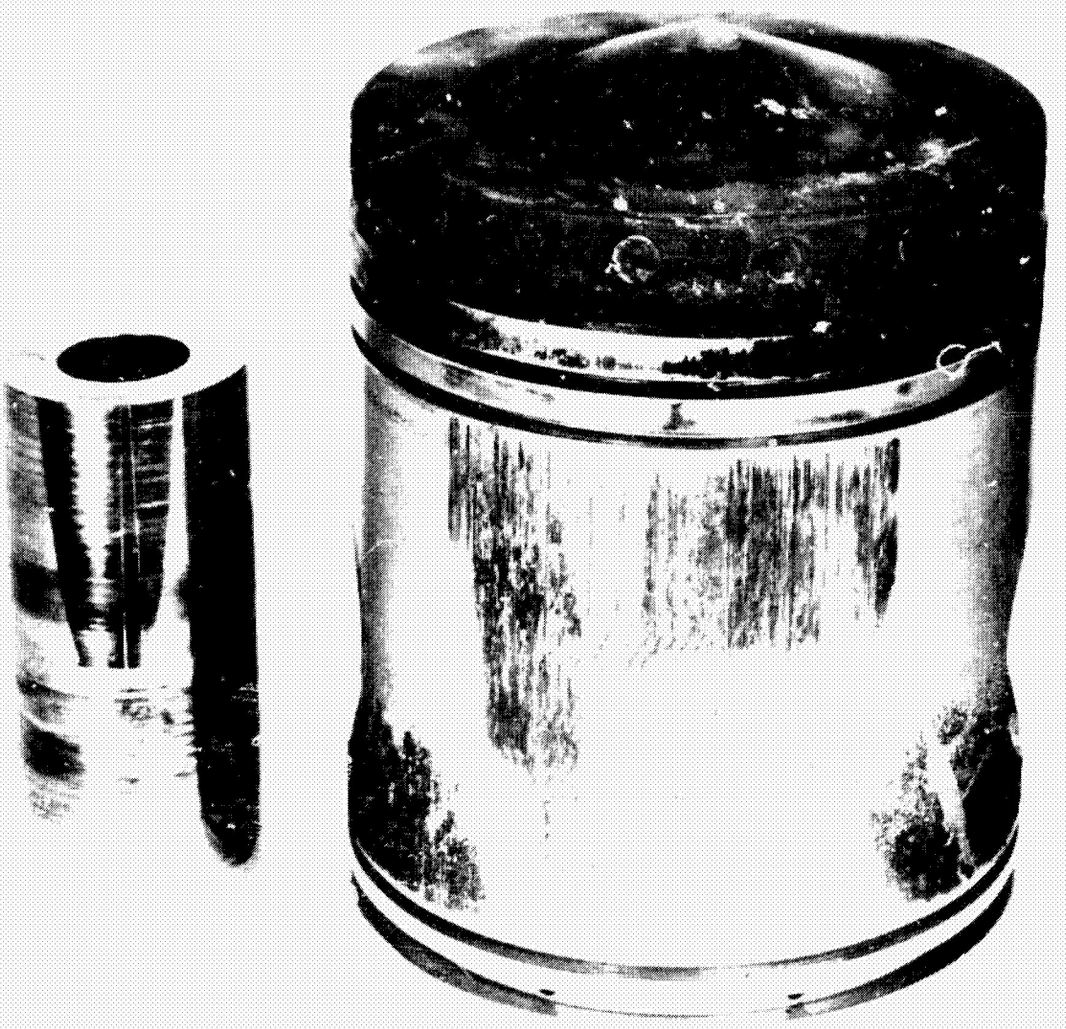

Figu 4.2-11. Scuffed Piston Removed from Configuration 4

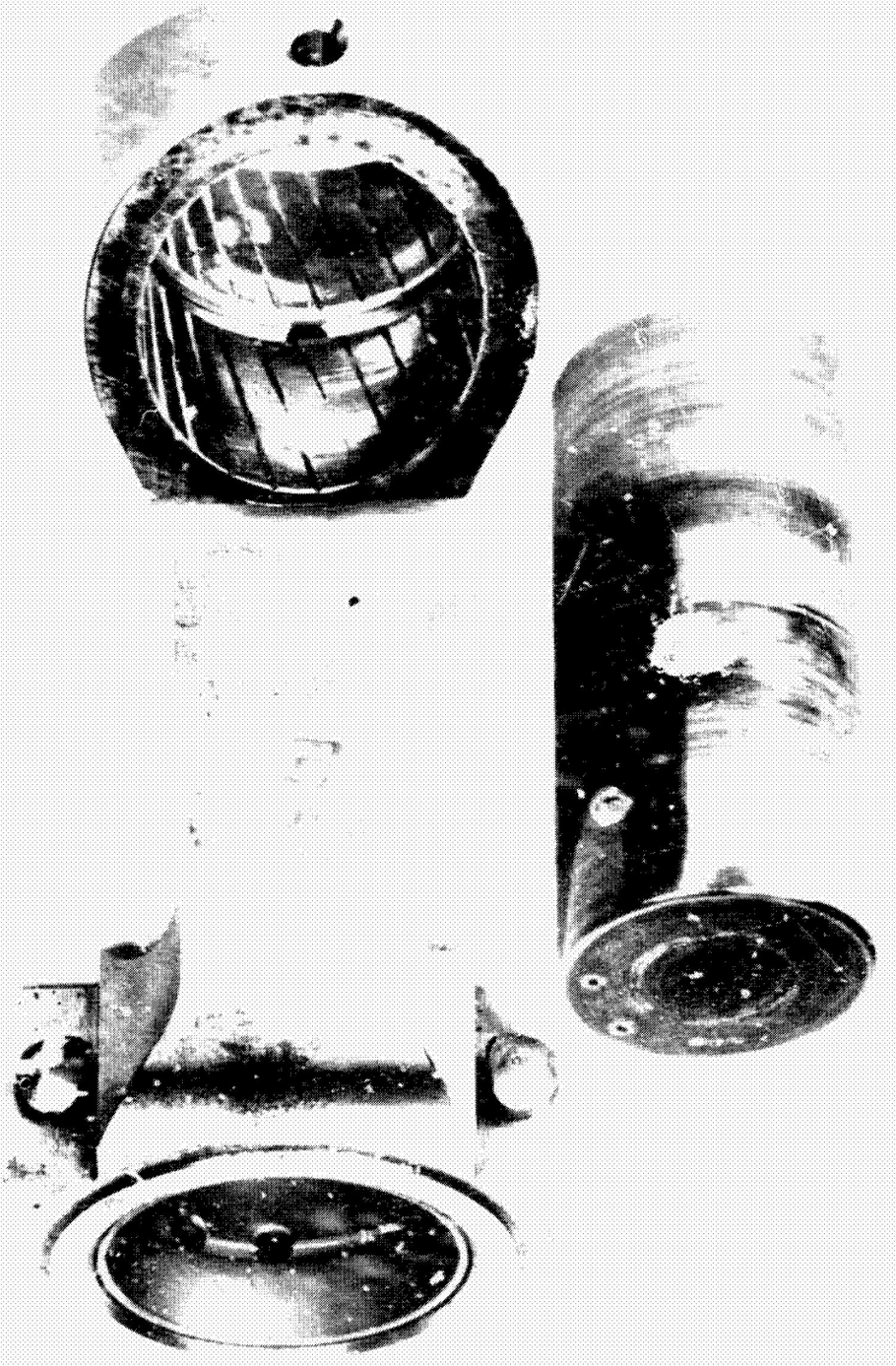

Figure 4.2-12. Connecting Rod Removed from Configuration 4

Figure 4.2-13. Steel Capped Aluminum Piston Assembly

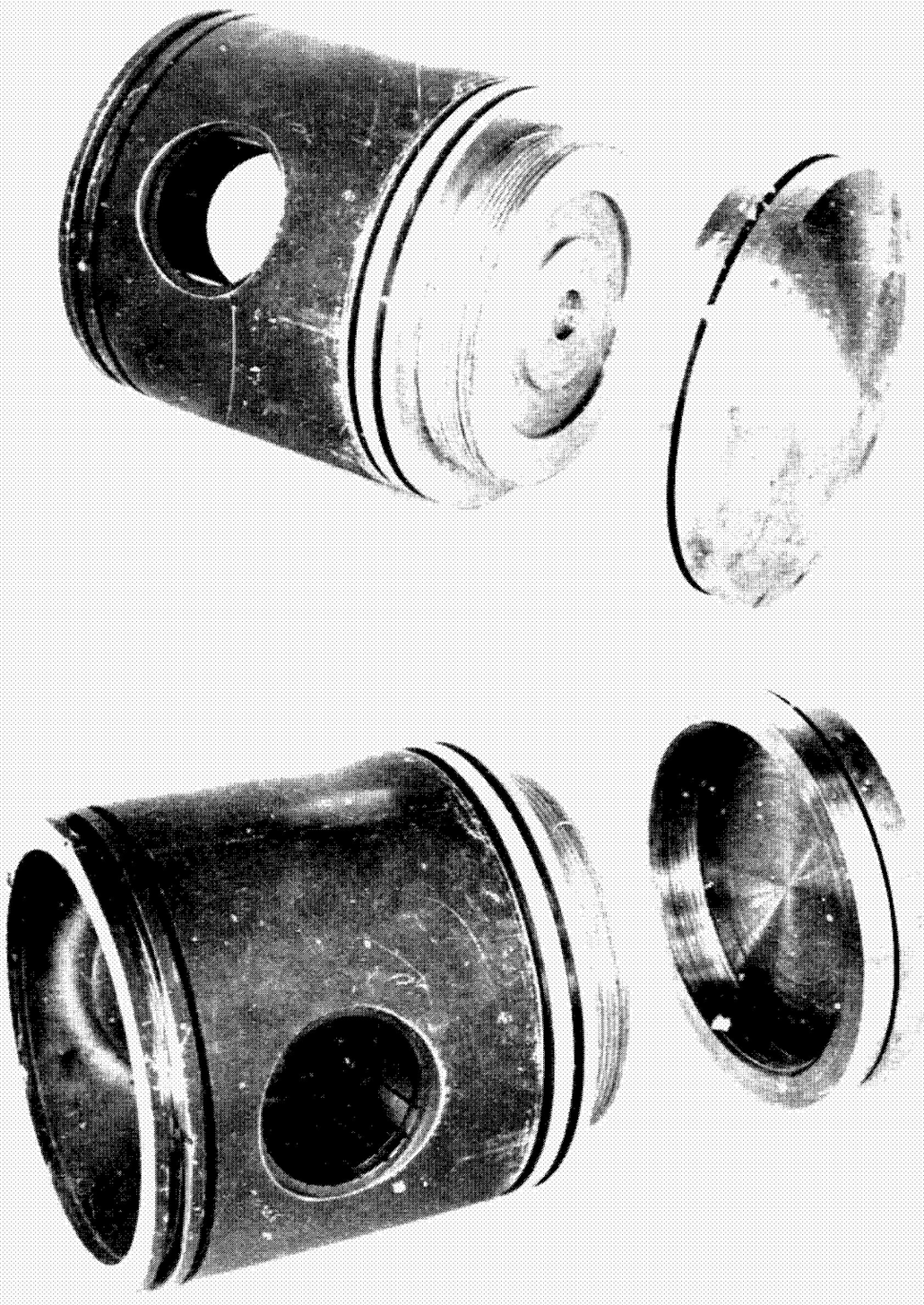

Figure 4.2-14. Aluminum Piston and Screwed on Steel Cap

Figure 4.2-15. Combustion Chamber and Injection Nozzle Components

Figure 4.2-16. Assembled Combustion Chamber and Injection Nozzle

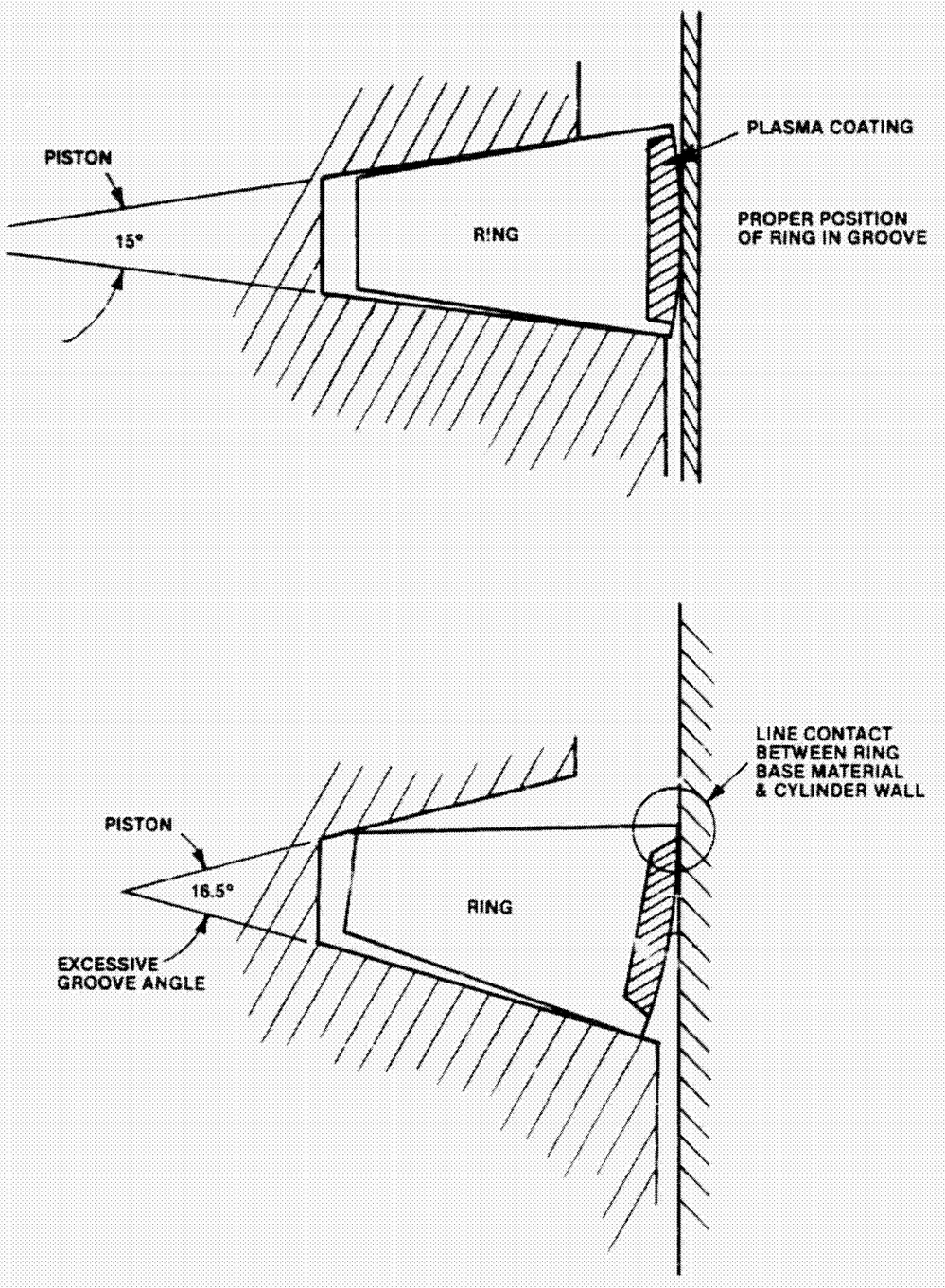

Figure 4.2-17. Effect of Improper Groove Angle on Ring Position

Figure 4.2-18. Ductile Iron Pistons for Configurations 6, 7, and 8

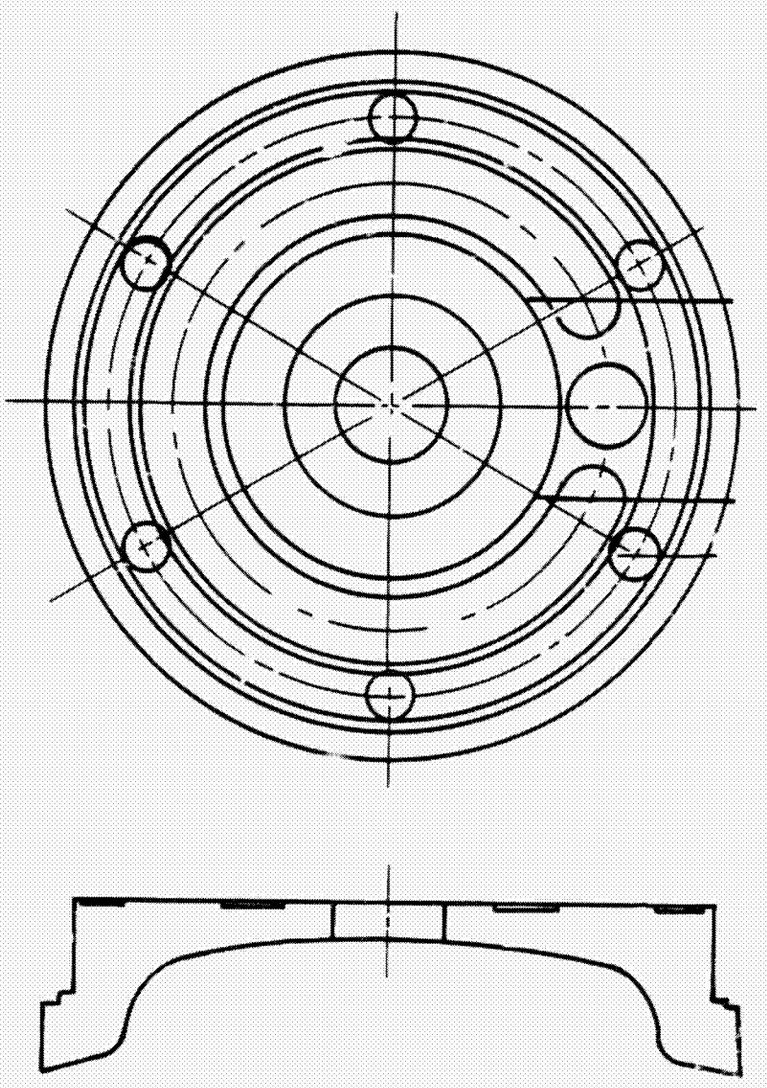

Figure 4.2-19. Combustion Chamber for Use with Domed Piston — Configurations 7, 8, and 9

Figure 4.2-20. "BOKOR" Finish of Piston Skirt for Oil Retention

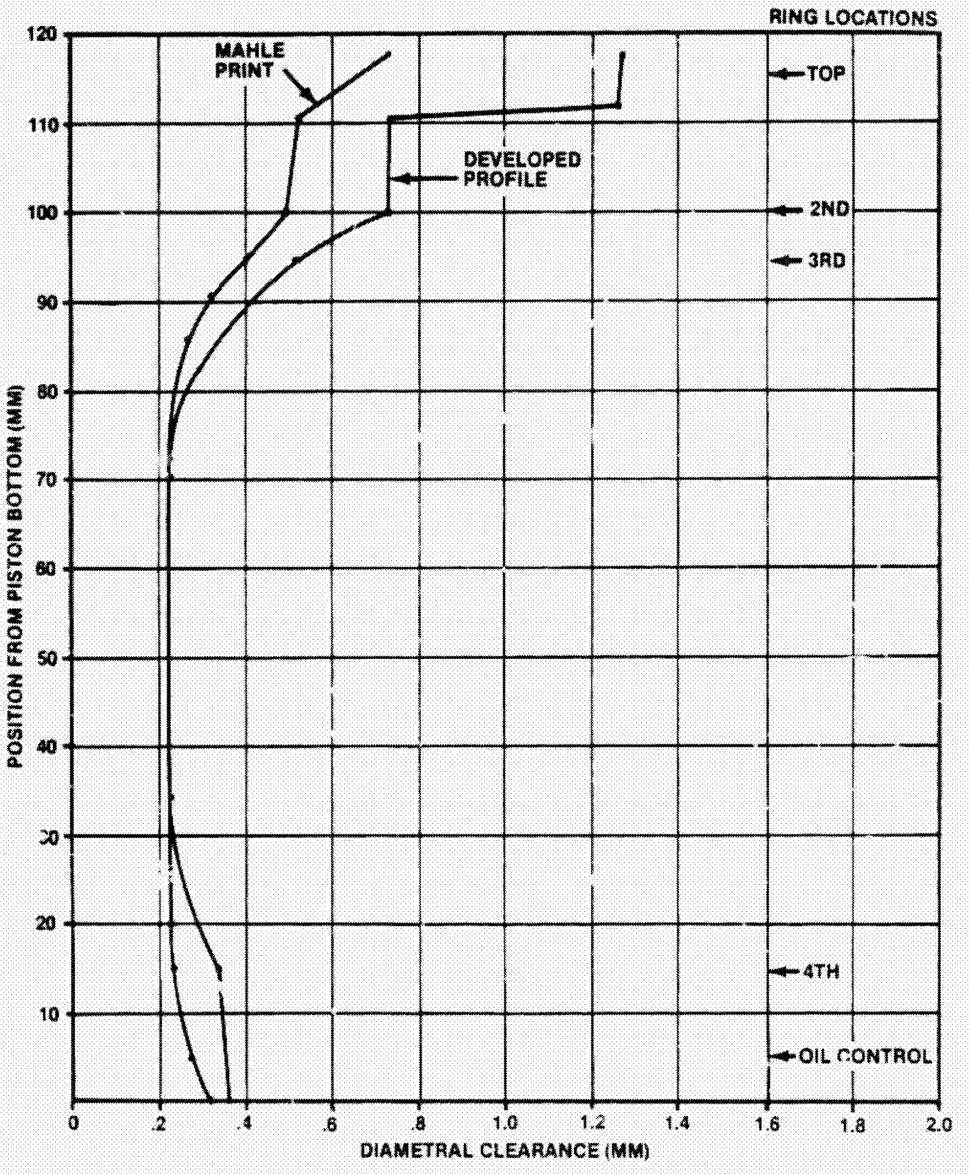

Figure 4.2-21. Piston Profile Developed for Cast Iron Piston

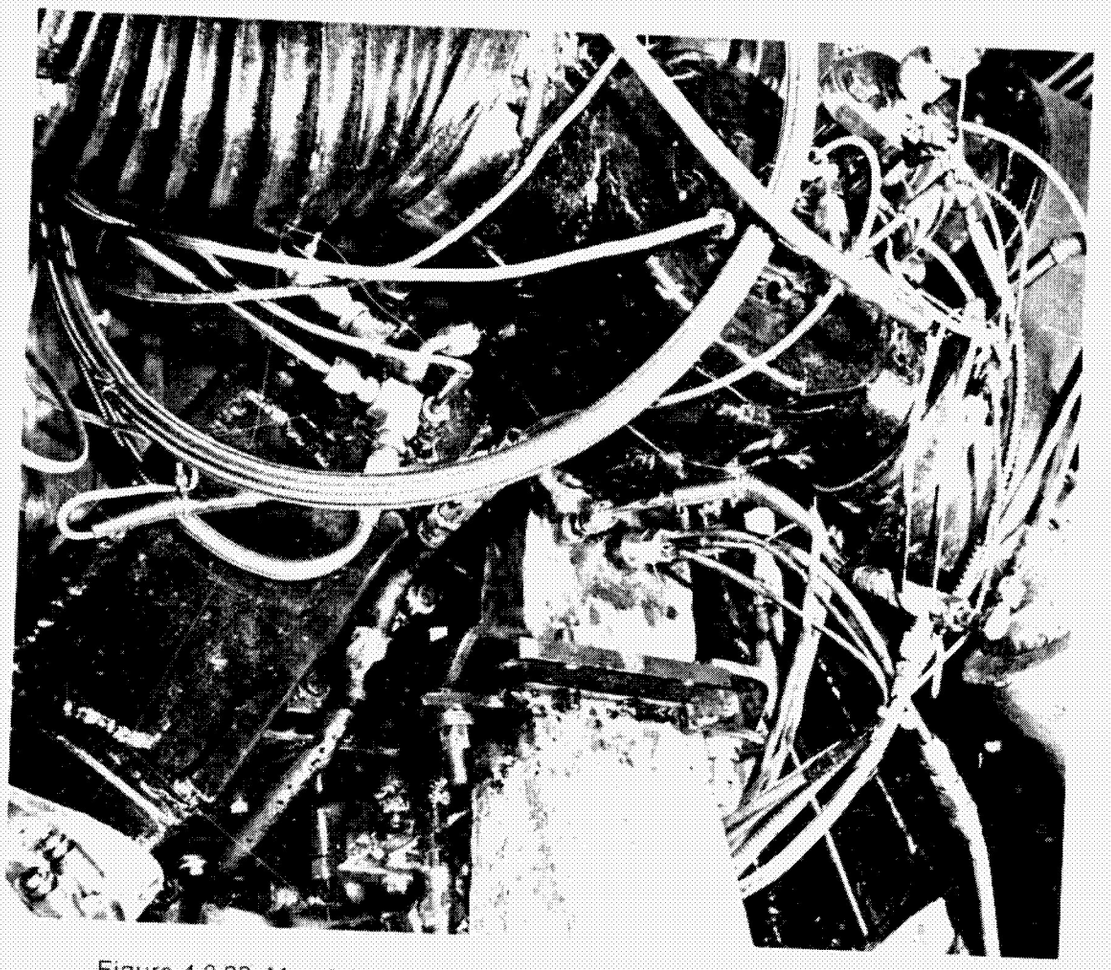

Figure 4.2-22 Manifold Configuration for Configurations 10 through 12

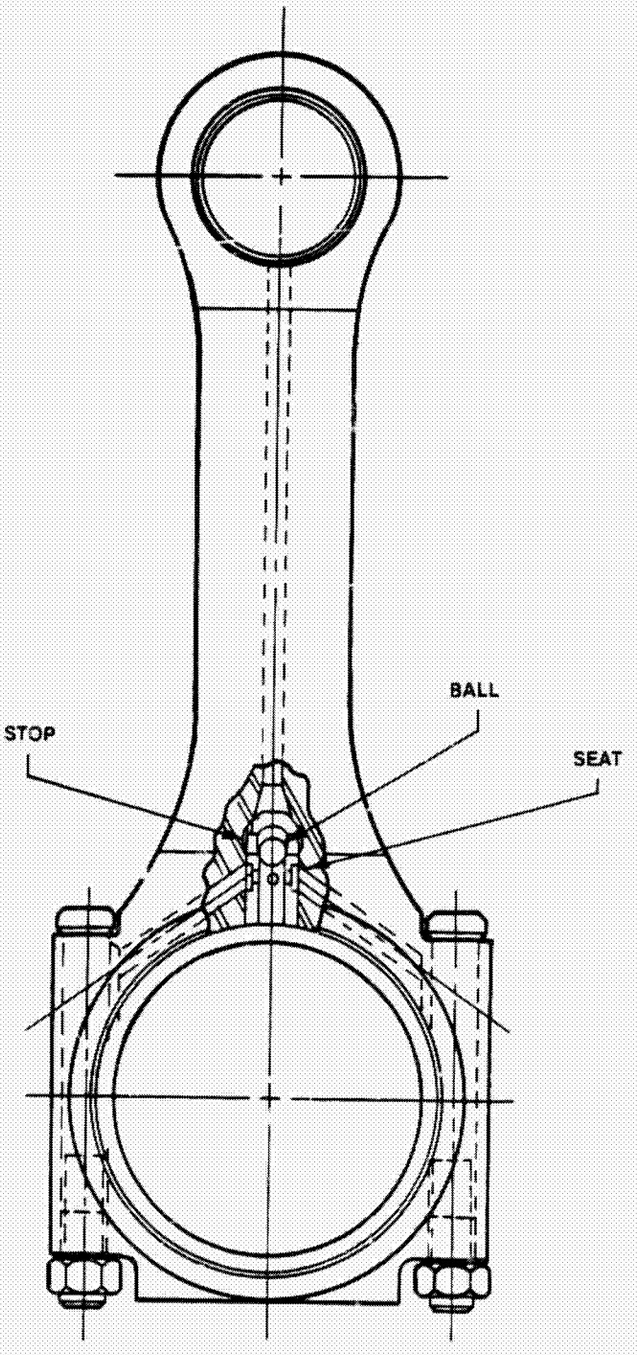

Figure 4.2-23. New Connecting Rod with "V" Drilled Oil Supply

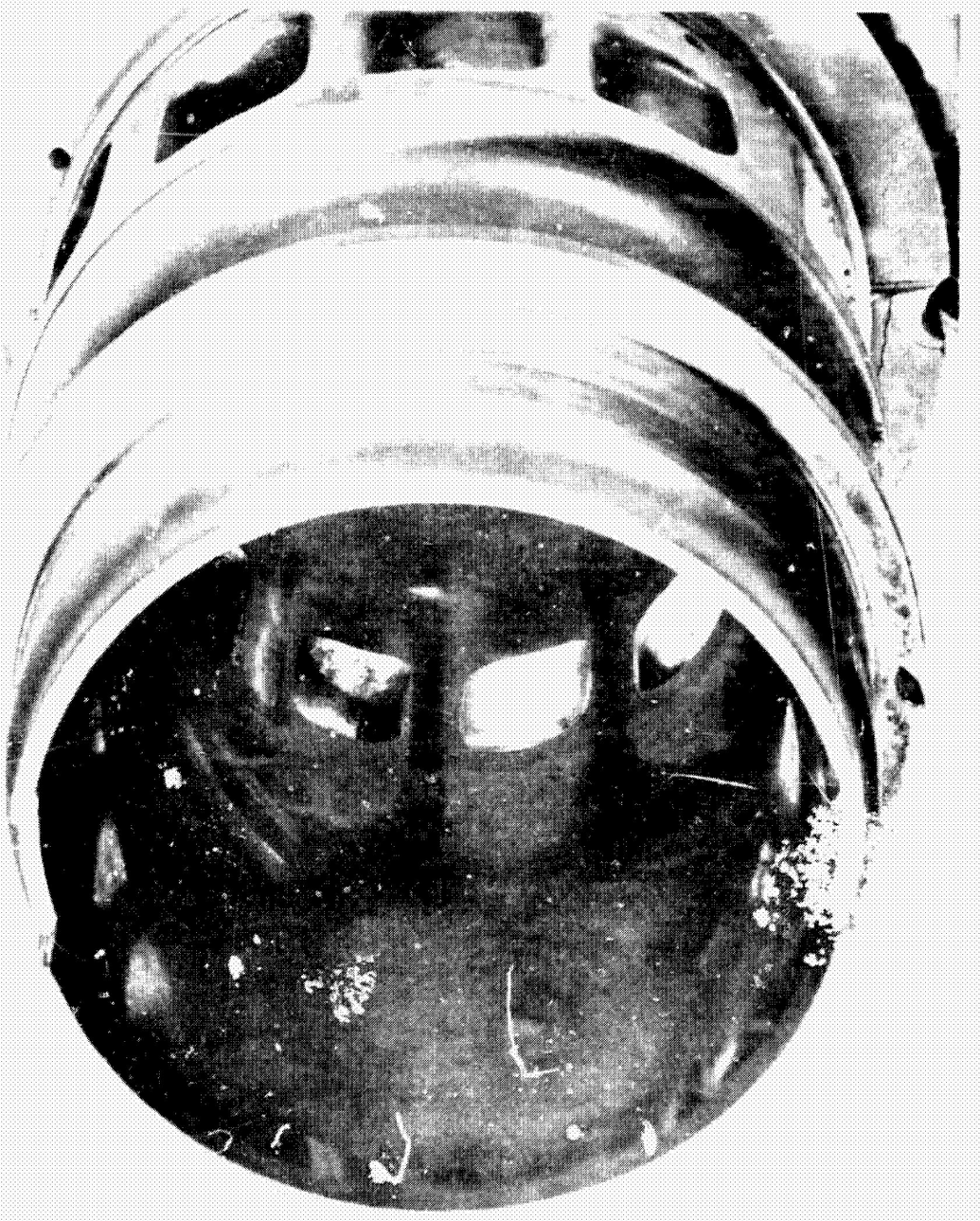

Figure 4.2-24. Interior View of Cylinder after 60 Hours of Running Configuration 10

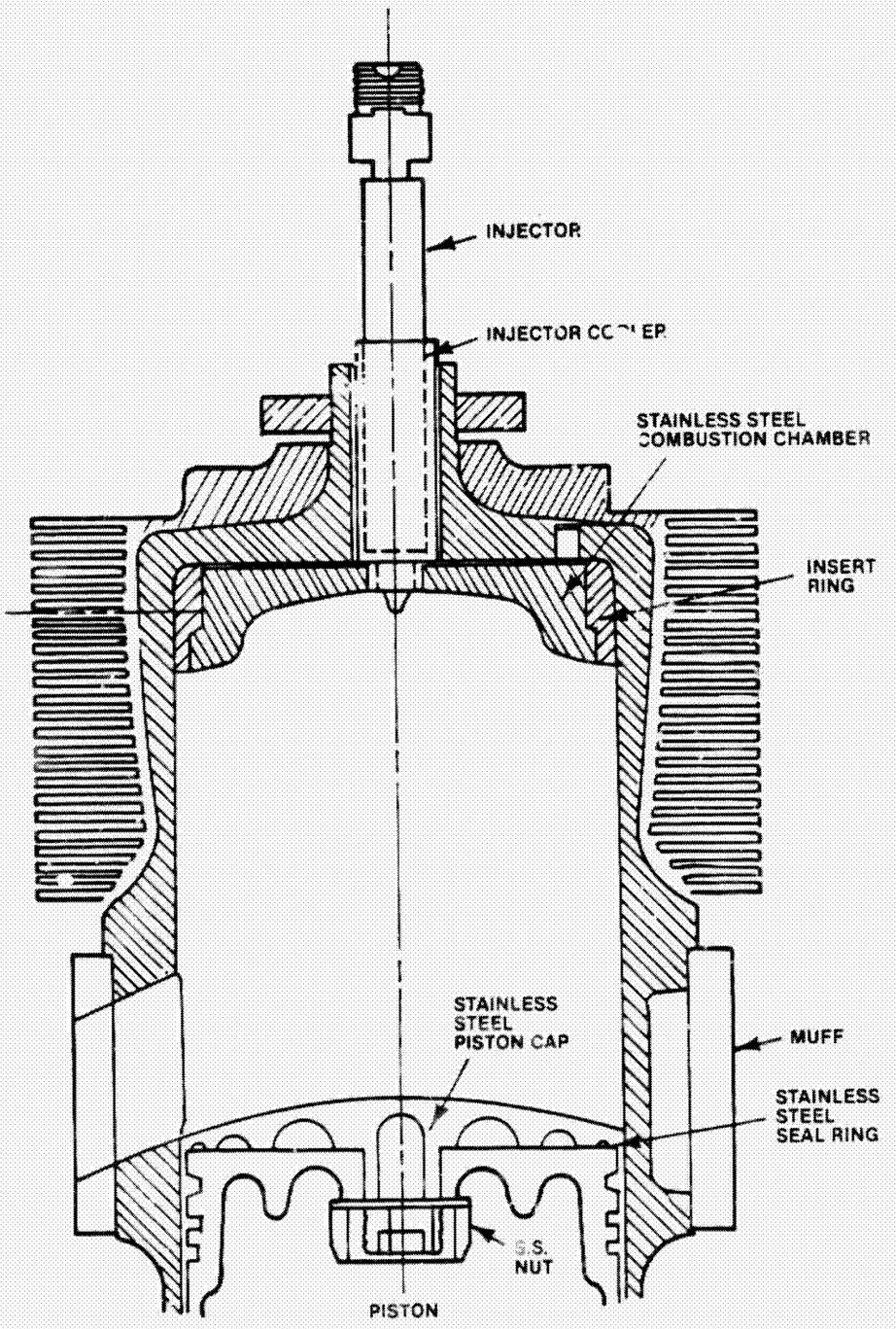

Figure 4.2-25. Air Gap Insulated Piston and Combustion Bowl Assembled in Cylinder

Figure 4.2-26. Air Gap Insulated Piston Cap

C-2

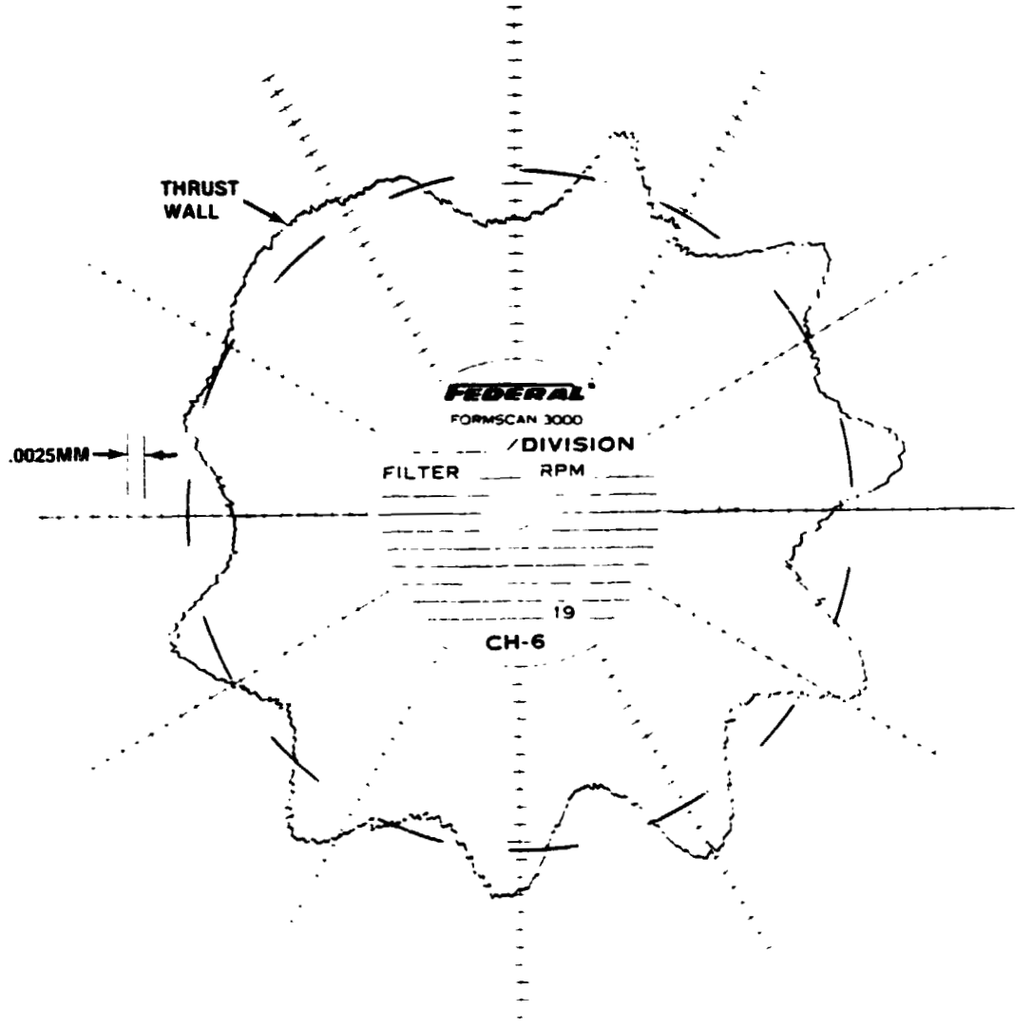

Figure 4.2-27. Inside Diameter Profile Trace of Cylinder, 6.35 mm Above Ports

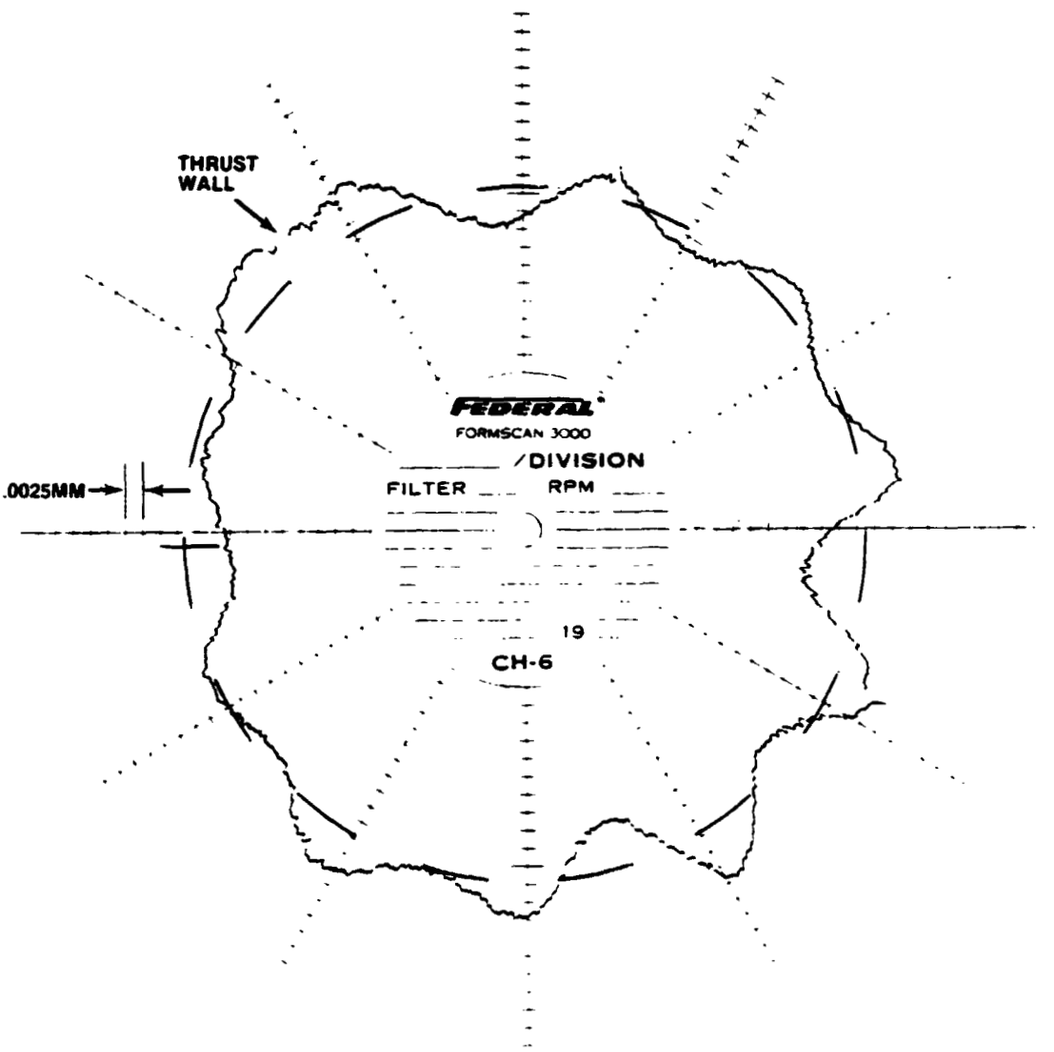

Figure 4.2-28. Inside Diameter Profile Trace of Cylinder No. 3, 6.35mm Below Ports

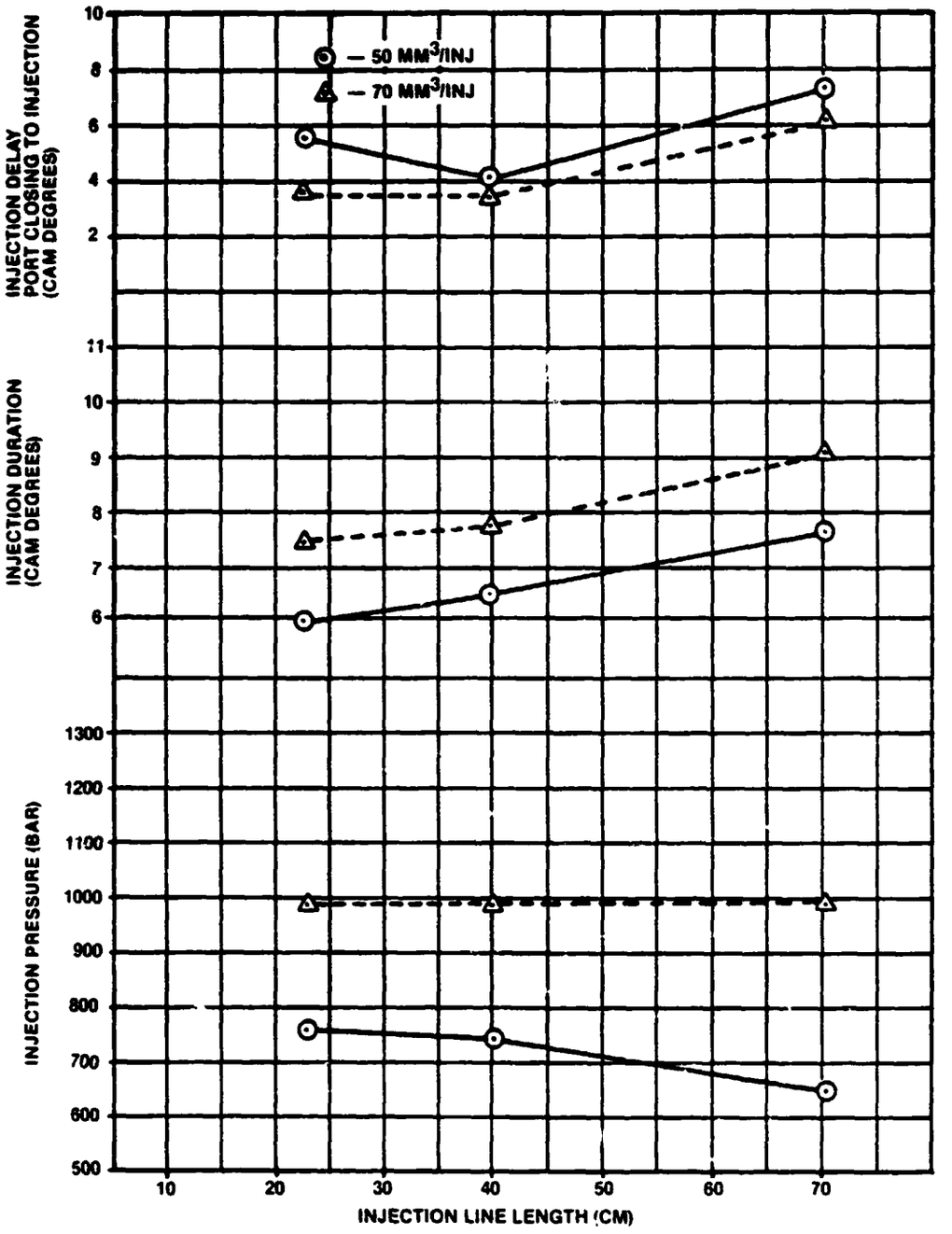

Figure 4.3-1. Injection Characteristics for CAE-X Pump at 1325 Pump RPM

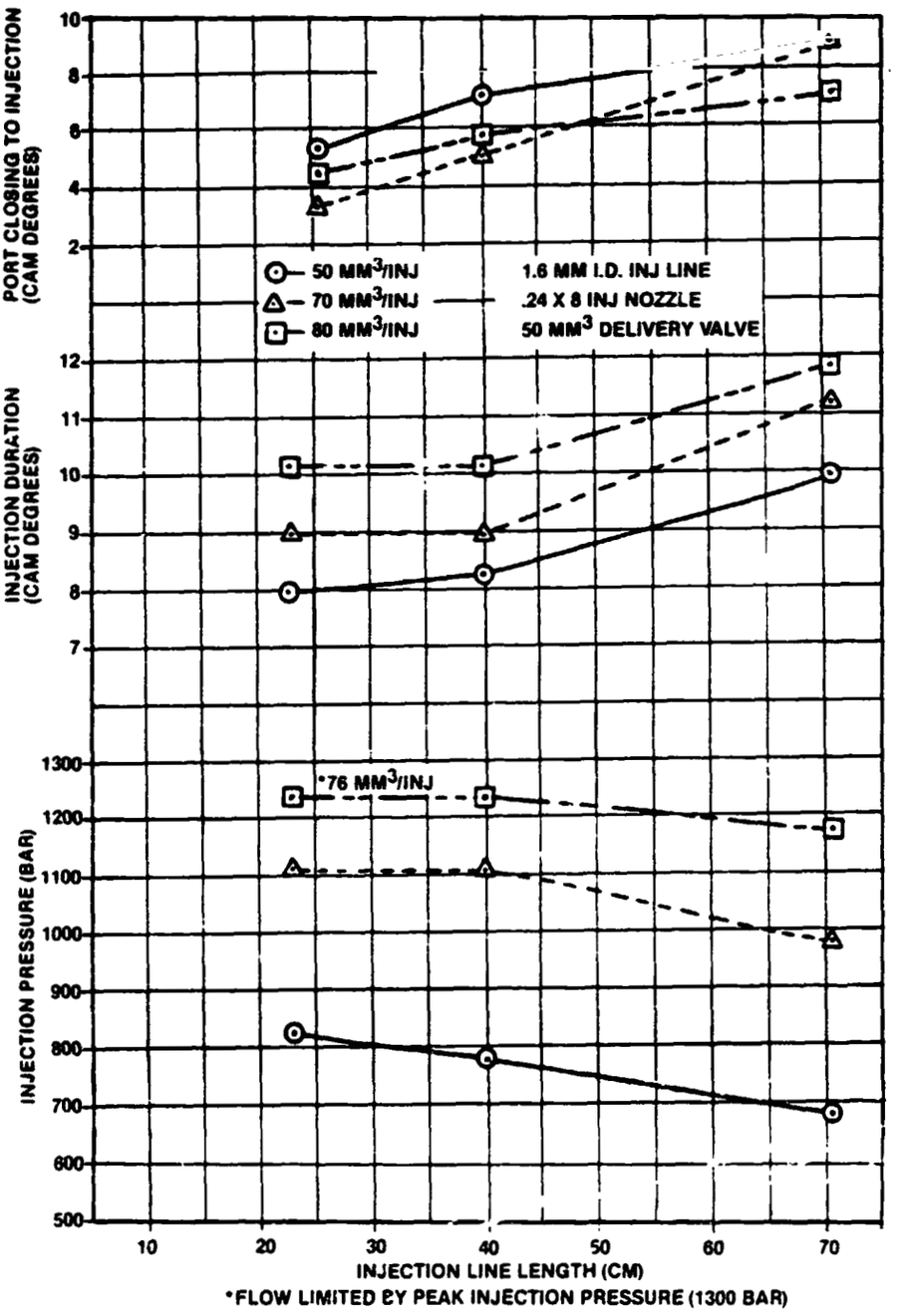

Figure 4.3-2. Injection Characteristics for CAE-X Pump at 1750 Pump RPM

Figure 4.3-3. CARE-X Pump with a 71.1cm Injecton Line Length as Installed on the SCTE

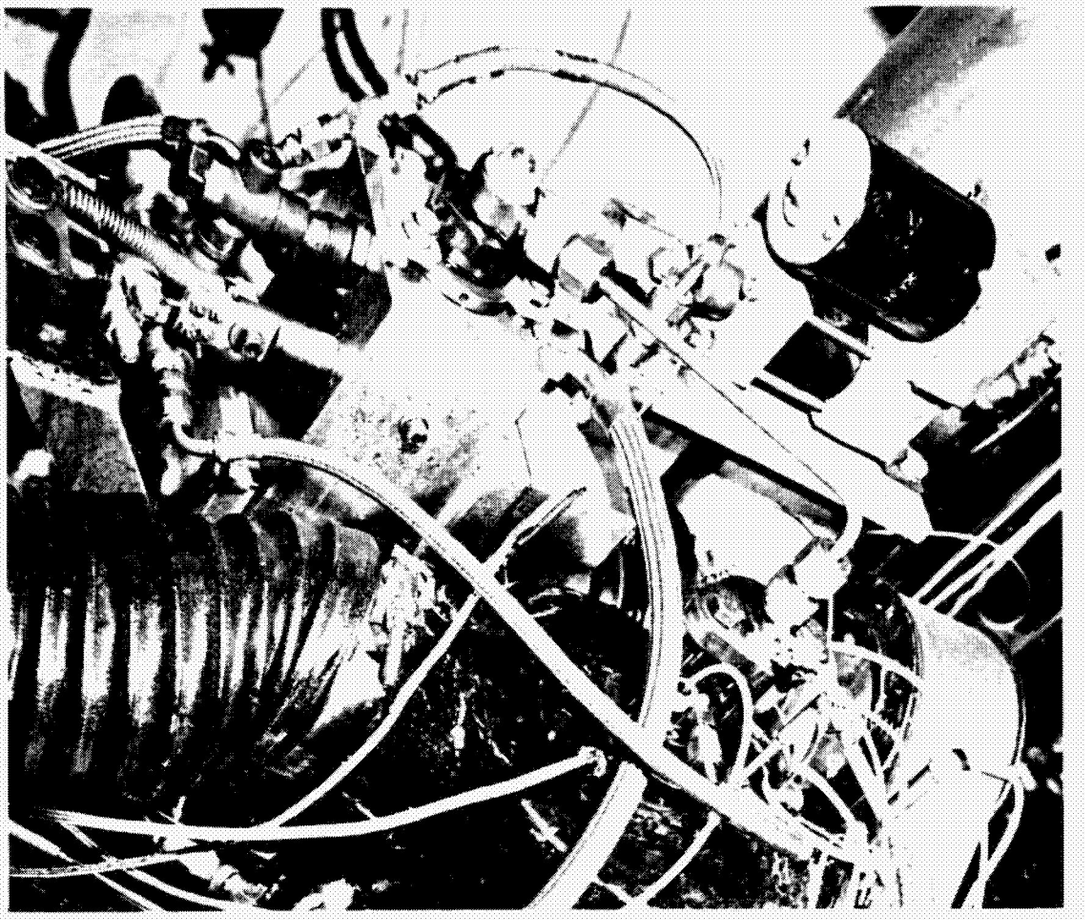

Figure 4.3-4. CAE-X Pump with a 17.8cm Injection Line Length as Installed on the SCTE

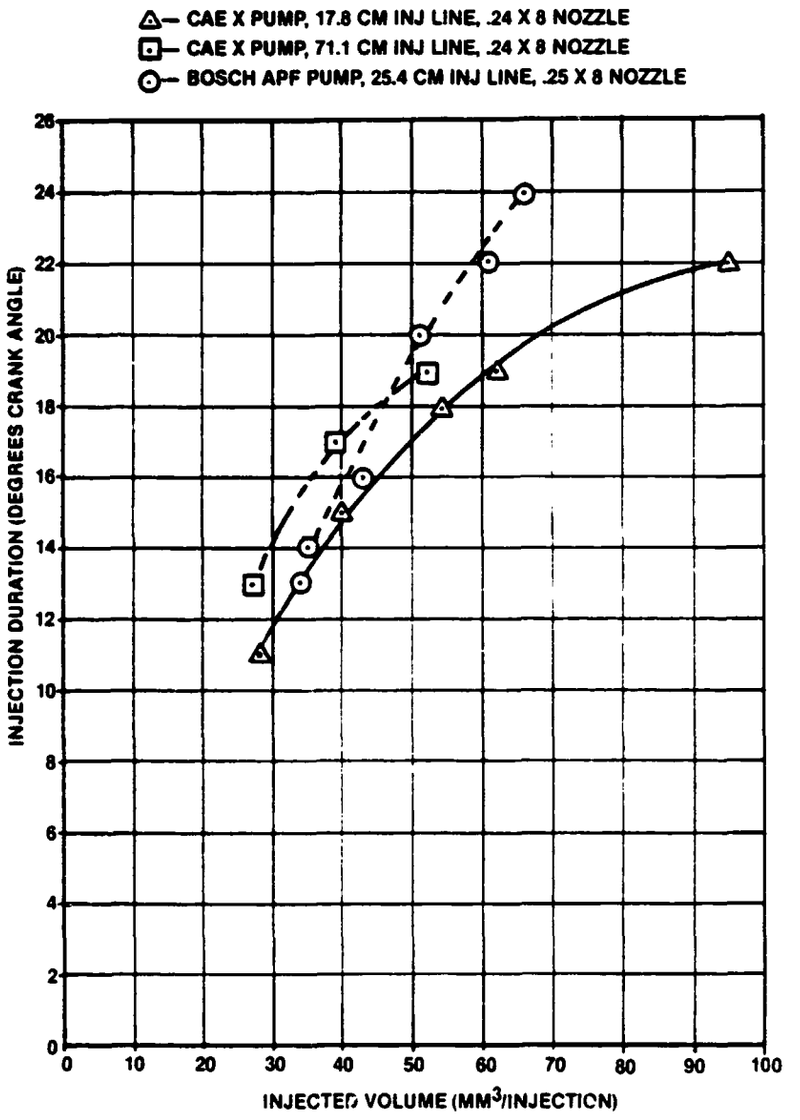

Figure 4.3-5. Injection Duration Versus Injected Volume for Three Injection Pump Configurations Tested at 3500 RPM

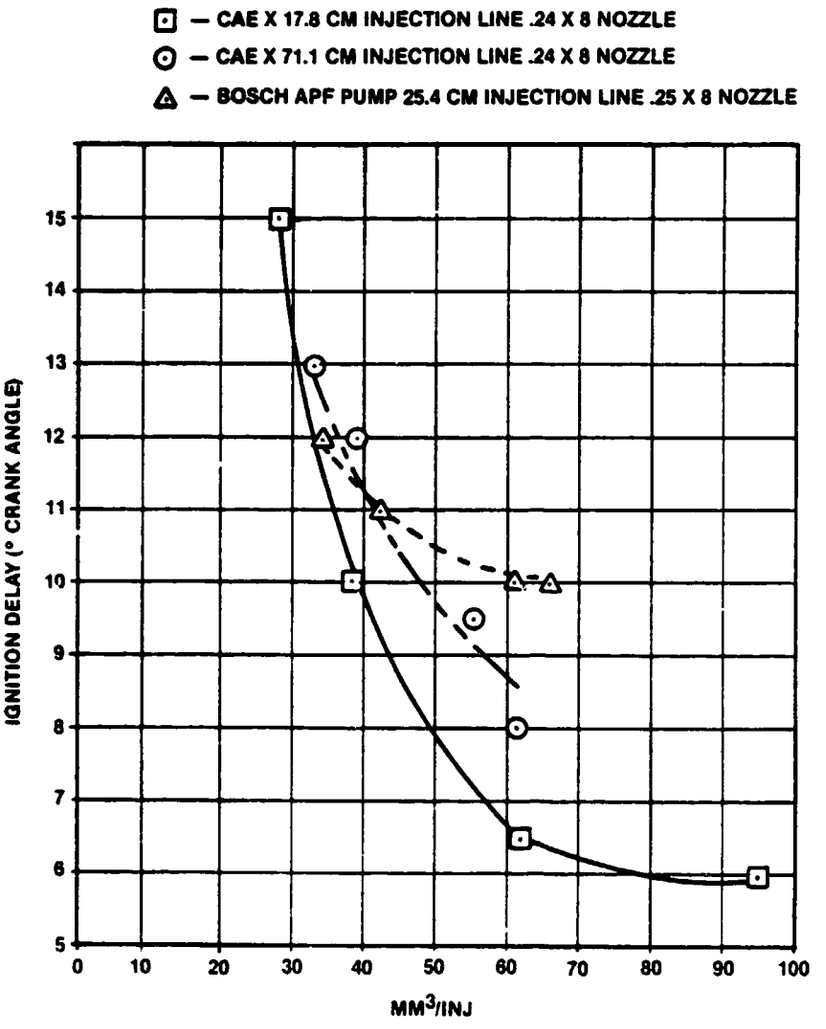

Figure 4.3-6. Ignition Delay Versus Injected Volume for Three Pump Configurations at 3500 RPM

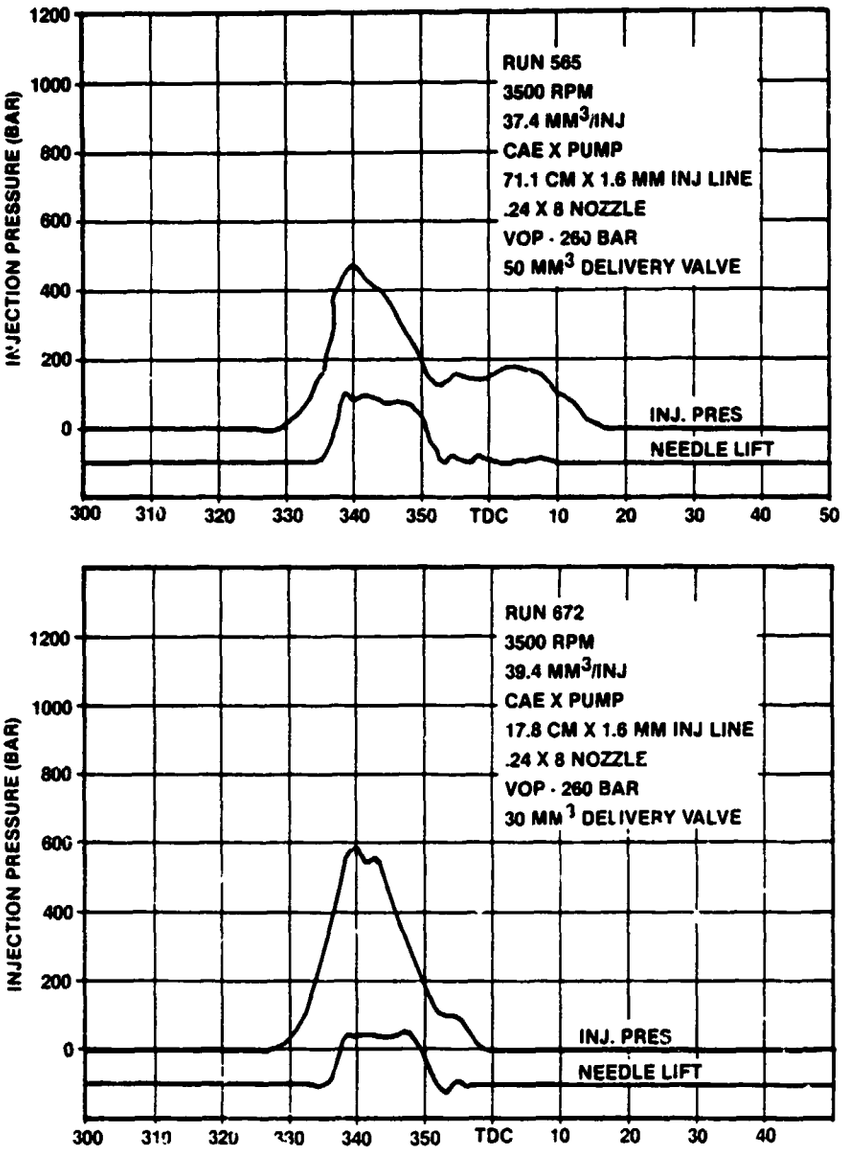

Figure 4.3-7. Dyanamic Pressure and Needle Lift Characteristics

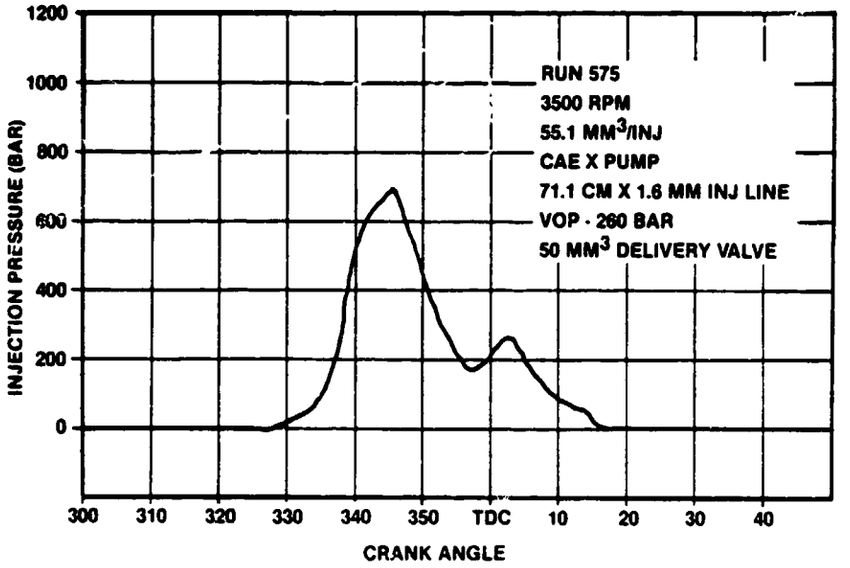

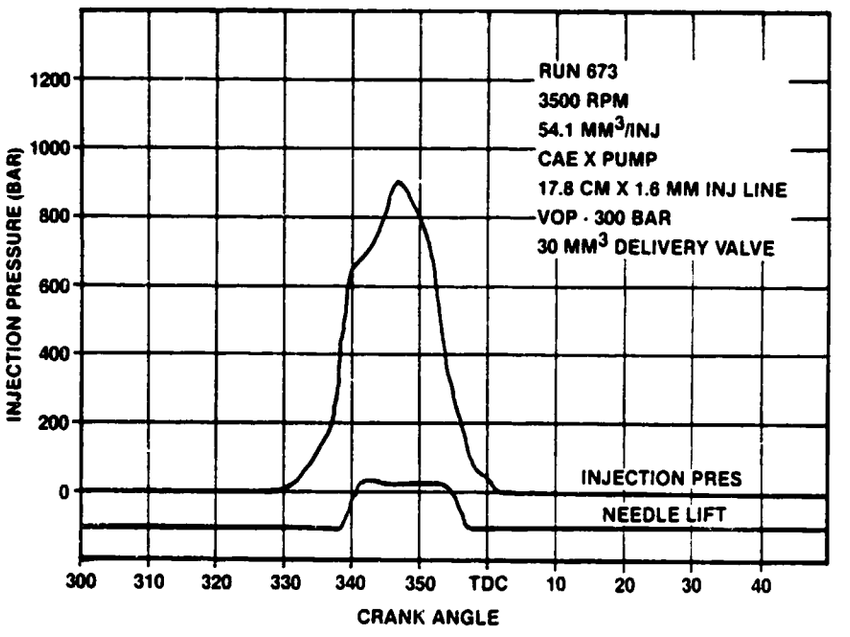

Figure 4.3-7. Dyanamic Pressure and Needle Lift Characteristics (Continued)

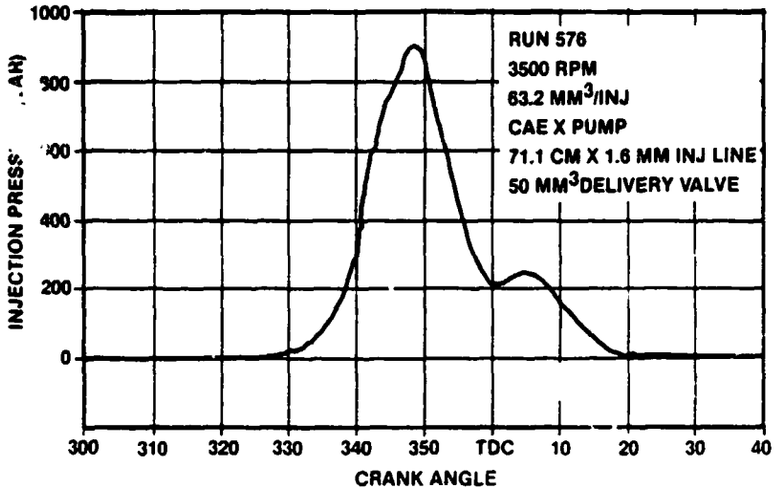

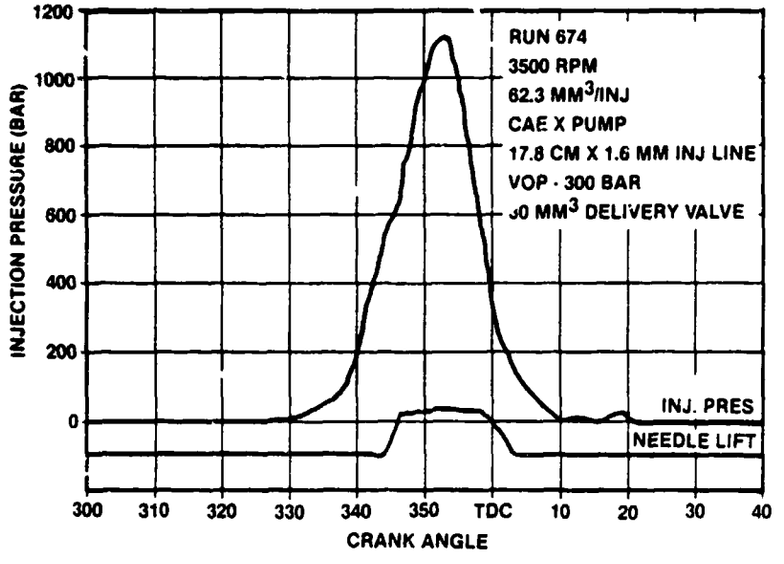

Figure 4.3-7. Dyanamic Pressure and Needle Lift Characteristics (Continued)

⬡ — CYL #1 ORIGINAL MANIFOLD
◇ — CYL #2 ORIGINAL MANIFOLD
○ — CYL #3 ORIGINAL MANIFOLD

3500 RPM
12.83 M/S PISTON SPEED

CYL #	INTAKE HEIGHT MM	A_i MM^2	EXHAUST HEIGHT MM	A_e MM^2	A_e/A_i
1	29	3084.1	44	2432	.788
2	28	2764.7	35	2076	.751
3	31	3296.7	43	2550	.774

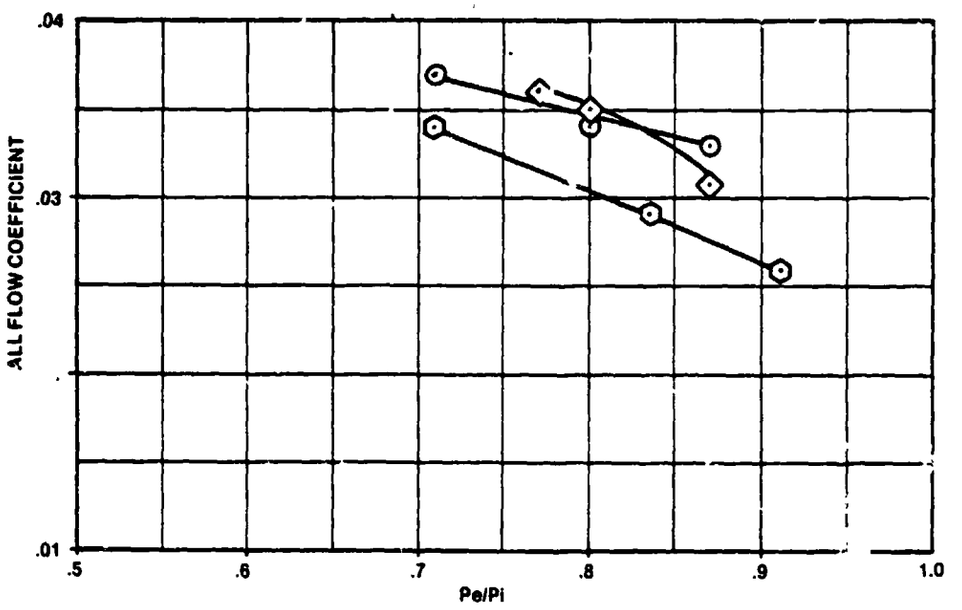

Figure 4.4-1. Comparison of Overall Flow Coefficients Using Original Manifold at 3500 RPM

⬡ — CYL #1 ORIGINAL MANIFOLD
◇ — CYL #2 ORIGINAL MANIFOLD
○ — CYL #3 ORIGINAL MANIFOLD
□ — AVL PREDICTION CYL #1

2650 RPM
9.72 M/S PISTON SPEED

CYL #	INTAKE HEIGHT MM	A_i MM^2	EXHAUST HEIGHT MM	A_e MM^2	A_e/A_i
1	29	3084.1	44	2432	.788
2	26	2764.7	35	2076	.751
3	31	3296.7	43	2550	.774

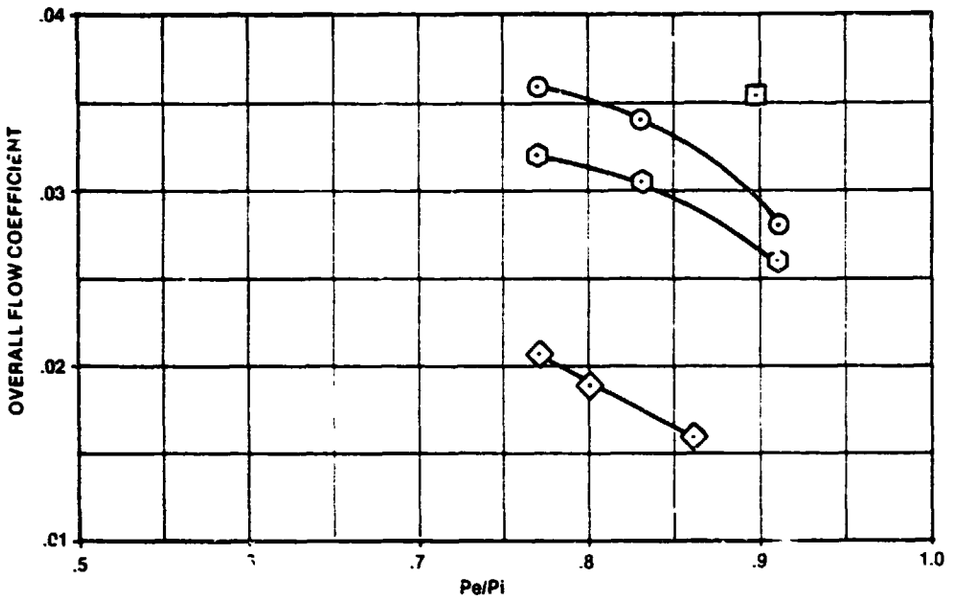

Figure 4.4-2. Compariso of Overall Flow Coefficients Using Original Manifold at 2650 RPM

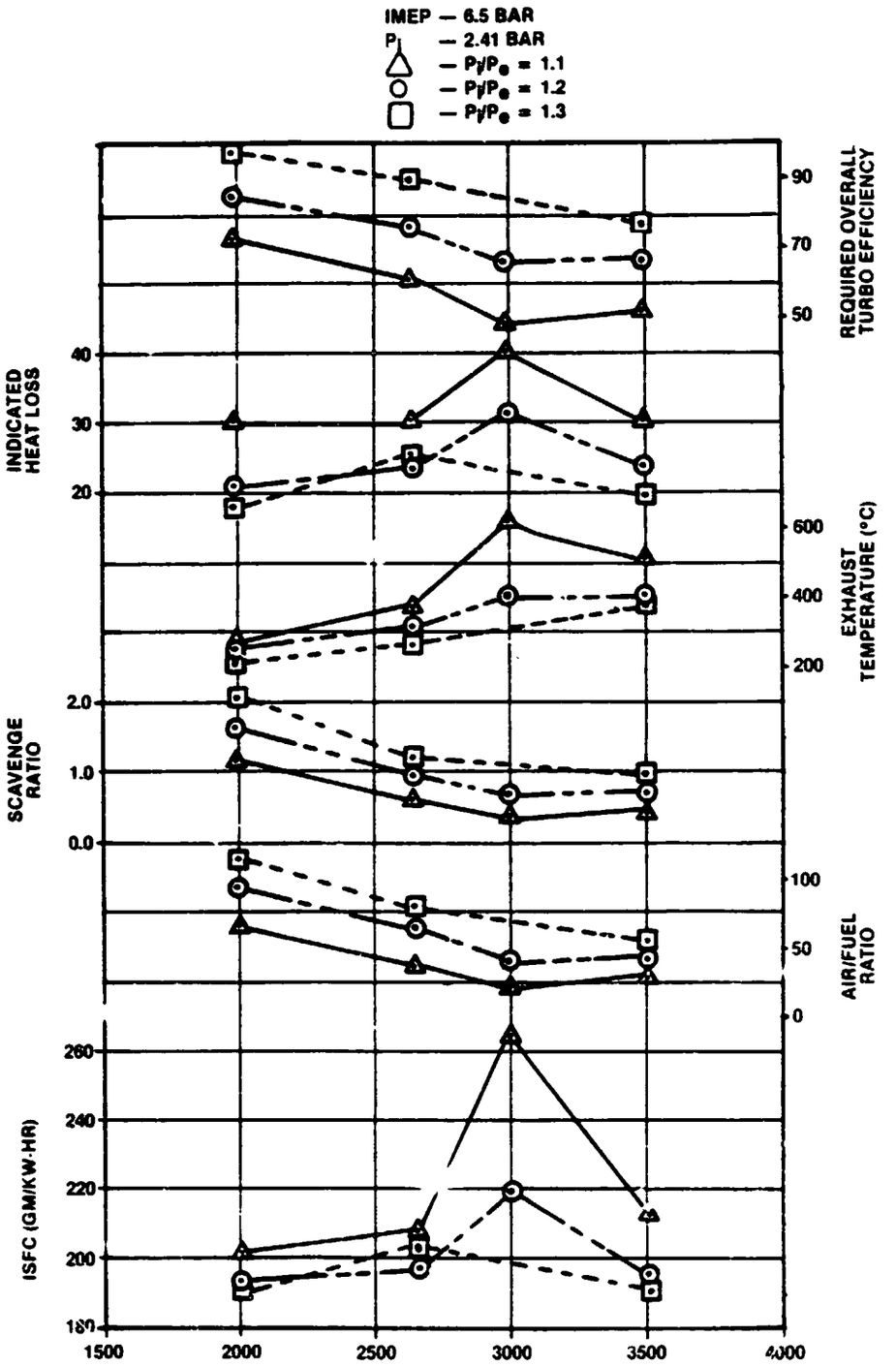

Figure 4.4-3. Engine Performance Versus Engine Speed for Cylinder #1 for Configurations 1, 2, and 3

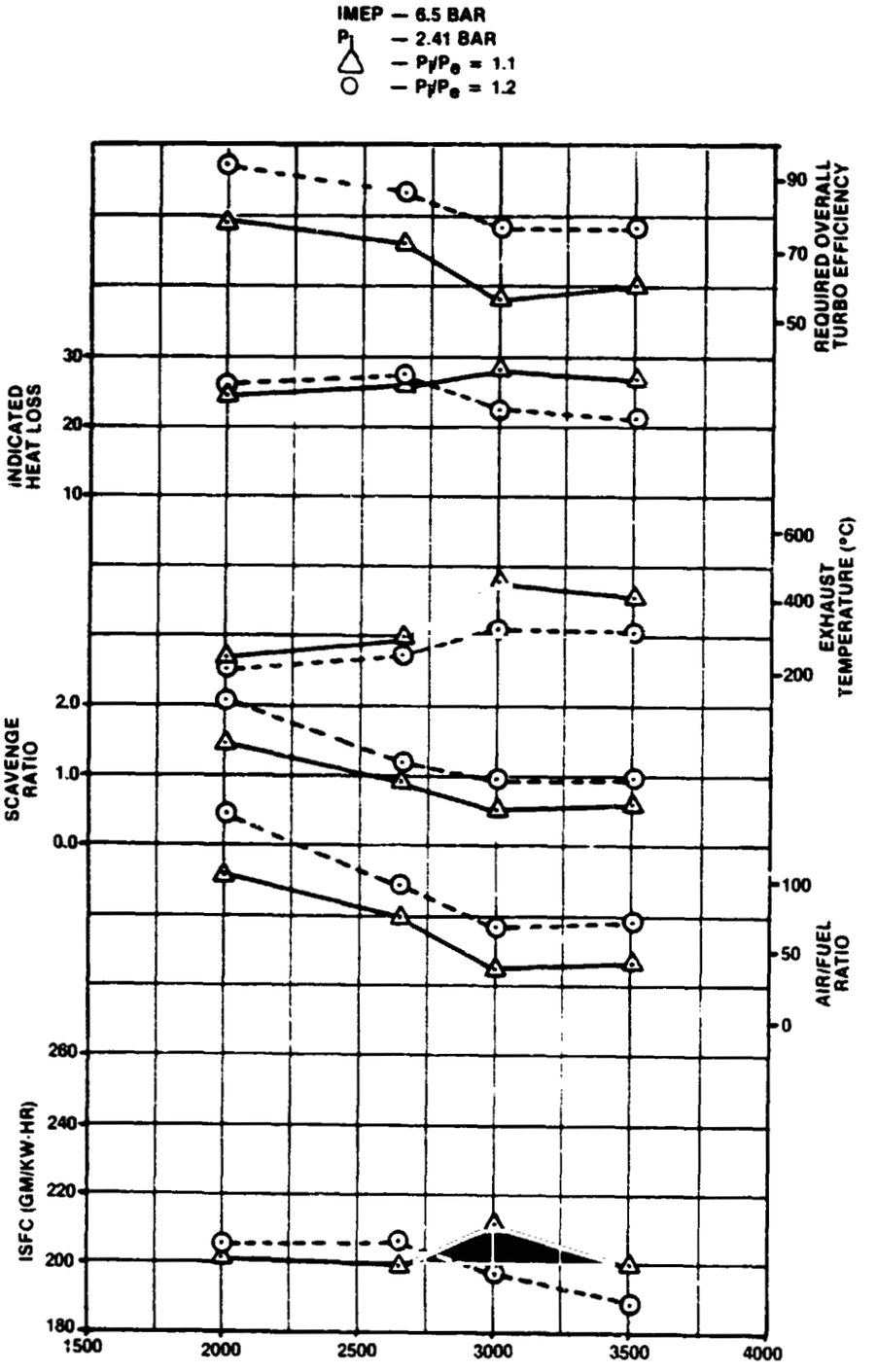

Figure 4.4-4. Engine Performance Versus Engine Speed for Cylinder #3 for Configurations 1, 2, and 3

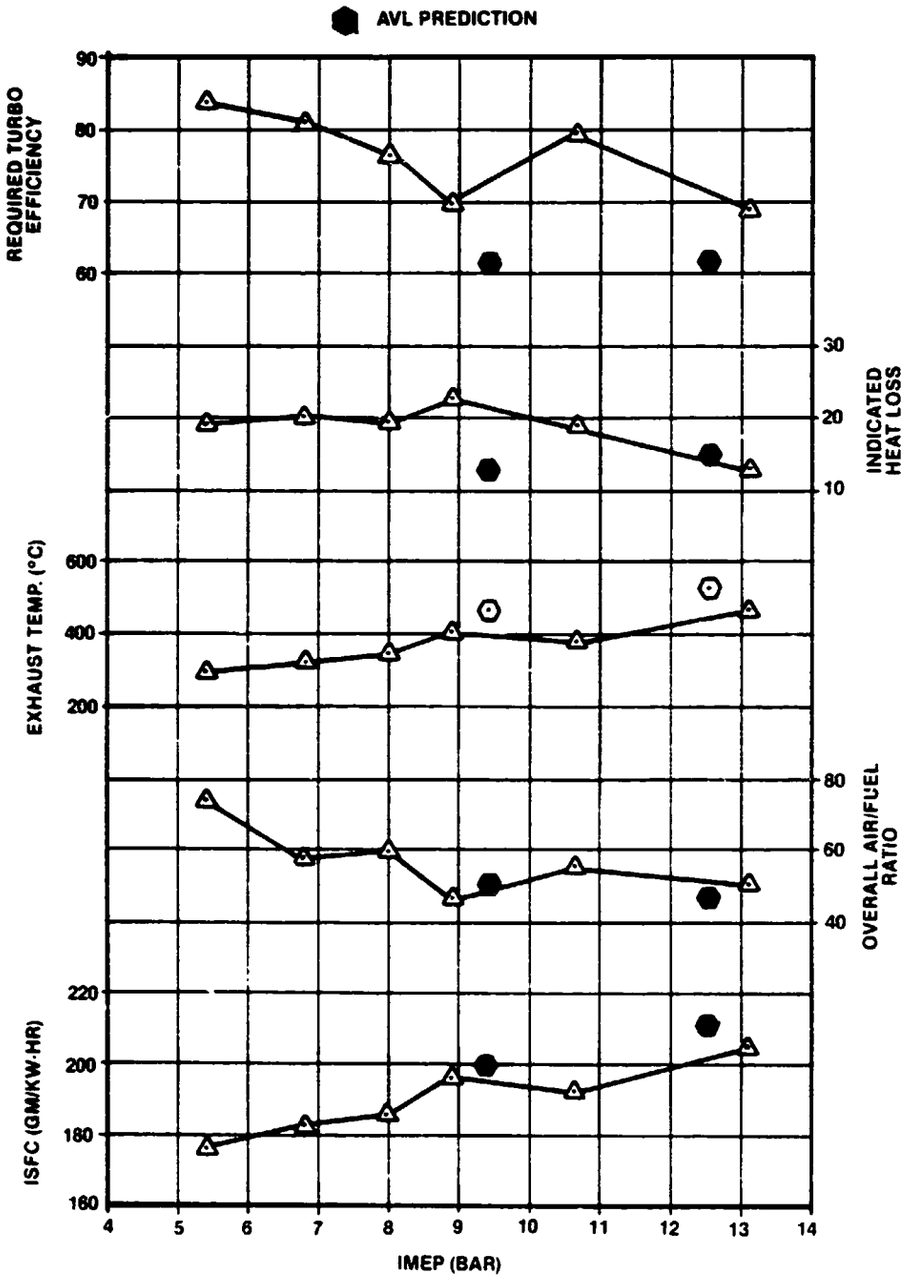

Figure 4.4-5. Engine Performance Versus IMEP for Cylinder 3 at 3500 RPM for Configuration 4

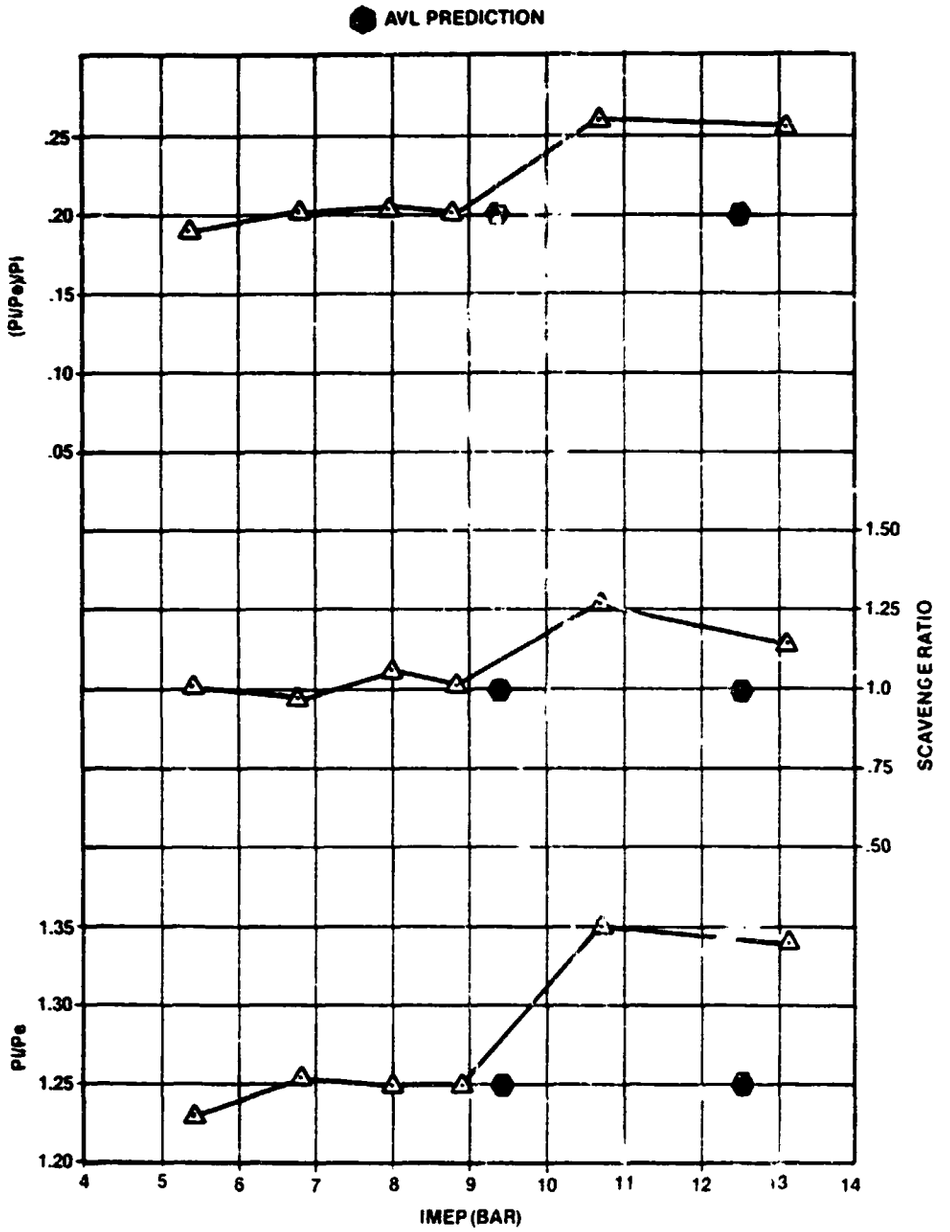

Figure 4.4-5. Engine Performance Versus IMEP for Cylinders at 3500 RPM for Configuration 4 (Continued)

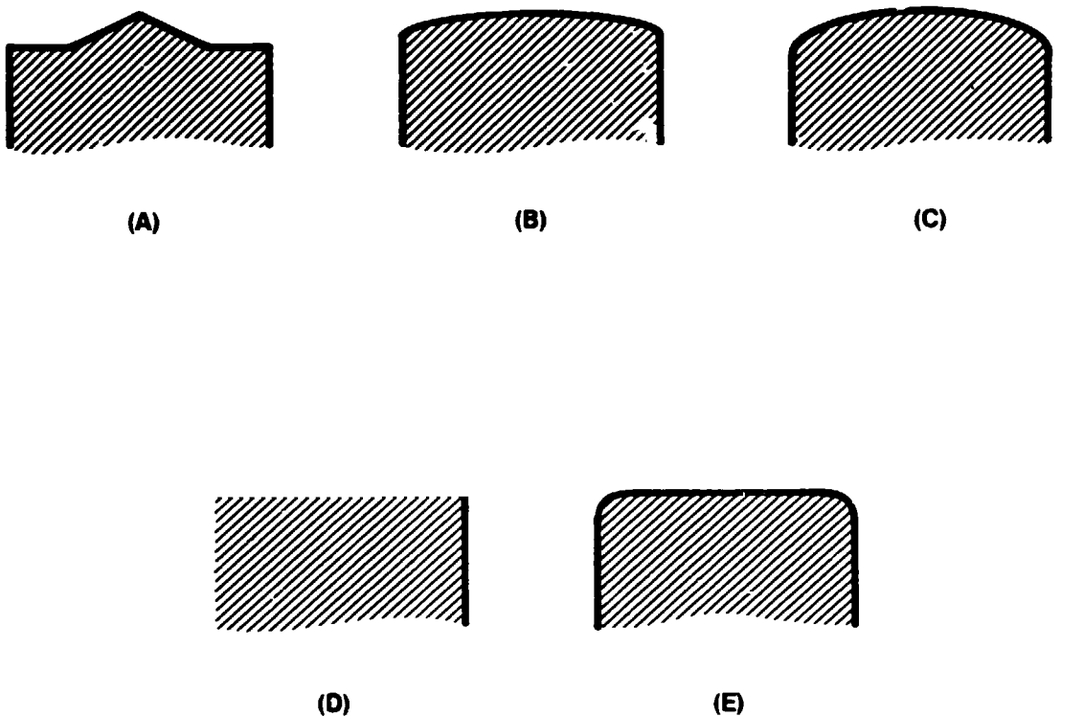

Figure 4.4-6. Piston Top Configurations Evaluated for Port Flow Coefficients

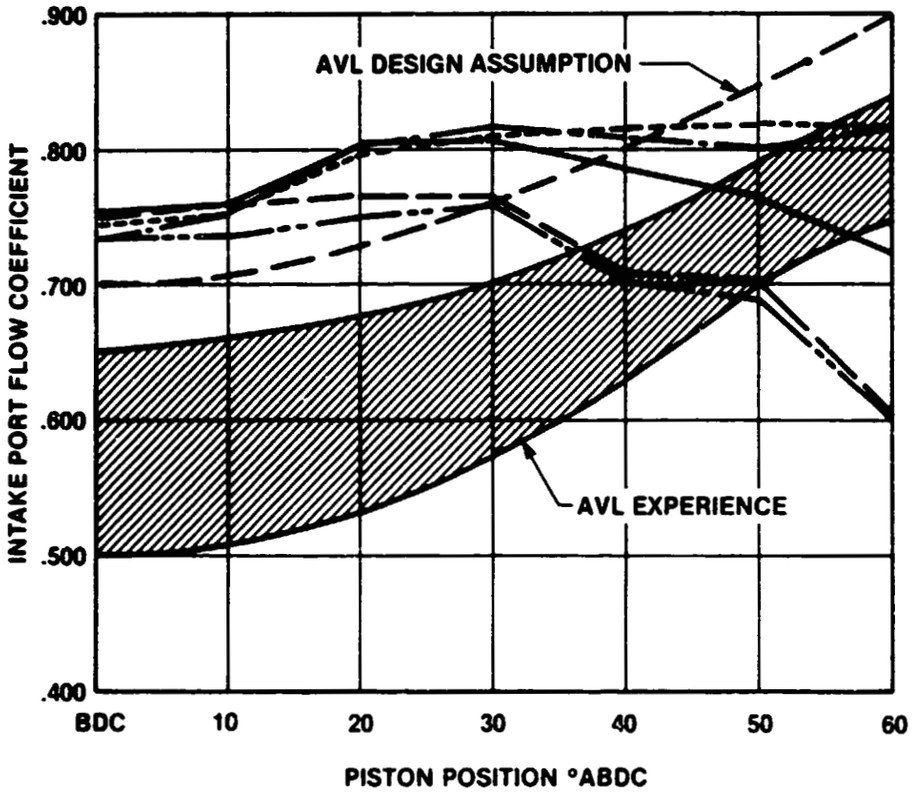

PISTON CONFIGURATIONS

CONE TOP SMOOTH EDGES
DOME TOP SHARP EDGES
DOME TOP SMOOTH EDGES
FLAT TOP SHARP EDGES
FLAT TOP SMOOTH EDGES

Figure 4.4-7. Intake Port Flow Coefficients

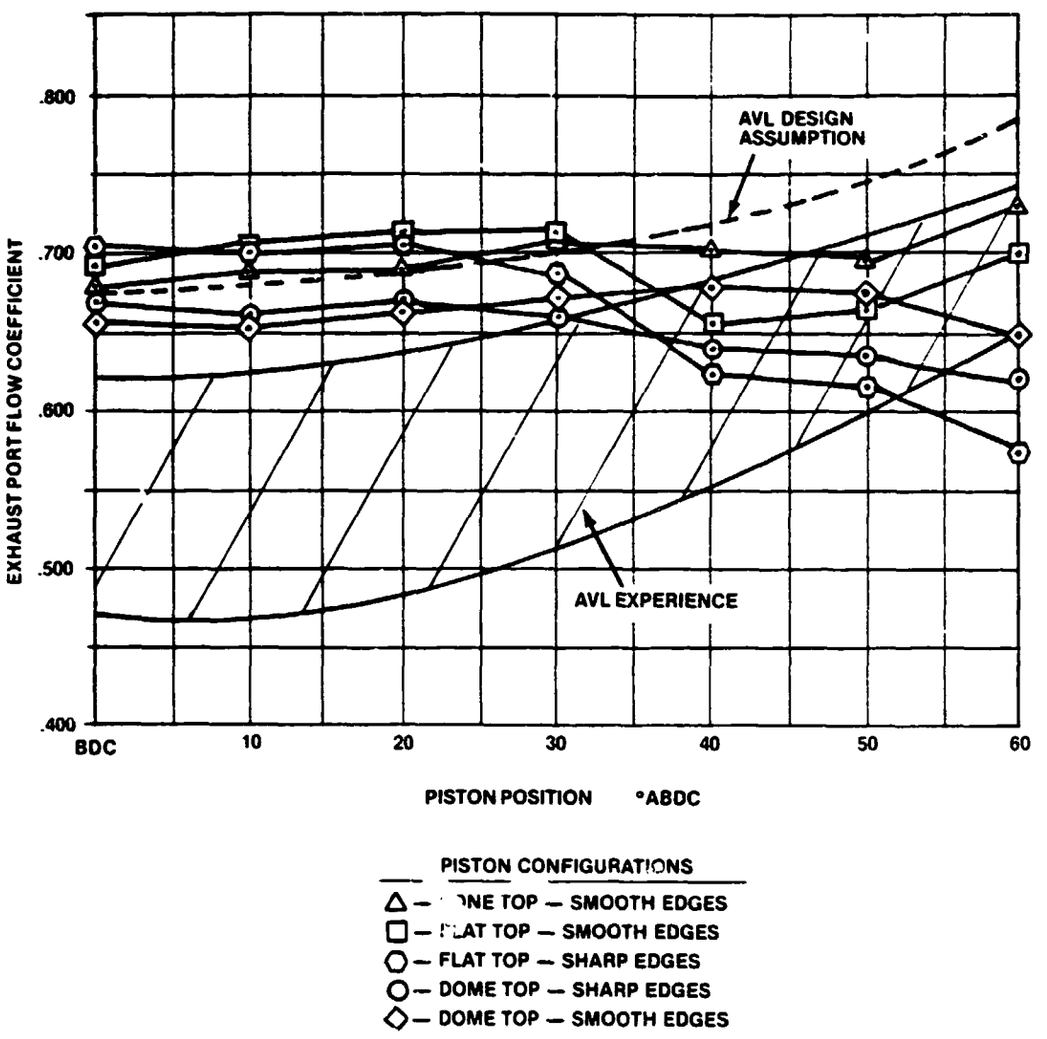

Figure 4.4-8. Exhaust Port Flow Coefficients

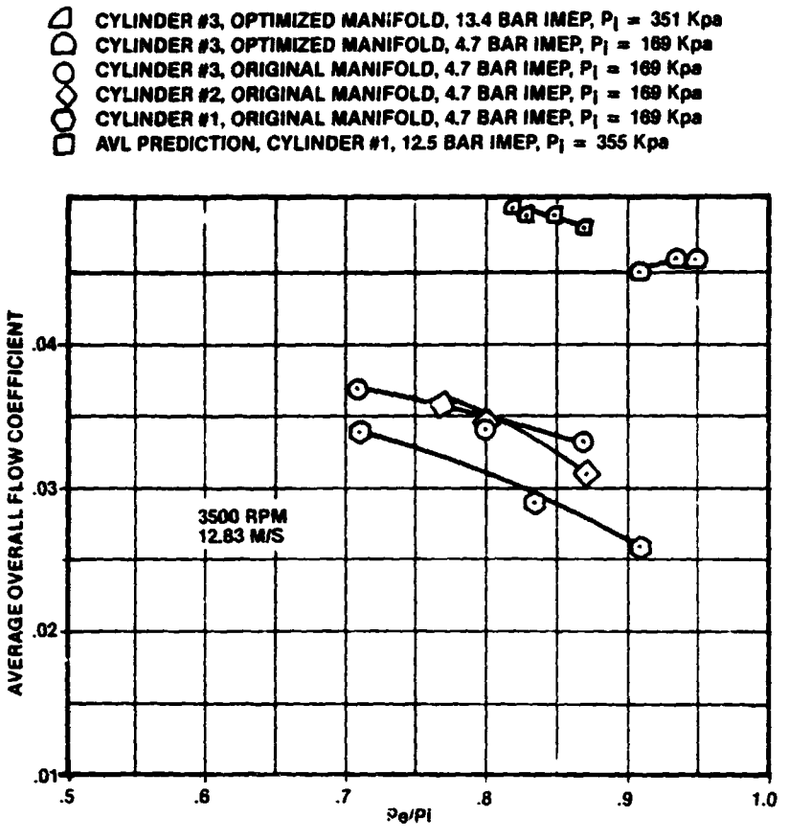

Figure 4.4-9. Average Overall Port Flow Coefficient with Optimized Manifolding at 3500 RPM

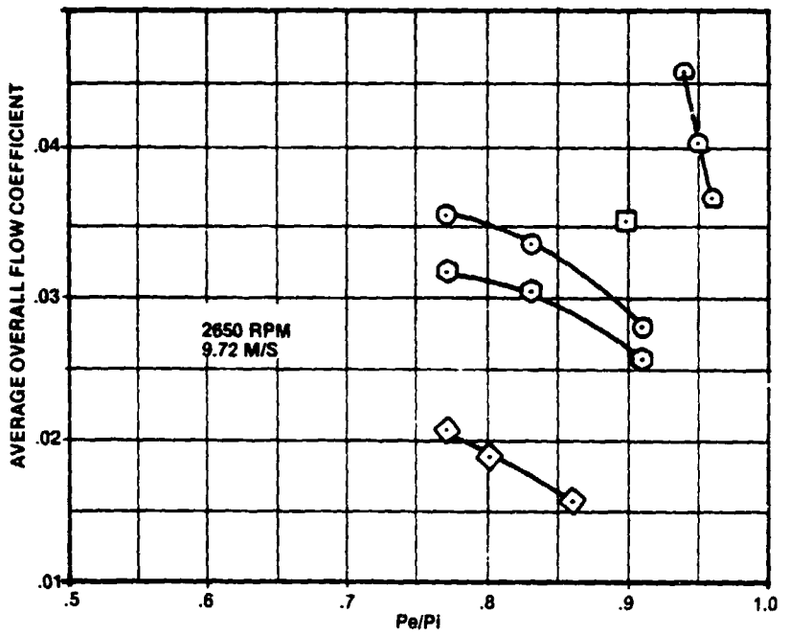

Figure 4.4-10. Average Overall Port Flow Coefficient with Optimized Manifolding at 2650 RPM

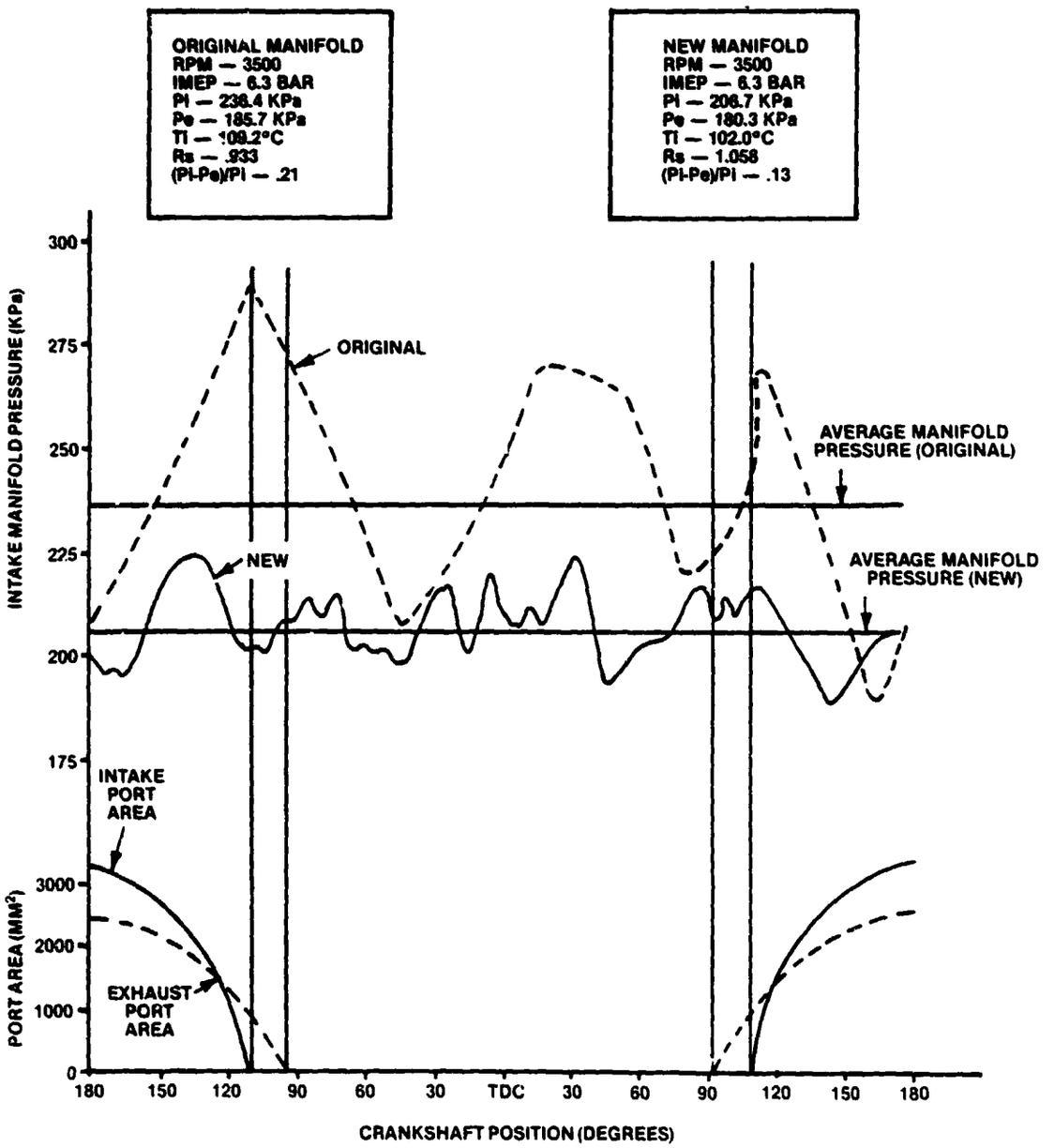

Figure 4.4-11. Dynamic Intake Manifold Pressure at 3500 RPM

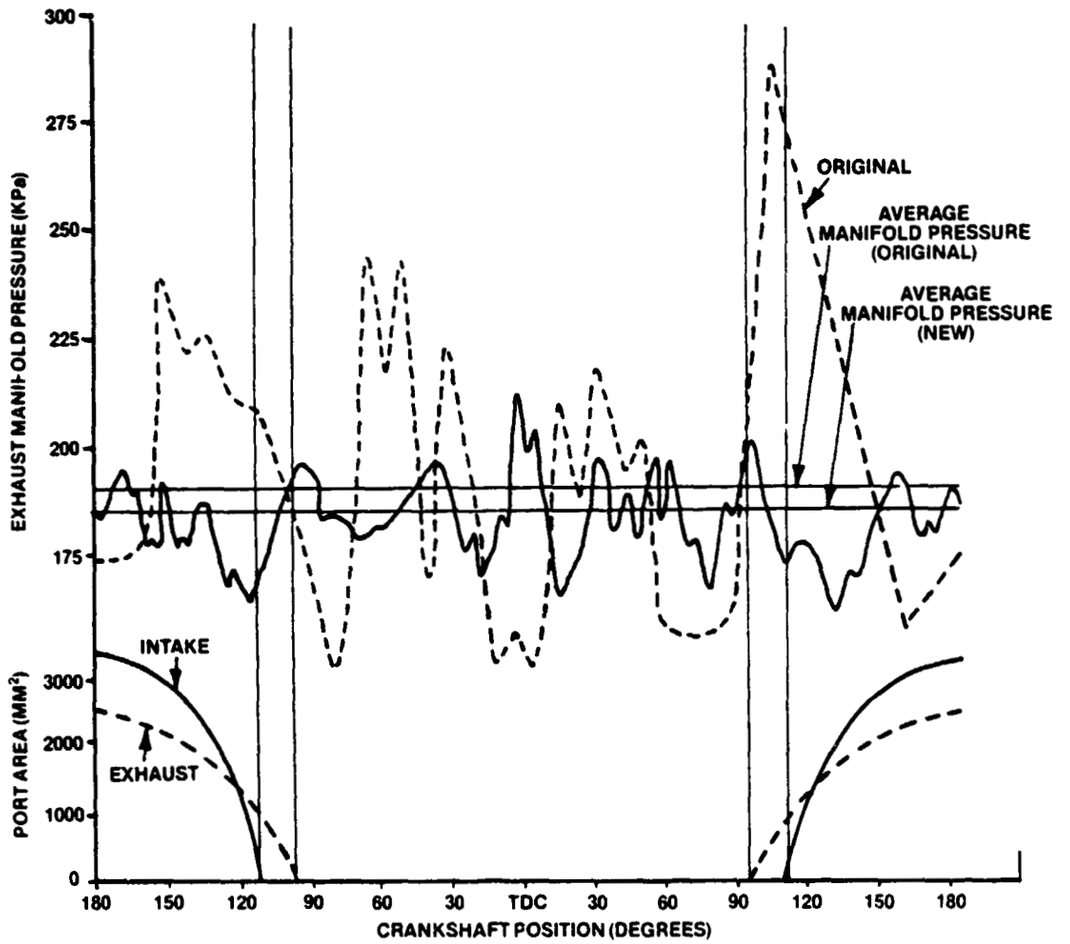

Figure 4.4-12. Dynamic Exhaust Manifold Pressure at 3500 RPM

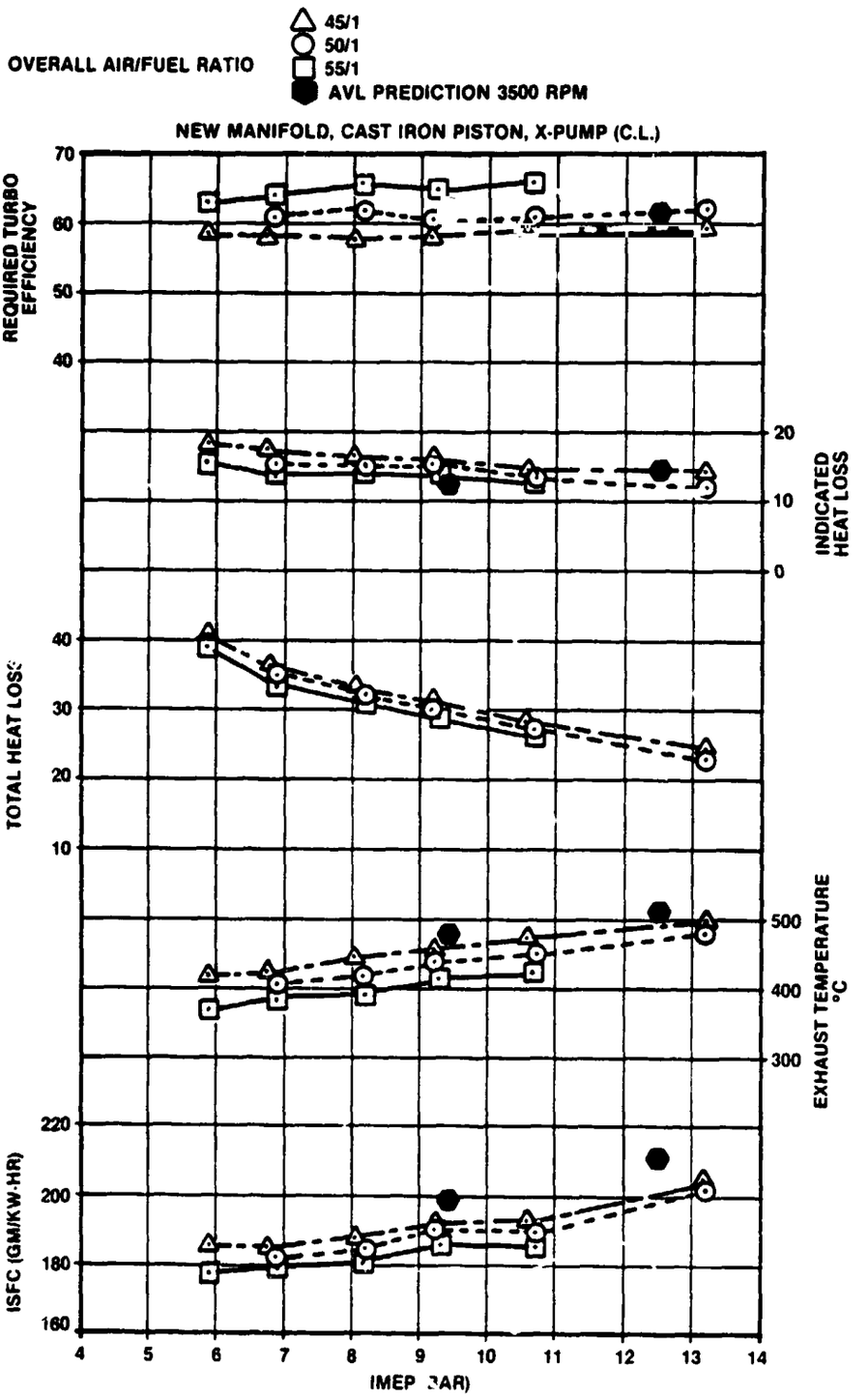

Figure 4.4-13. Engine Performance for Configuration 10 at 3500 RPM

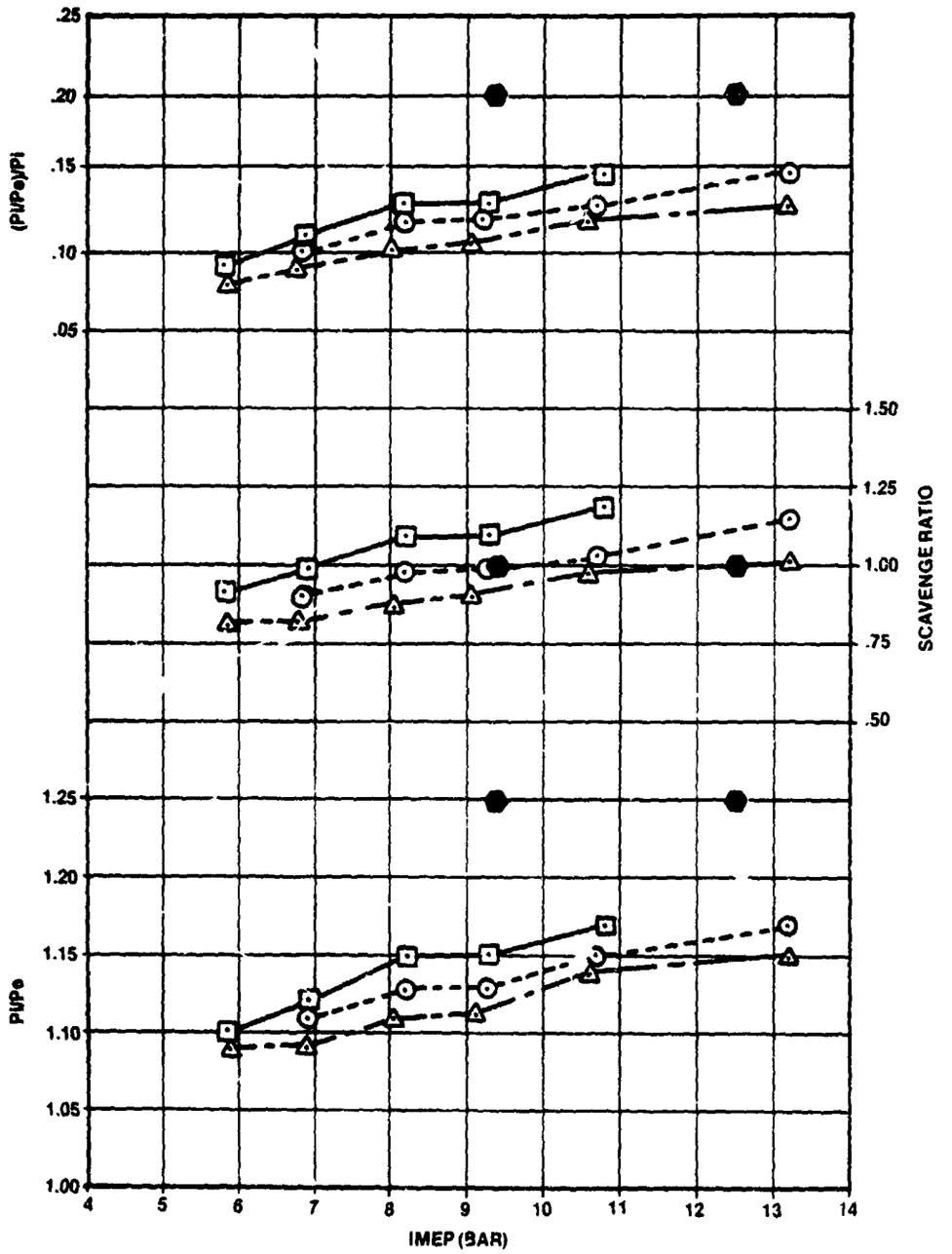

Figure 4.4-13. Engine Performance for Configuration 10 at 3500 RPM (Continued)

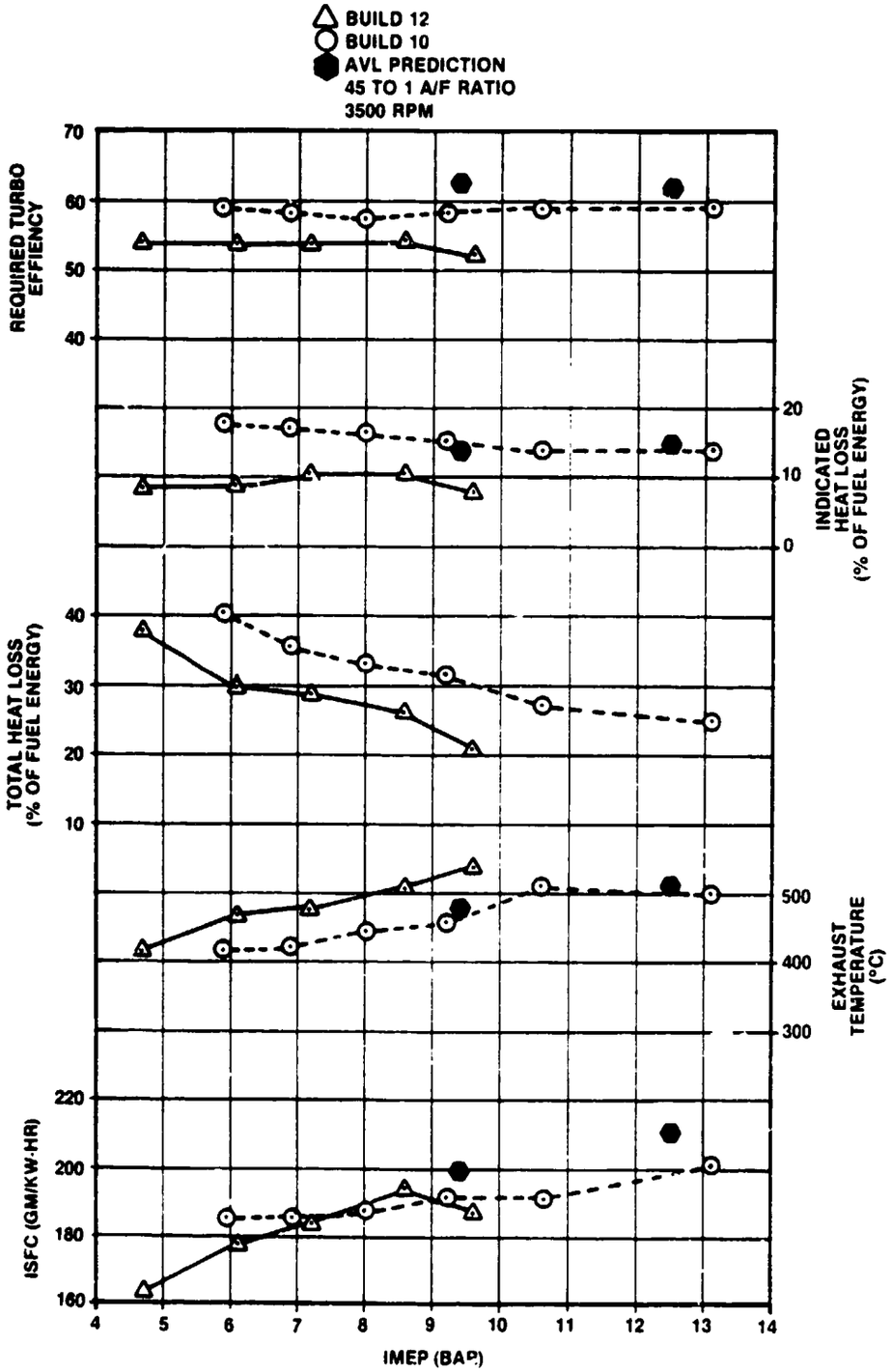

Figure 4.4-14. Engine Performance Comparisons at 3500 RPM for Configurations 10 and 12

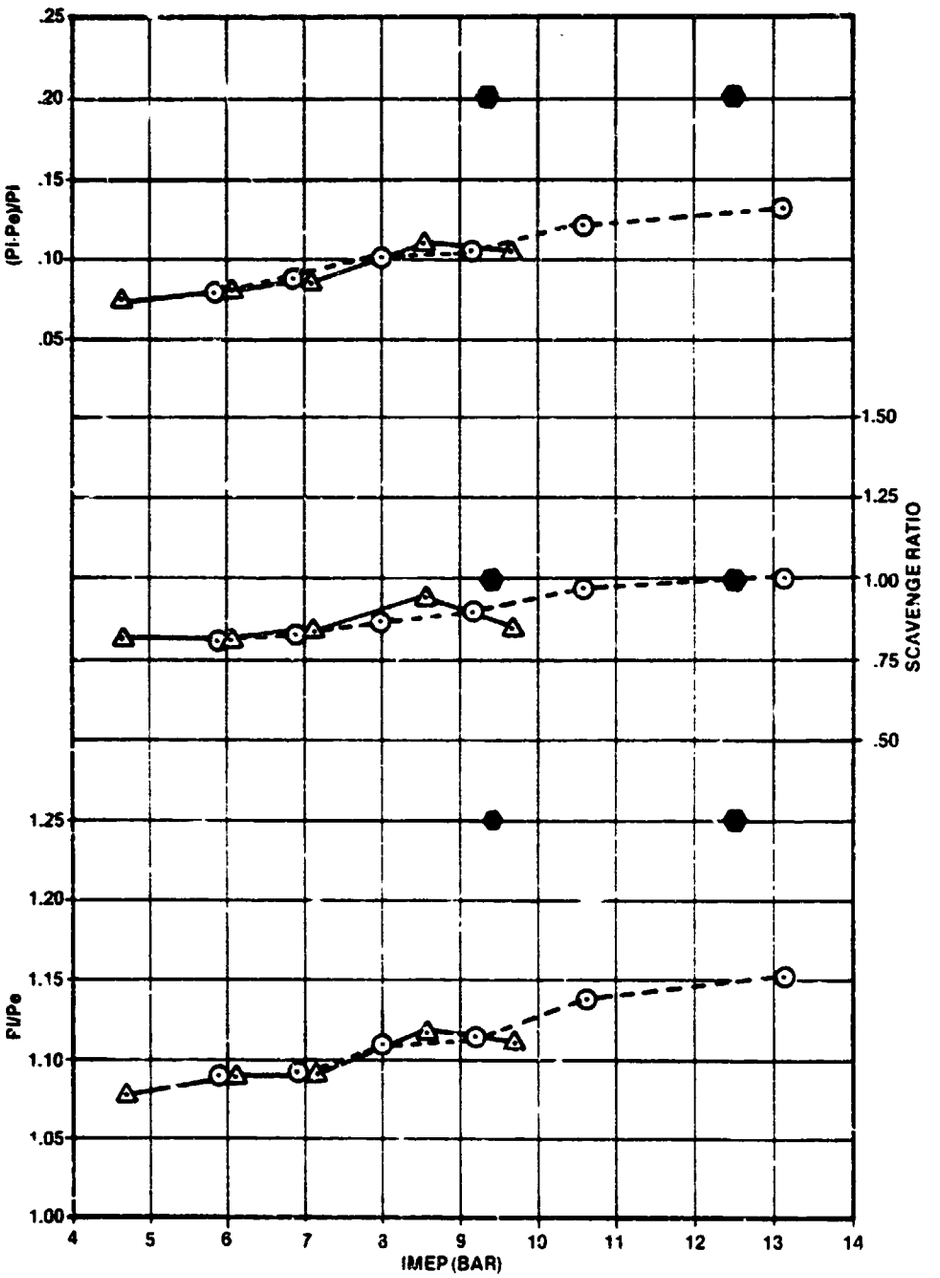

Figure 4.4-14 Engine Perfo- -ance Comparisons at 3500 RPM for Configurations 10 and 12 (Continued)

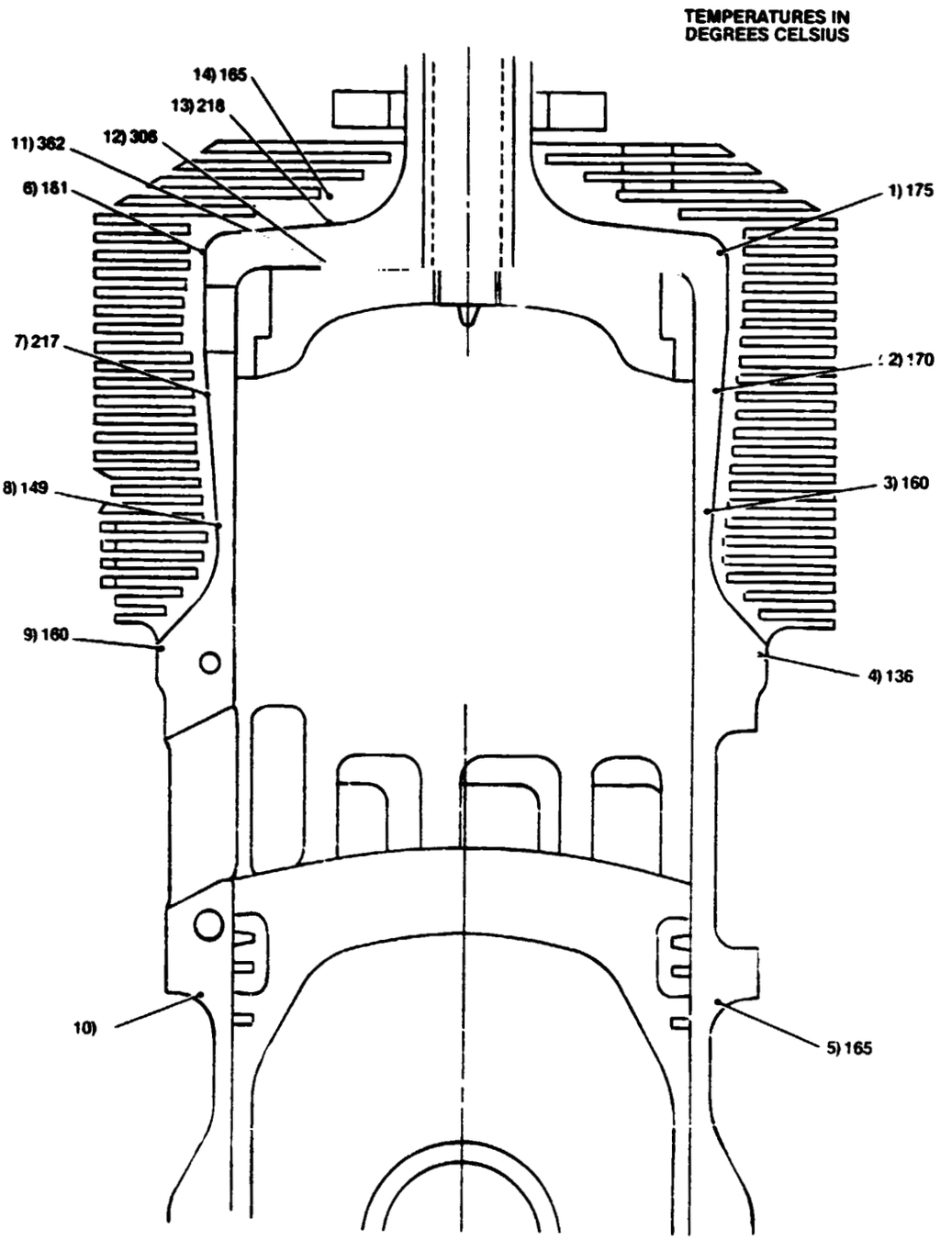

Figure 4.4-15. Cylinder Temperature Distribution for Configuration 10 at 3500 RPM and 9.6 BAR IMEP

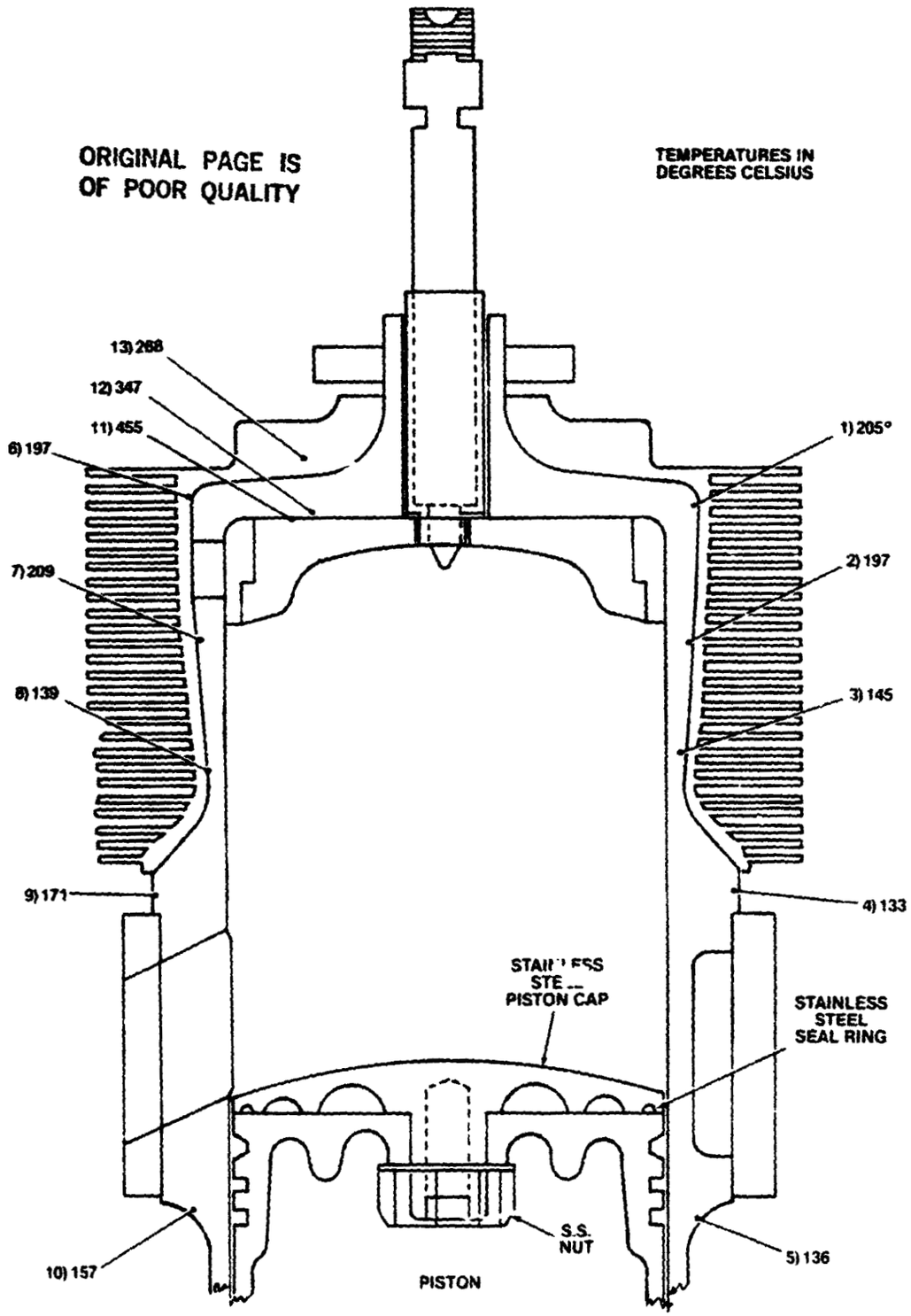

Figure 4.4-16. Cylinder Temperature Distributions for Configuration 12 at 3500 RPM and 3.6 BAR IMEP

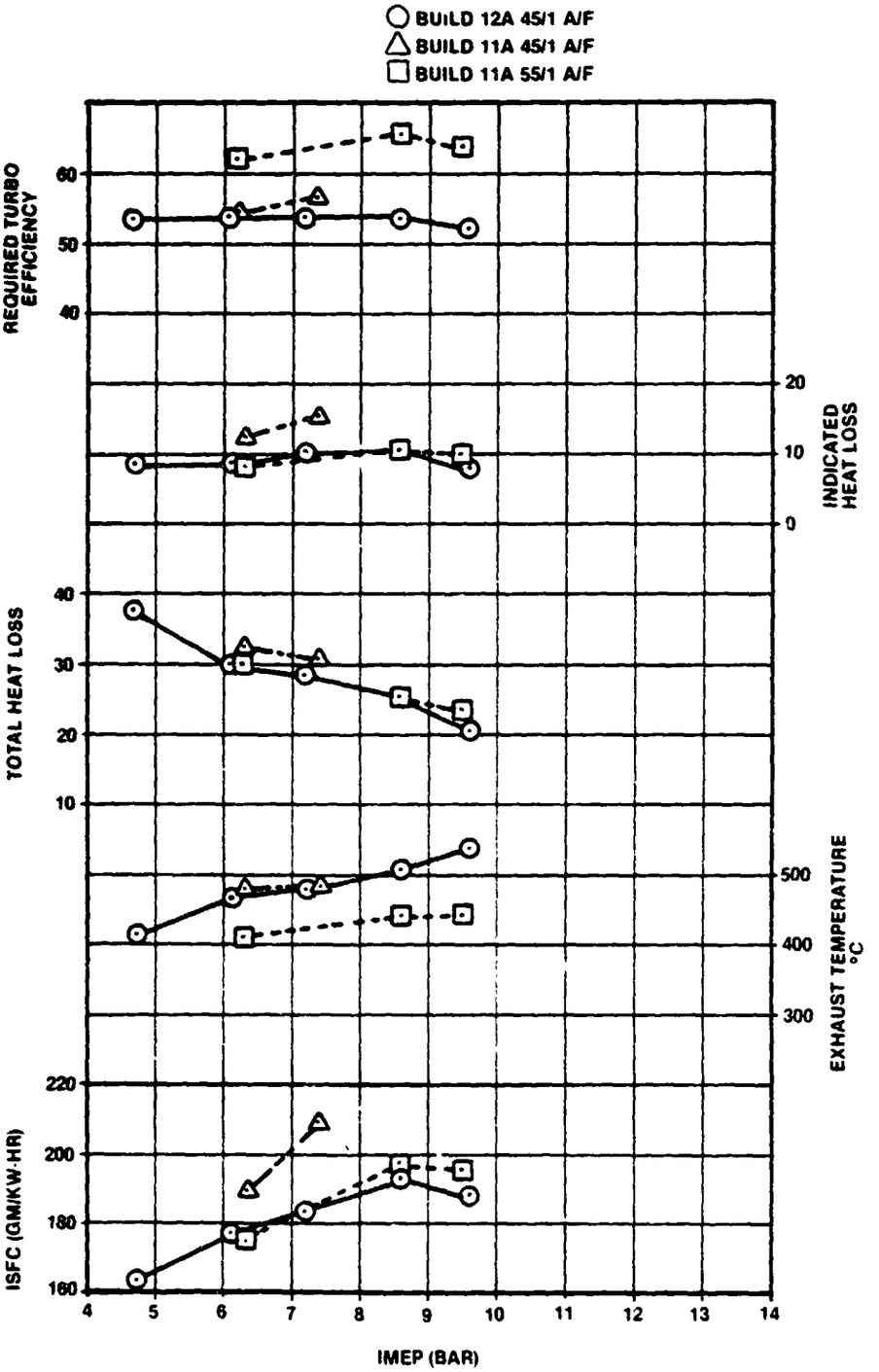

Figure 4.4-17. Engine Performance Comparison for Configurations 11 and 12 at 3500 RPM

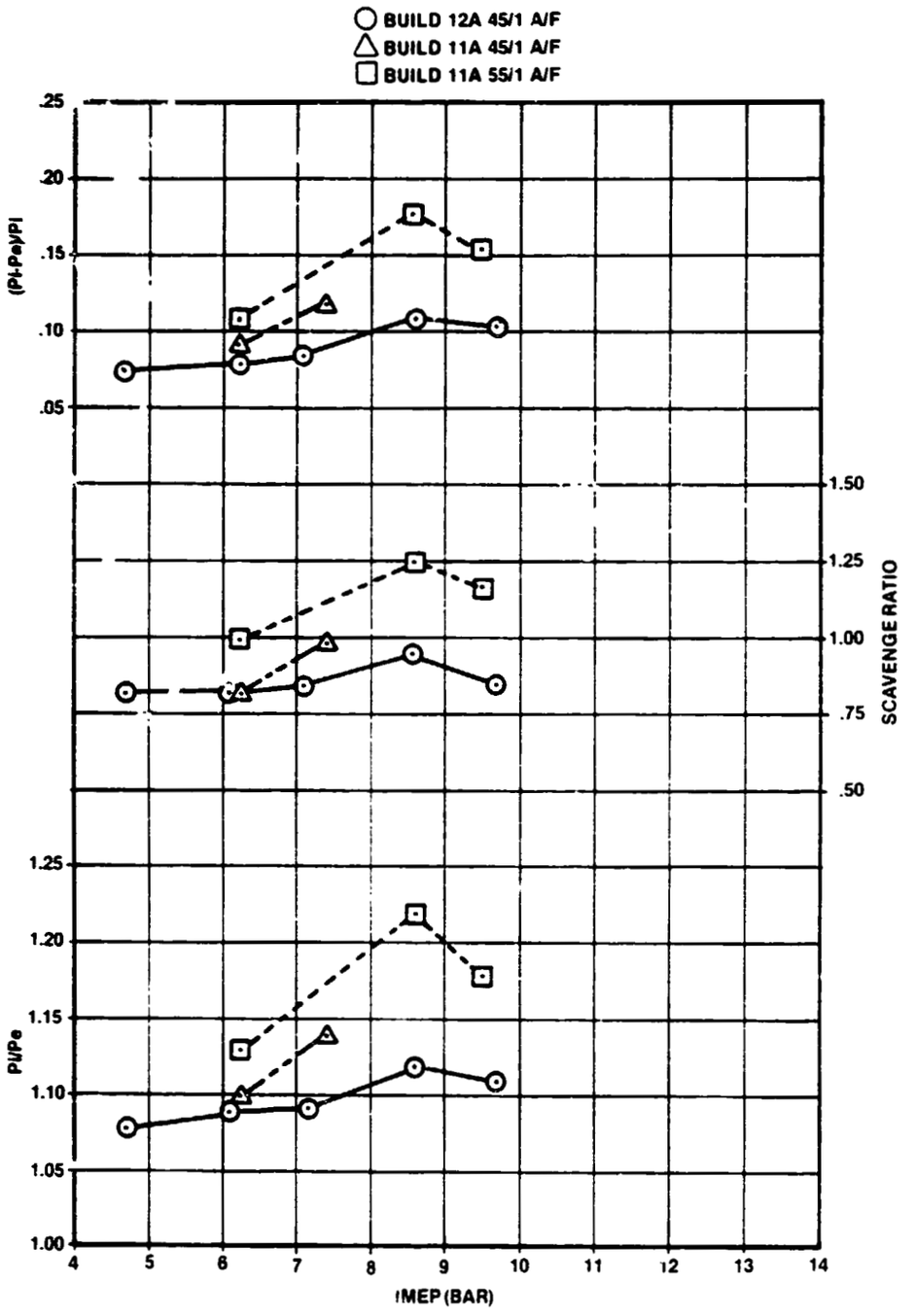

Figure 4.4-17 Engine Performance Comparison for Configurations 11 and 12 at 3500 RPM (Continued)

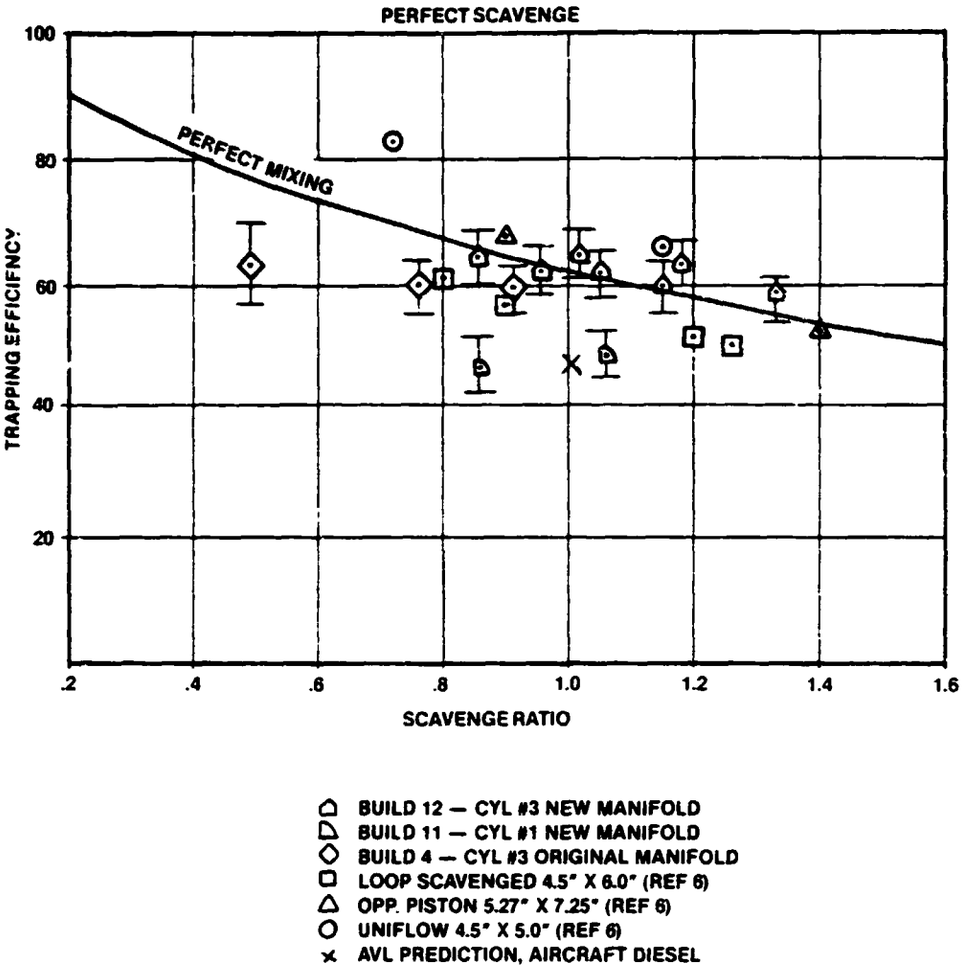

Figure 4.4-18. Calculated Trapping Efficiencies Based on Methods Described in Reference 6

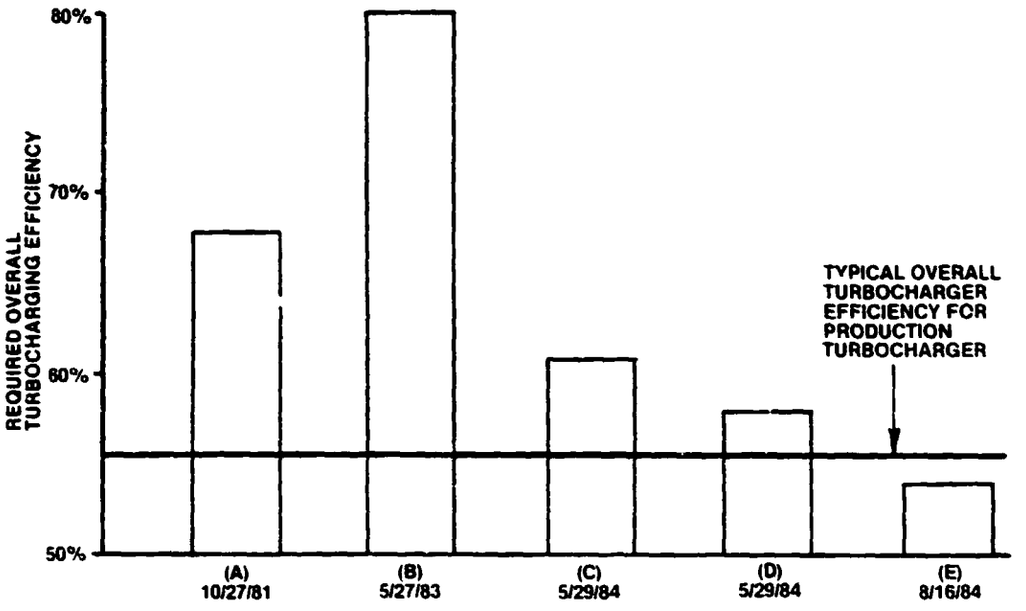

A. BUILD THREE: ALUMINUM PISTON, .63 SQUISH RATIO STAINLESS STEEL COMBUSTION CHAMBER CYLINDER NUMBER THREE, ORIGINAL MANIFOLD, BOSCH APF INJECTION SYSTEM, 53 TO 1 AIR/FUEL RATIO

B. BUILD FOUR: ALUMINUM PISTON, .63 SQUISH RATIO STAINLESS STEEL COMBUSTION CHAMBER, CYLINDER NUMBER THREE, ORIGINAL MANIFOLD, CAE-X INJECTION SYSTEM, 59 to 1 AIR/FUEL RATIO

C. BUILD TEN: CAST IRON PISTON, .8 SQUISH RATIO STAINLESS STEEL COMBUSTION CHAMBER, CYLINDER NUMBER THREE, NEW MANIFOLD, CLOSE COUPLED CAE-X INJECTION SYSTEM, 51 to 1 AIR/FUEL RATIO

D. BUILD TEN: CAST IRON PISTON, .8 SQUISH RATIO STAINLESS STEEL COMBUSTION CHAMBER CYLINDER NUMBER THREE, NEW MANIFOLD, CLOSE COUPLED CAE-X INJECTION SYSTEM, 46 TO 1 AIR/FUEL RATIO

E. BUILD TWELVE: CAST IRON PISTON WITH STAINLESS STEEL CAP, .8 SQUISH RATIO STAINLESS STEEL COMBUSTION CHAMBER, CYLINDER NUMBER THREE, CLOSE COUPLED CAE-X INJECTION SYSTEM, 45 TO 1 AIR/FUEL RATIO

Figure 4.4-19. Required Overall Turbocharger Efficiency at 6.90 BAR IMEP and 3500 RPM for Five Engine Comfigurations

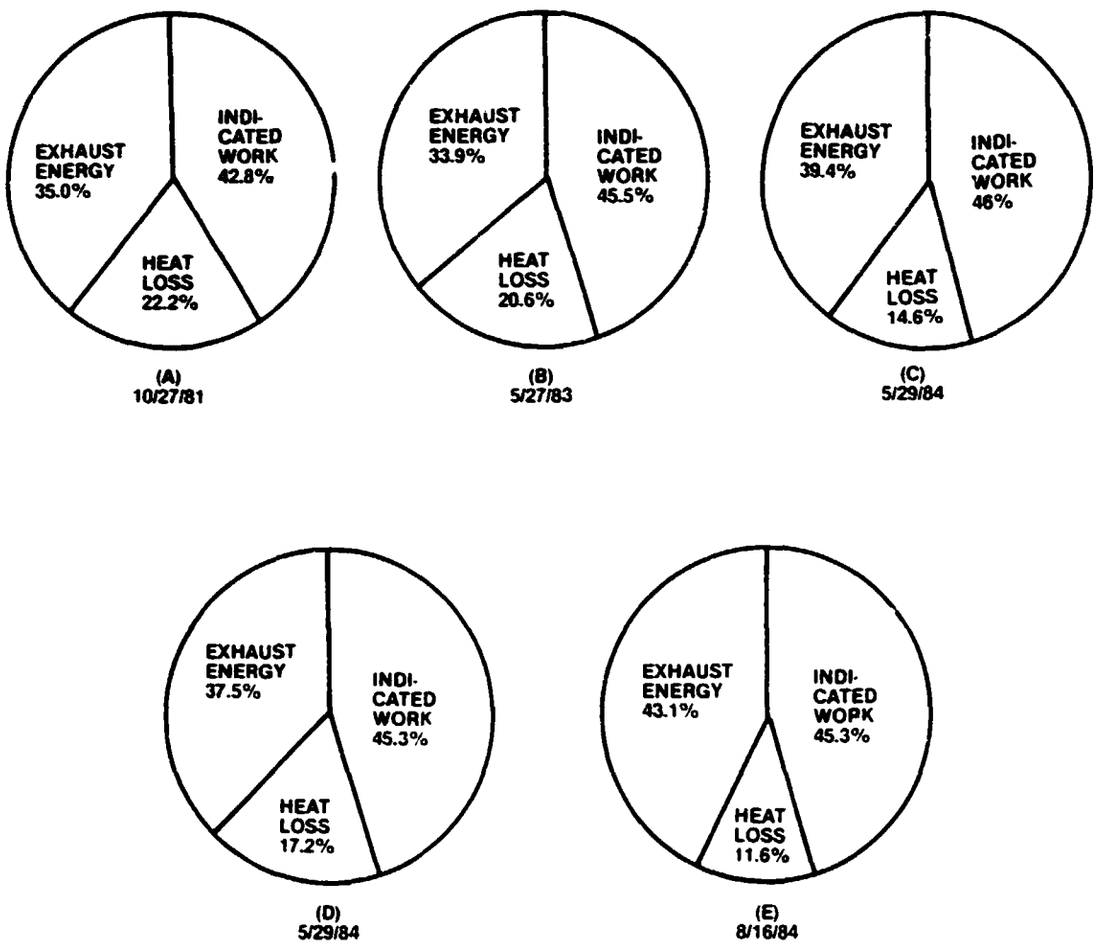

Figure 4.4-20. Engine Heat Balance at 6.9 Bar IMEP and 3500 RPM for Five Engine Configurations

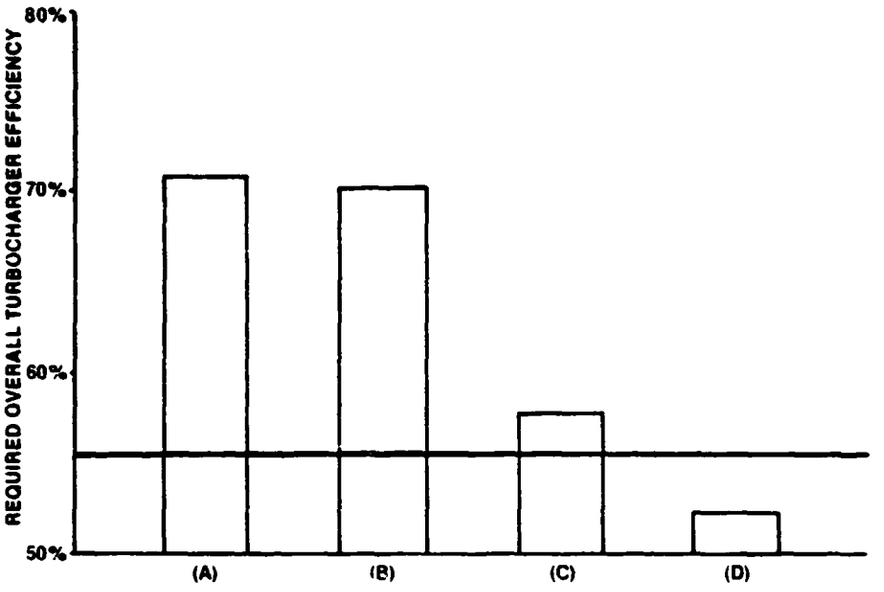

A. BUILD THREE: ALUMINUM PISTON, .63 SQUISH RATIO STAINLESS STEEL COMBUSTION CHAMBER CYLINDER NUMBER THREE, ORIGINAL MANIFOLD, BOSCH APF INJECTION SYSTEM, 46.8 TO 1 AIR/FUEL RATIO

B. BUILD FOUR: ALUMINUM PISTON, .63 SQUISH RATIO STAINLESS STEEL COMBUSTION CHAMBER, CYLINDER NUMBER THREE, ORIGINAL MANIFOLD, CAE-X INJECTION SYSTEM, 46.7 to 1 AIR/FUEL RATIO

C. BUILD TEN: CAST IRON PISTON, .8 SQUISH RATIO STAINLESS STEEL COMBUSTION CHAMBER, CYLINDER NUMBER THREE, NEW MANIFOLD, CLOSE COUPLED CAE-X INJECTION SYSTEM, 45.6 to 1 AIR/FUEL RATIO

D. BUILD TWELVE: CAST IRON PISTON WITH STAINLESS STEEL CAP, .8 SQUISH RATIO STAINLESS STEEL COMBUSTION CHAMBER, CYLINDER NUMBER THREE, CLOSE COUPLED CAE-X INJECTION SYSTEM, 45 TO 1 AIR/FUEL RATIO

Figure 4.4-21. Required Overall Turbocharger Efficiency at 9.0 BAR IMEP and 3500 RPM for Four Engine Configurations

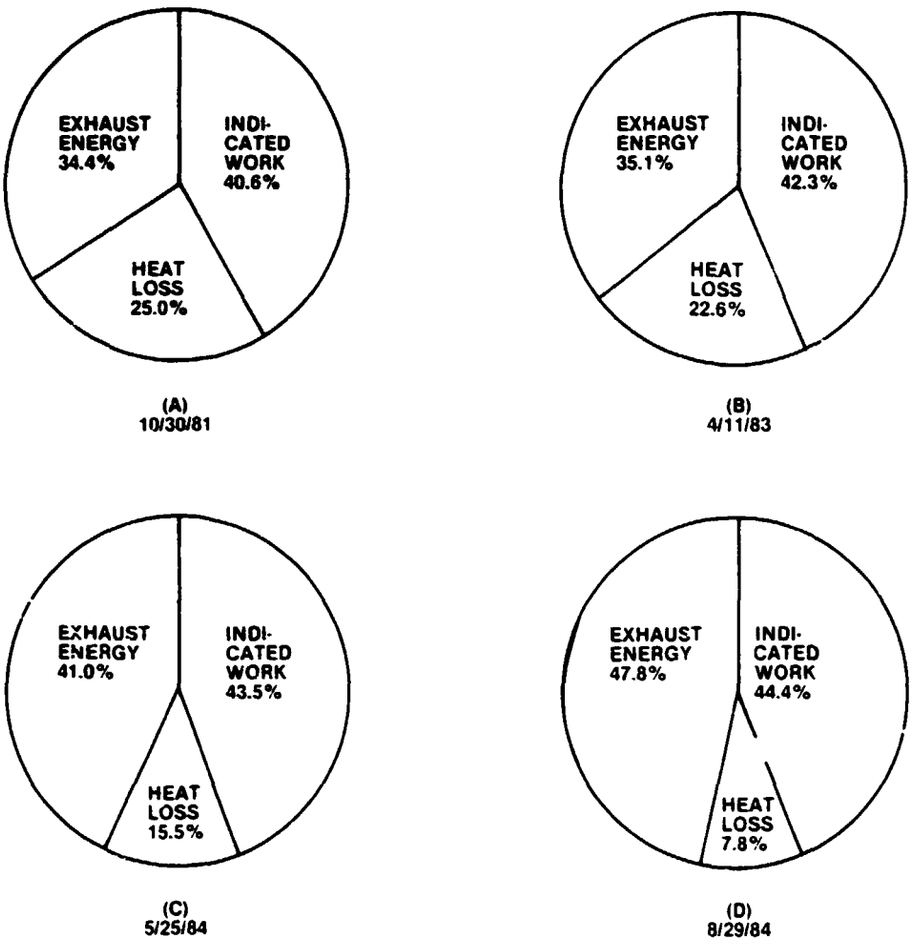

Figure 4.4-22. Engine Heat Balance at 9.0 bar IMEP and 3500 RPM

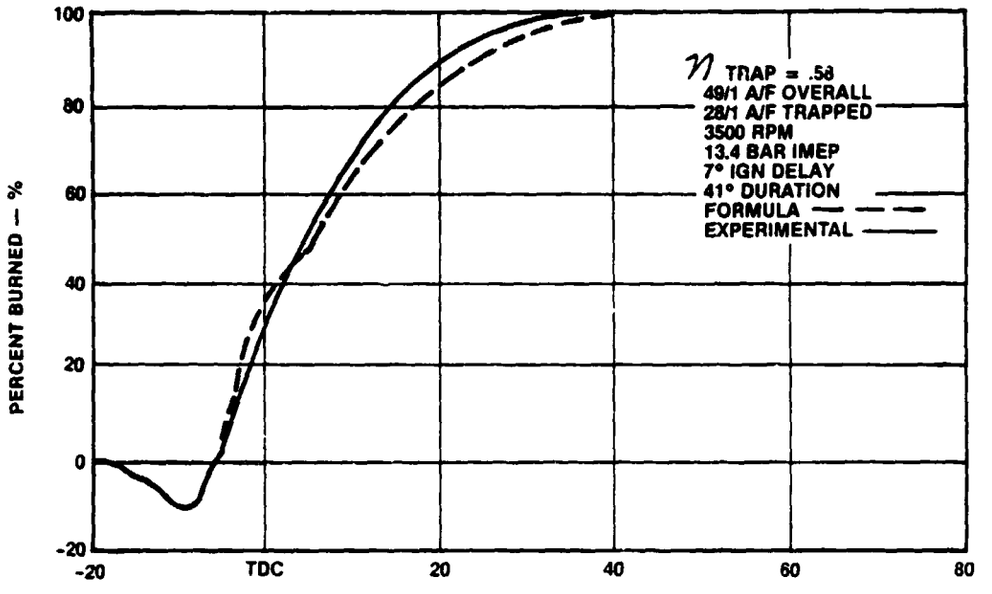

Figure 4.4-23. Mass Fraction Burn Rates for Three Selected Points for Configuration 12

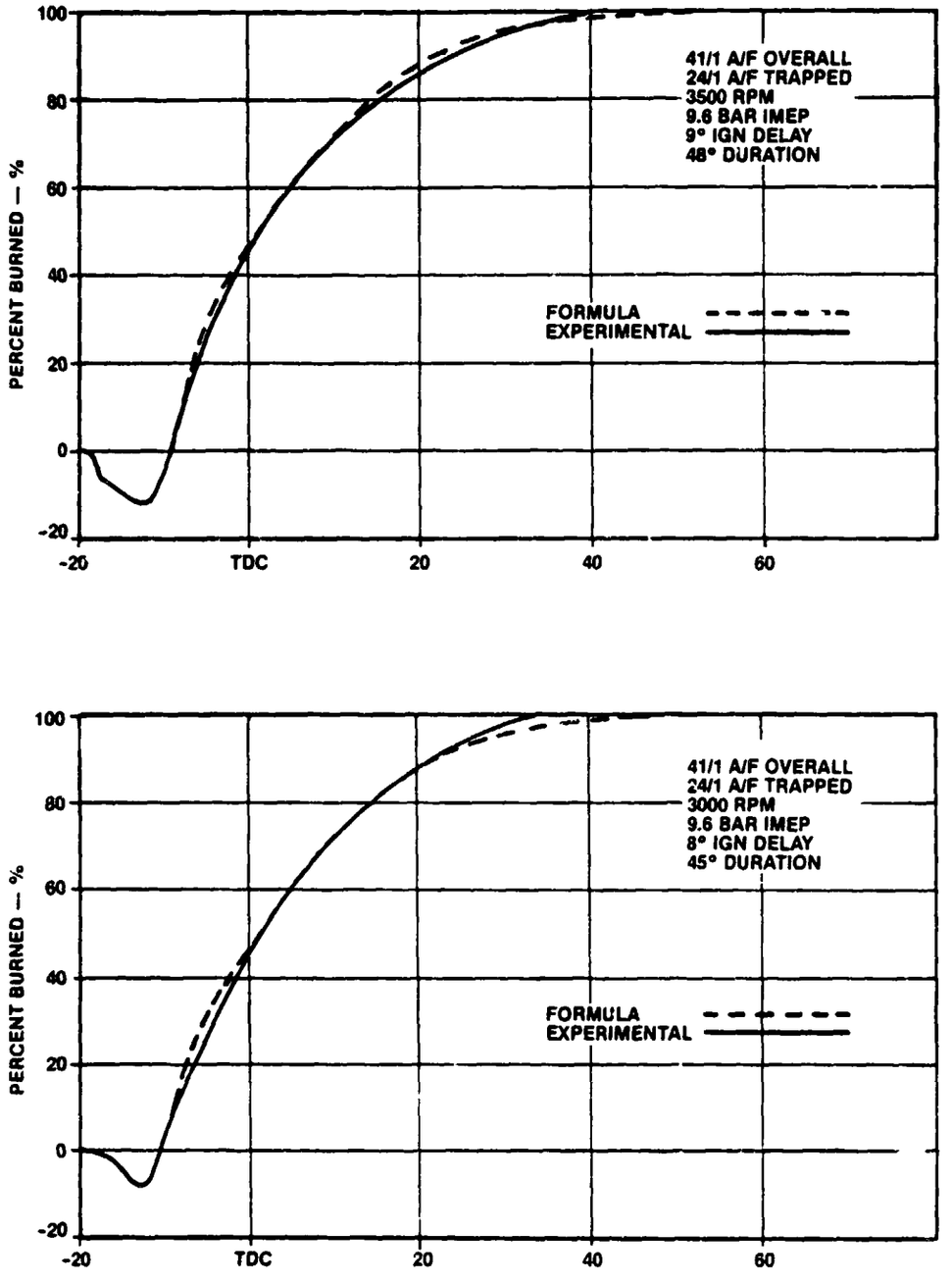

Figure 4.4-23. Mass Fraction Burn Rates for Three Selected Points for Configuration 12 (Continued)

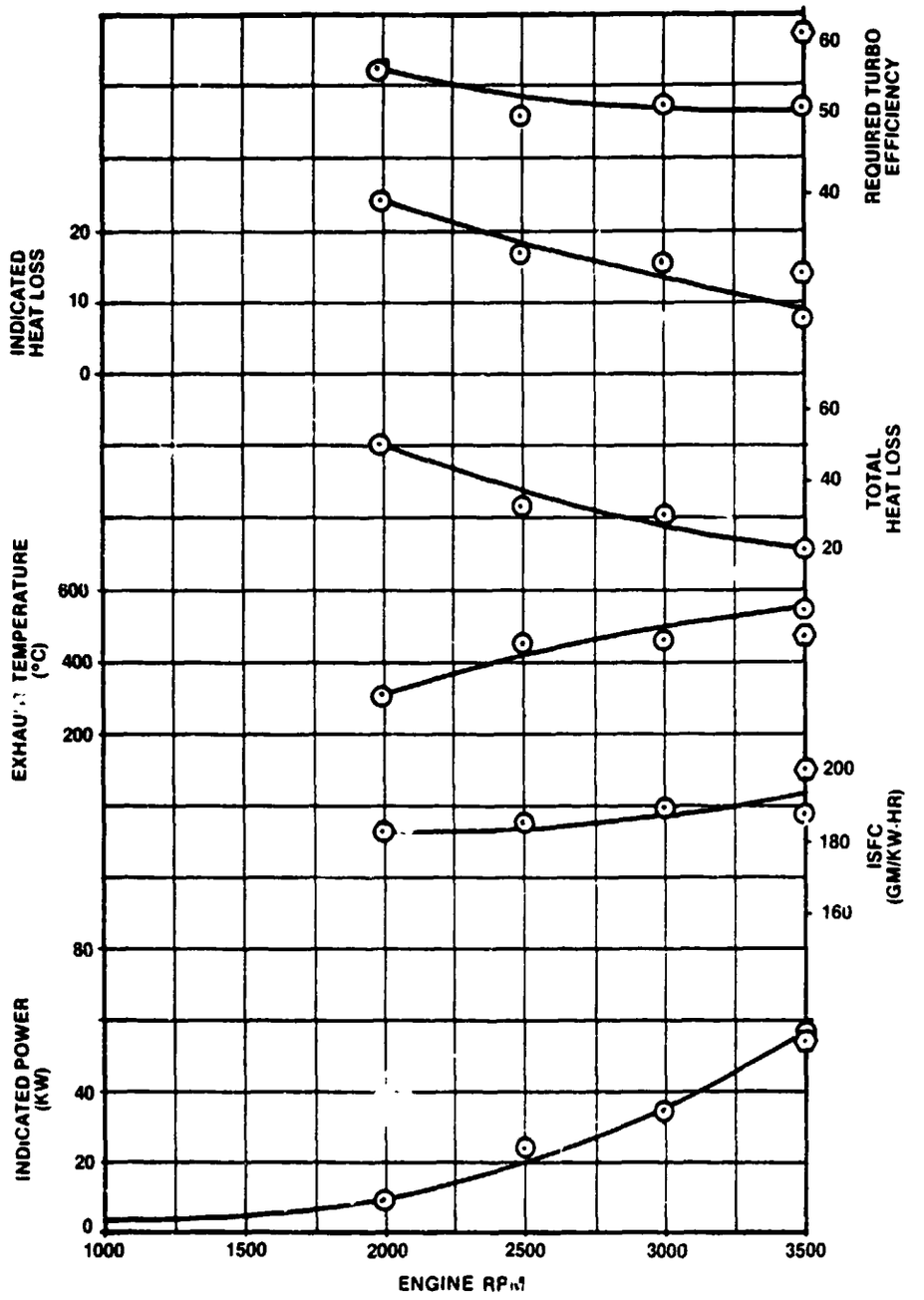

Figure 4.4-24. Single Cylinder Aircraft Diesel Performance of Configuration 12A 3/4 Load Curve Propeller

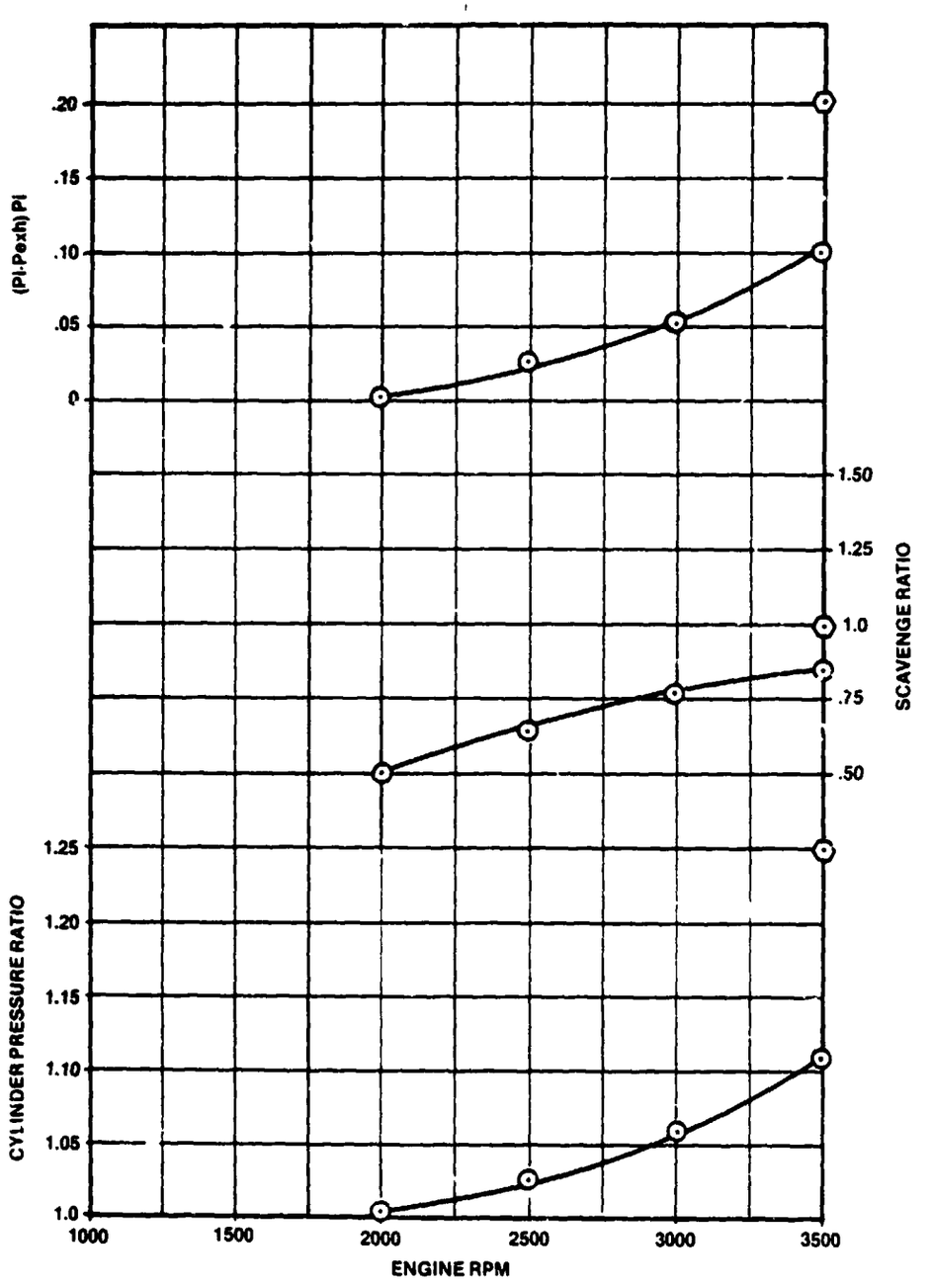

Figure 4.4-24. Single Cylinder Aircraft Diesel Performance of Configuration 12A 3/4 Load Propeller Curve (Continued)

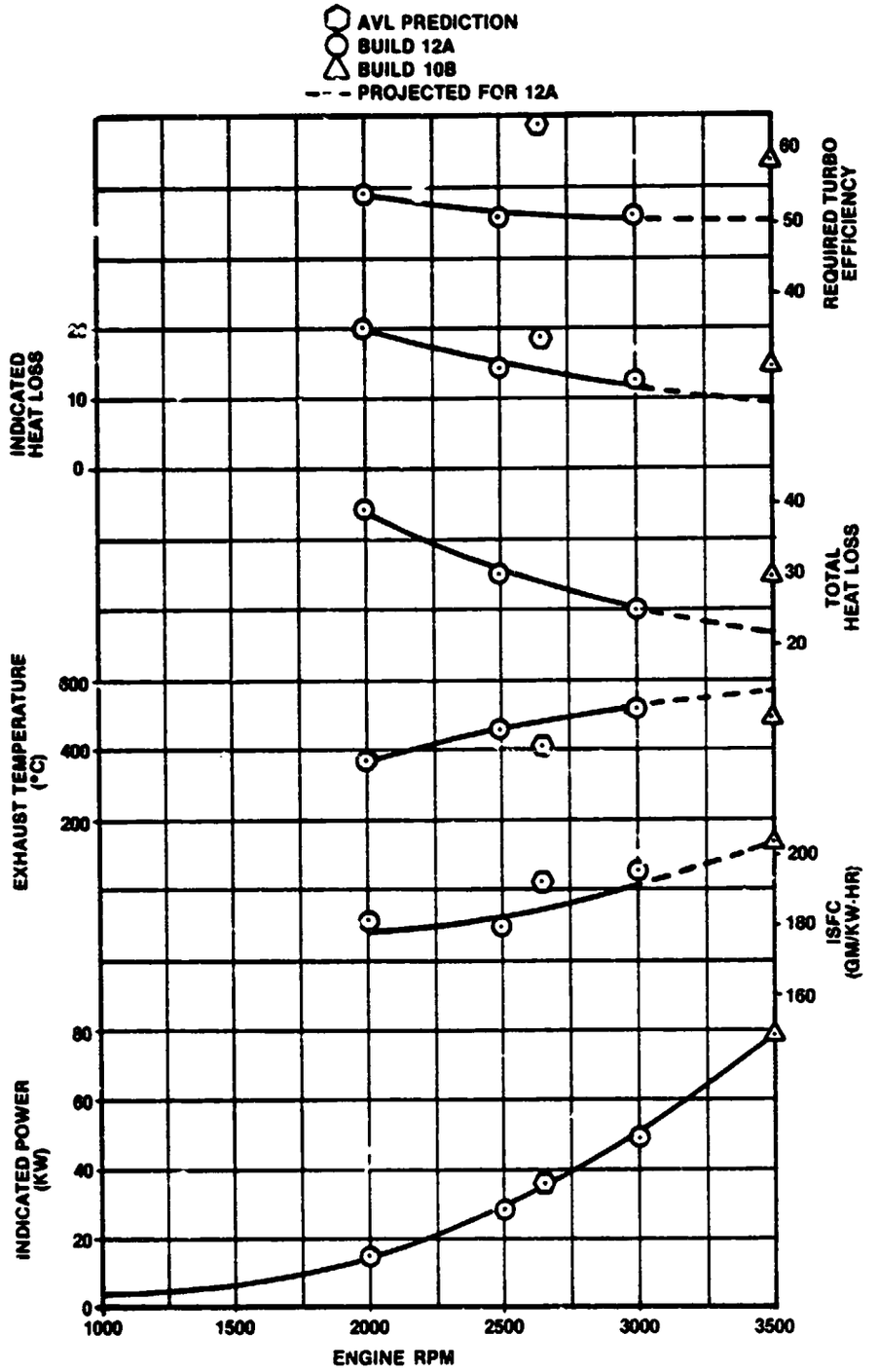

Figure 4.4-25. Single Cylinder Aircraft Performance of Configuration 12A, Full Load Propeller Curve

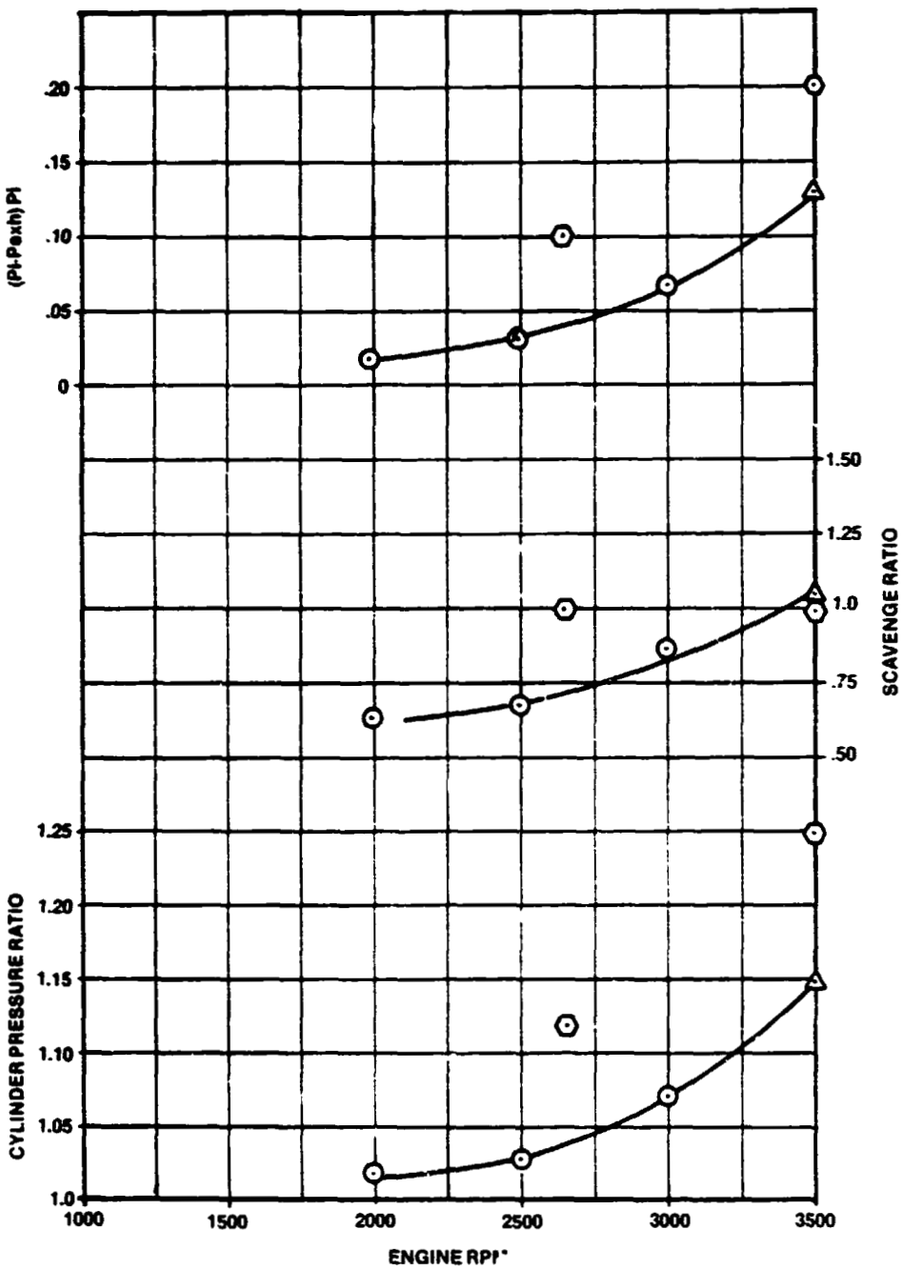

Figure 4.4-25. Single Cylinder Aircraft Performance of Configuration 12A, Full Load Propeller Curve (Continued)

ORIGINAL PAGE IS
OF POOR QUALITY

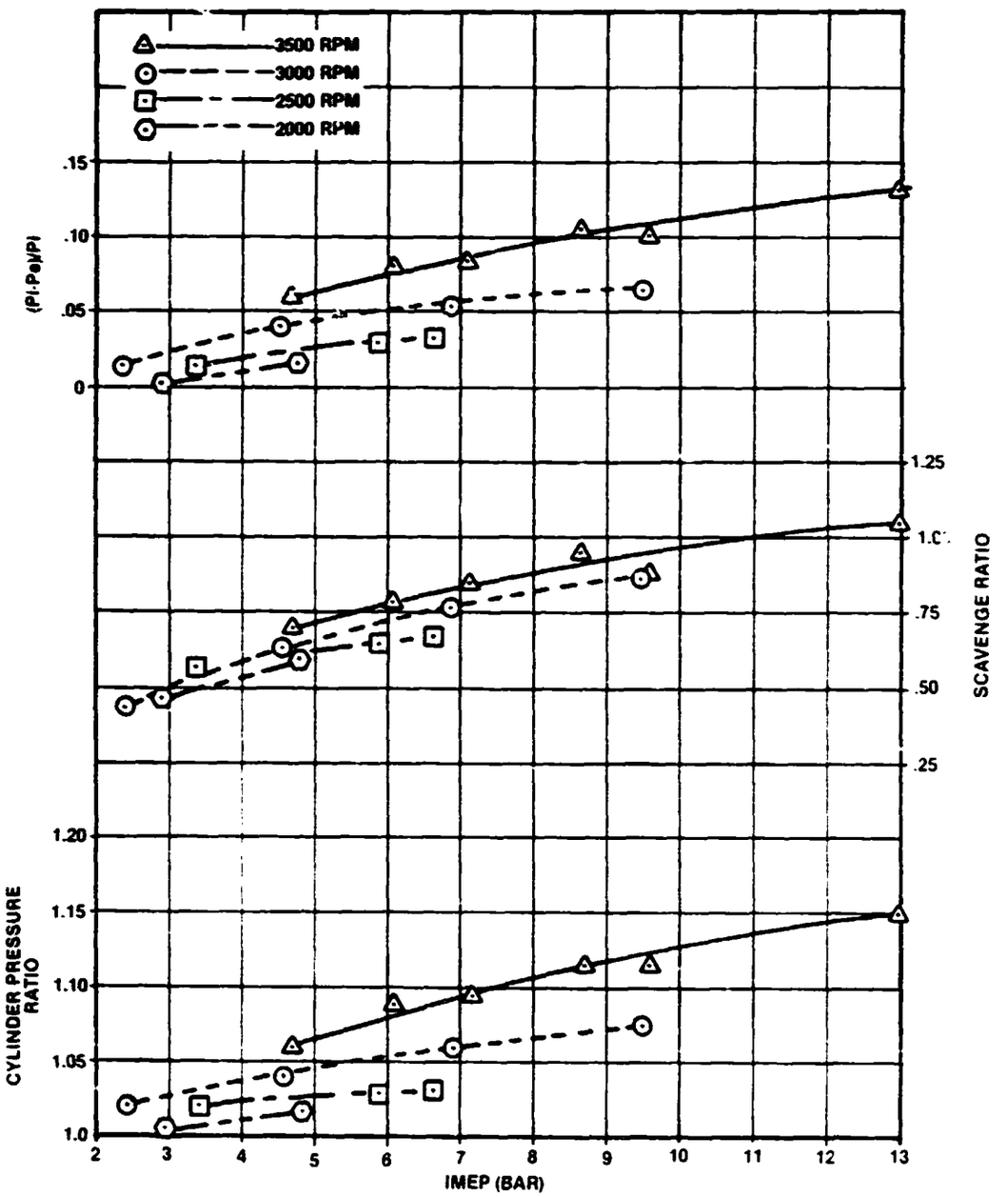

Figure 4.4-26. Airflow Parameters for Configuration 12A

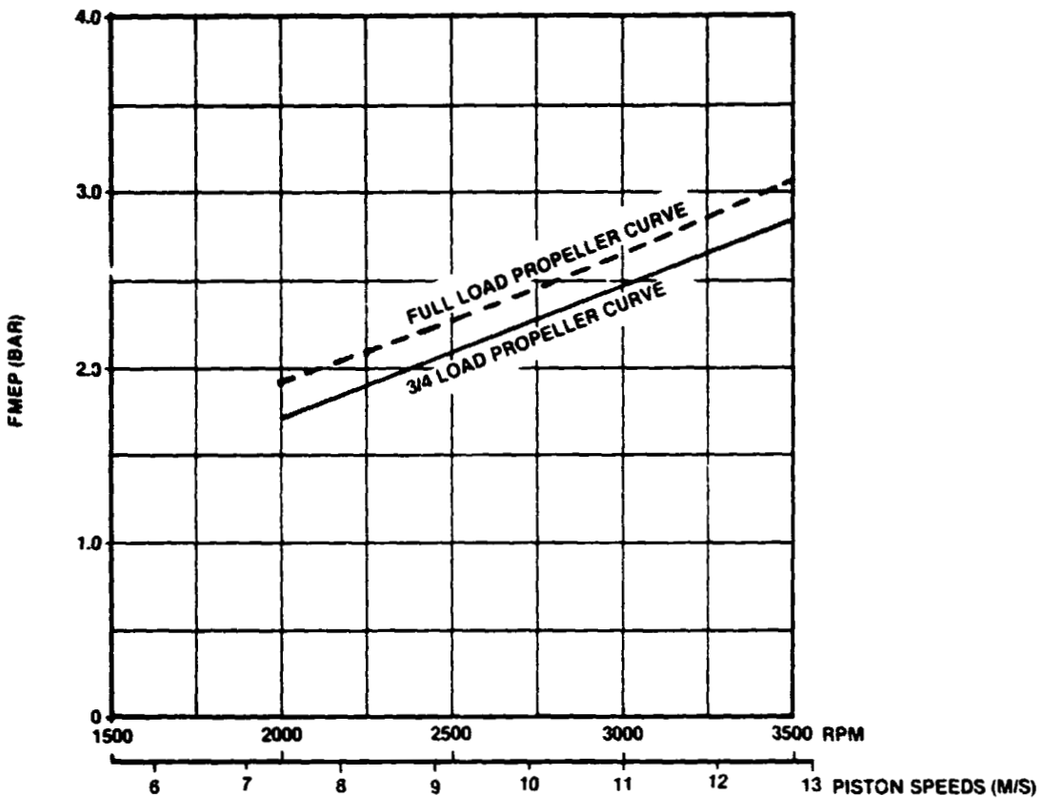

Figure 4.4-27. FMEP Versus RPM and Piston Speed for SCTE

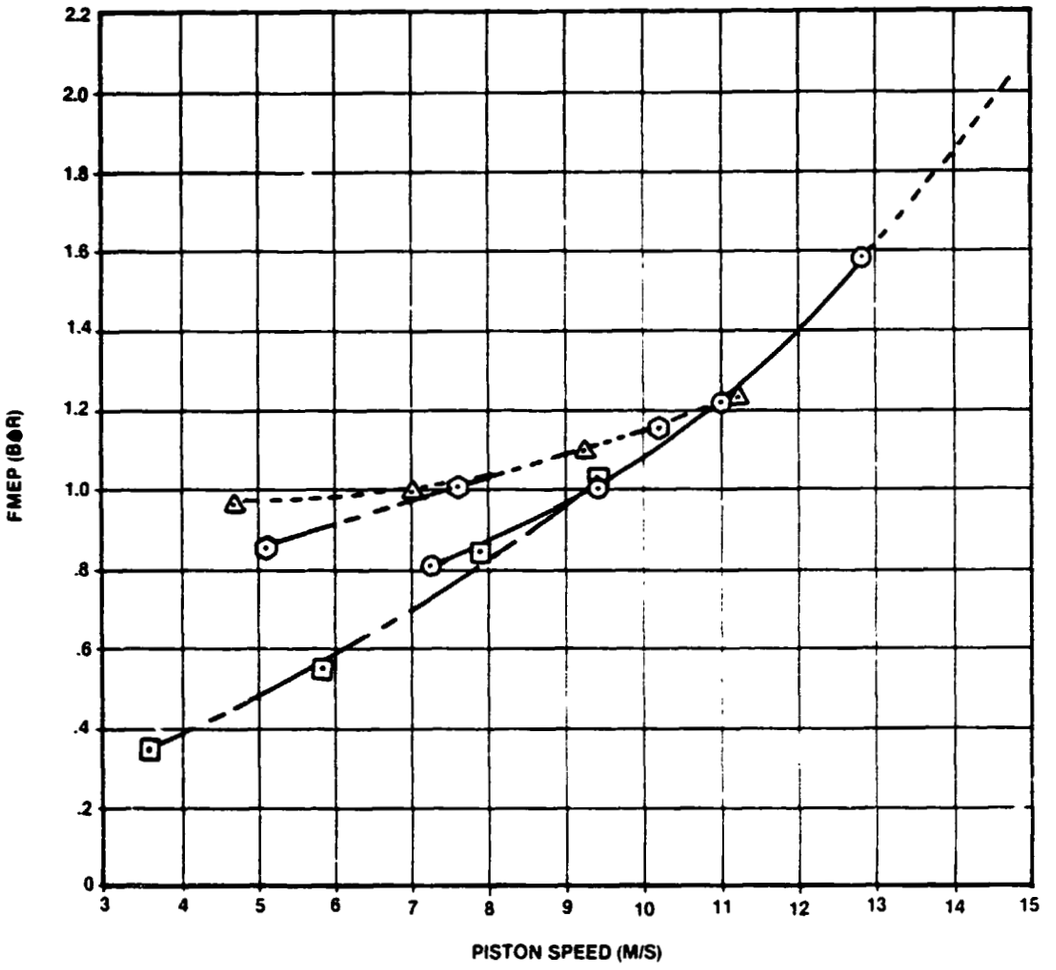

○ AIRCRAFT DIESEL, 4 CYLINDER RADIAL, TWO-STROKE, LOOP SCAVENGED 108 MM X 110 MM, 11 TO 1 C.R. (EFF), 2 COMPRESSION RINGS AND 1 OIL CONTROL RING. *PREDICTED FRICTION FROM SCTE DATA

⬡ GM 6-71, INLINE 6 CYLINDERS, TWO-STROKE, UNIFLOW SCAVENGED, 4 EXHAUST VALVES, 108 MM X 127 MM, 17 to 1 C.R. (NOMINAL), 4 COMPRESSION RINGS AND 2 OIL CONTROL RINGS

△ AVM 310, 4 CYLINDER, 90 DEGREE V, TWO-STROKE, LOOP SCAVENGE, 108 MM X 139.7 MM, 18.7 TO 1 C.R. (EFF), 4 COMPRESSION RINGS AND 1 OIL CONTROL RING

□ R670, 7 CYLINDER RADIAL, FOUR-STROKE, GASOLINE, ONE INLET AND ONE EXHAUST VALVE 130 MM X 118 MM, 6 TO 1 C.R., 3 COMPRESSION RINGS AND 1 OIL CONTROL RING

Figure 5.1-1. FMEP Versus Piston Speed for GTDR 246 and Other Similar Engines

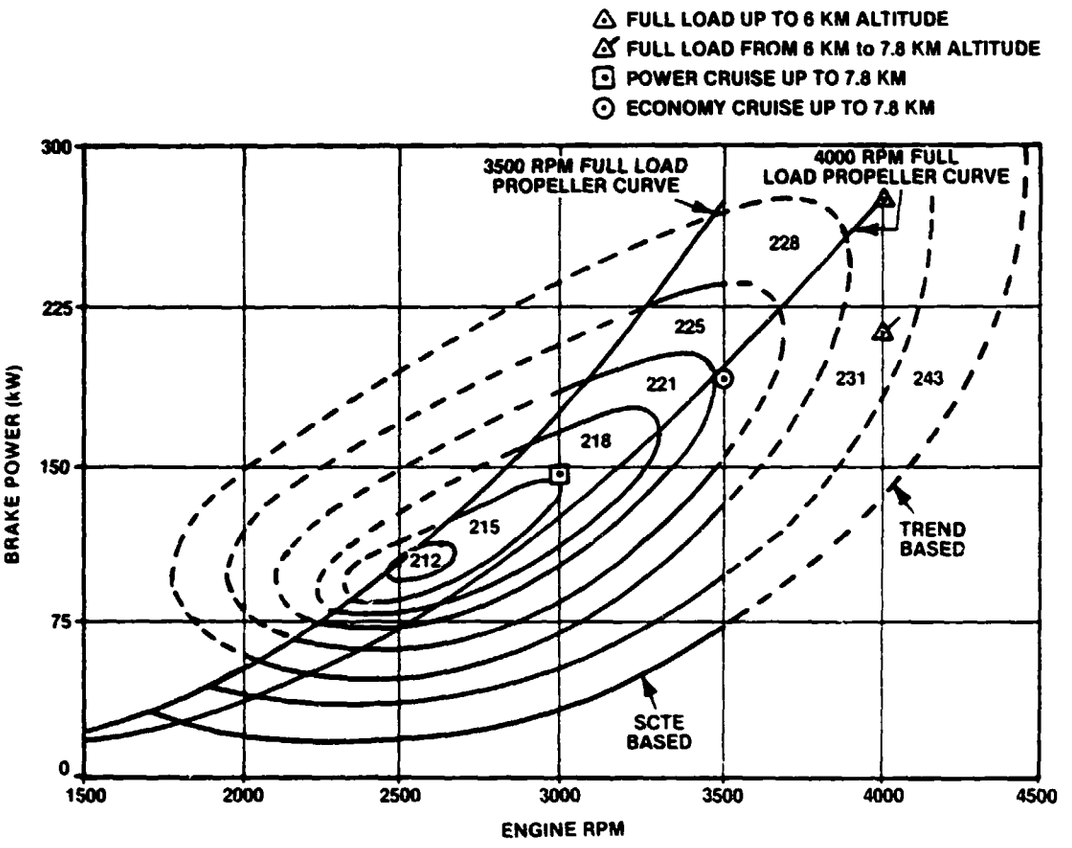

Overall Air/Fuel Ratio = 42

Fuel Consumption — GM/KW-HR

Figure 5.1-2. Predicted GTDR 246 Fuel Map

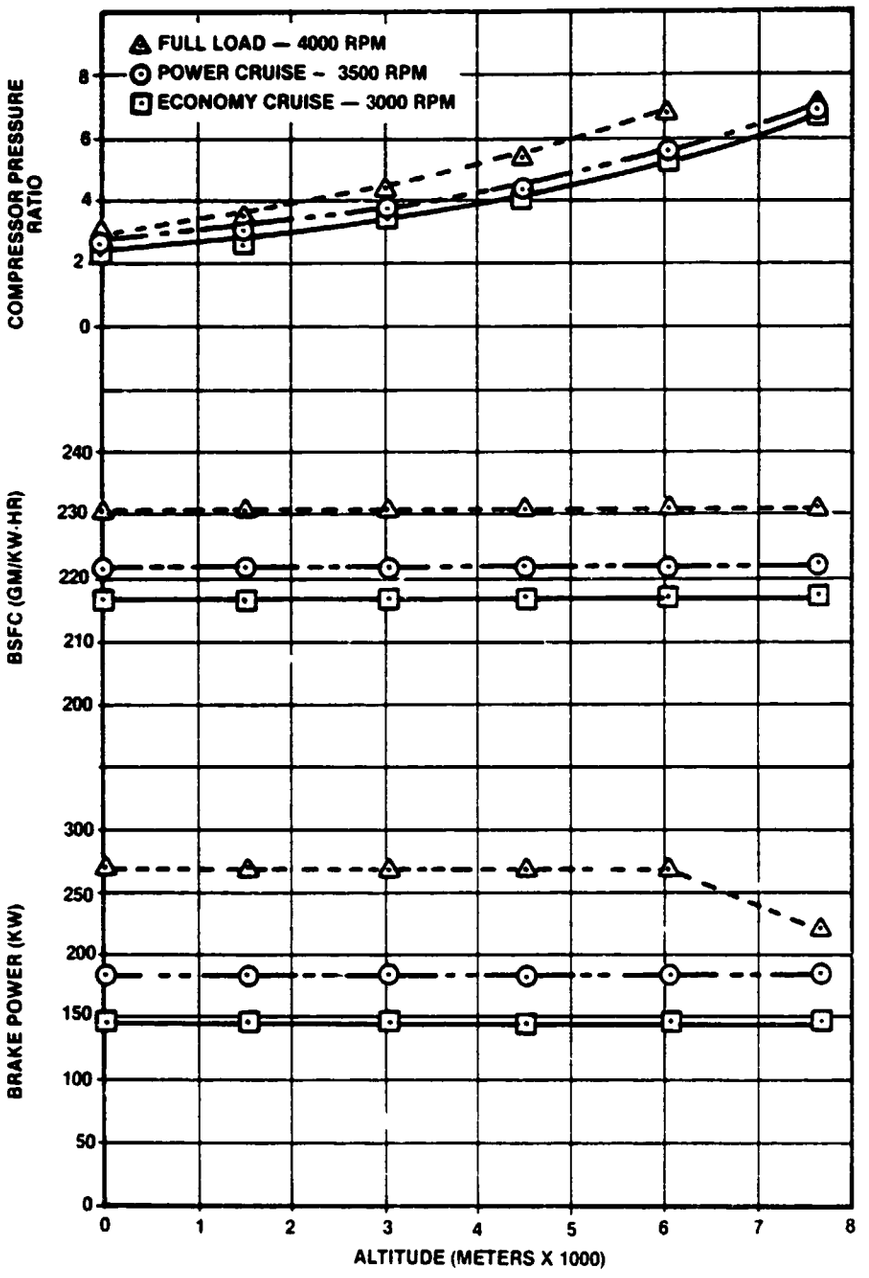

Figure 5.1-3. Predicted Altitude Performance of Multicylinder Engine

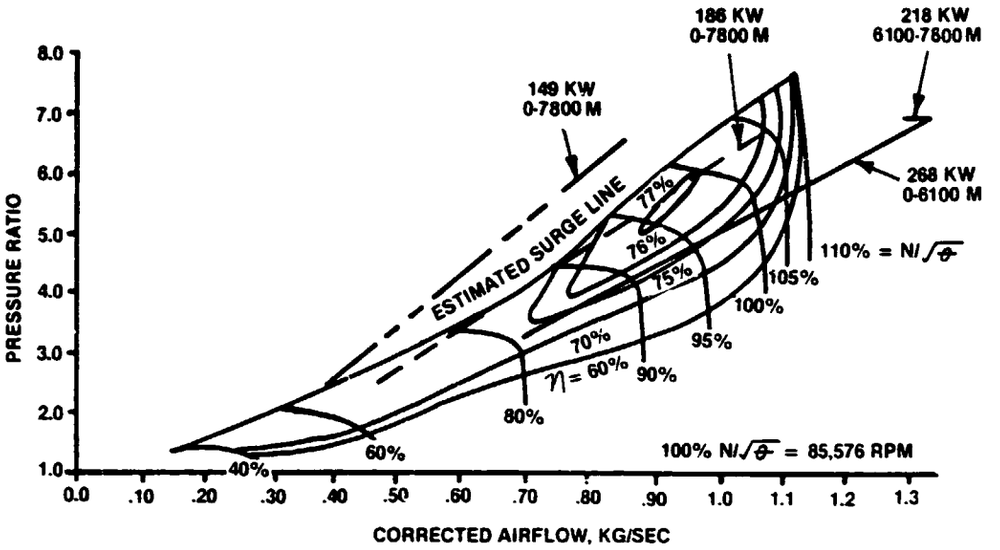

Figure 5.2-1. Compressor Flow Requirement Plotted on an Advanced Compressor Map Generated for NASA under Contract NAS3-22750

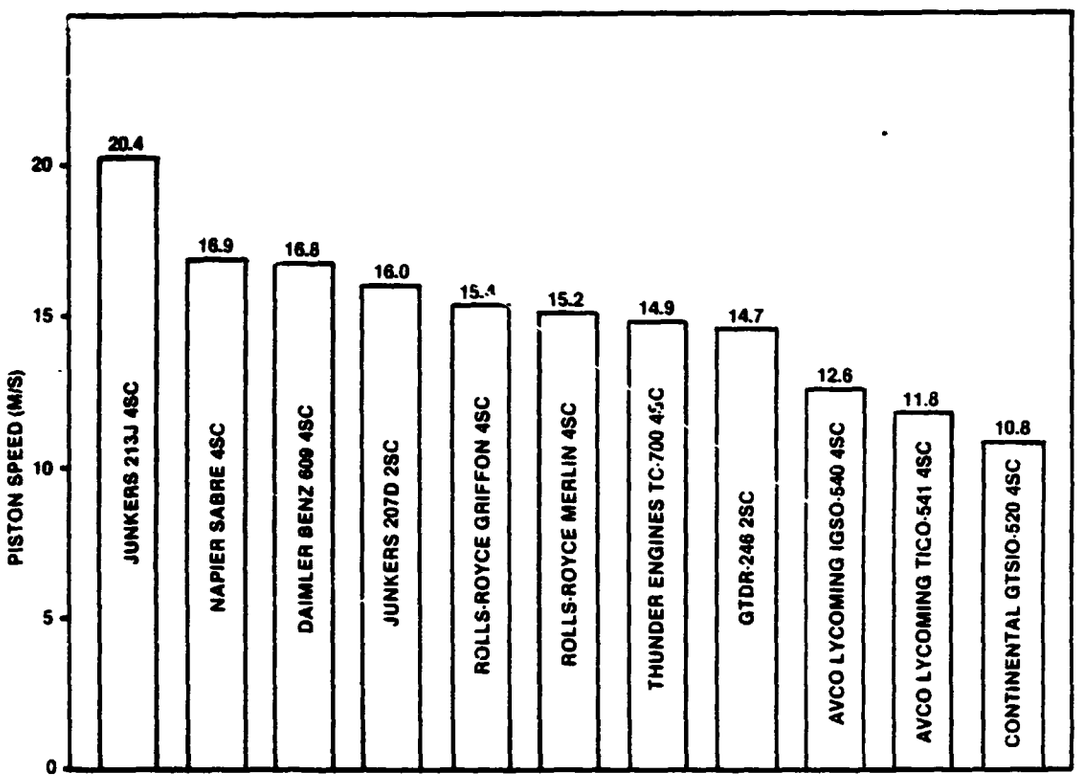

Figure 5.3-1. Piston Speed of Eleven Selected Aircraft Engines

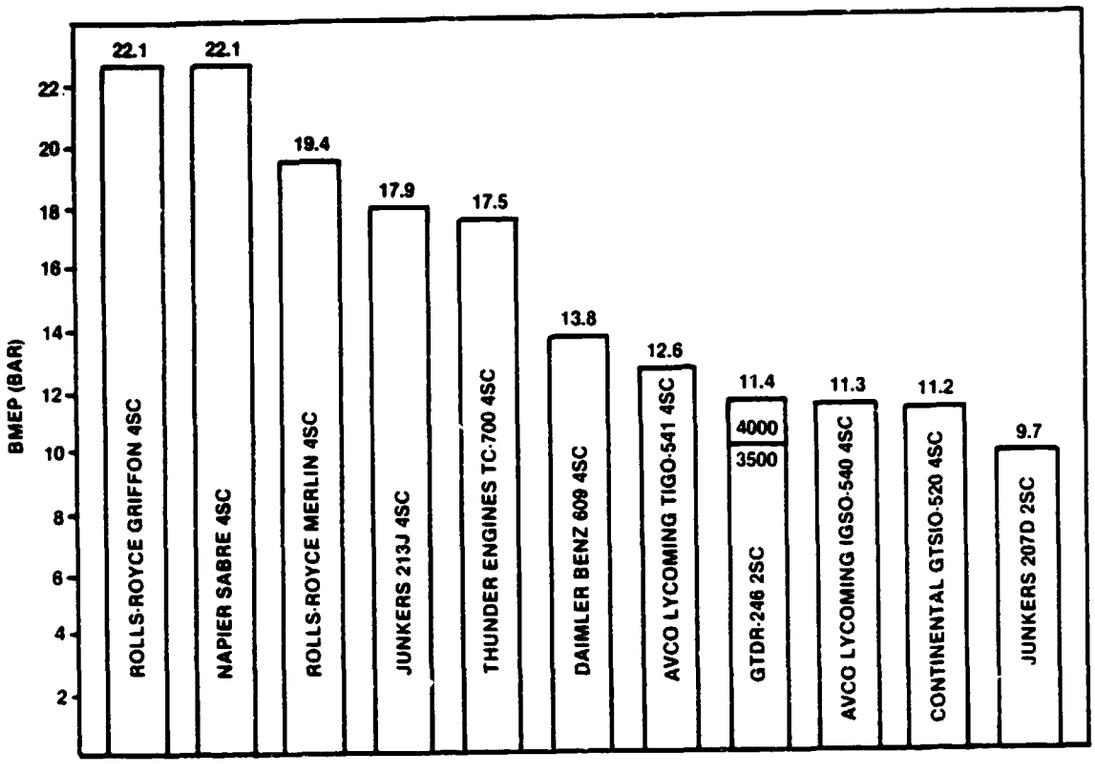

Figure 5.3-2. BMEP of Eleven Selected Aircraft Engines

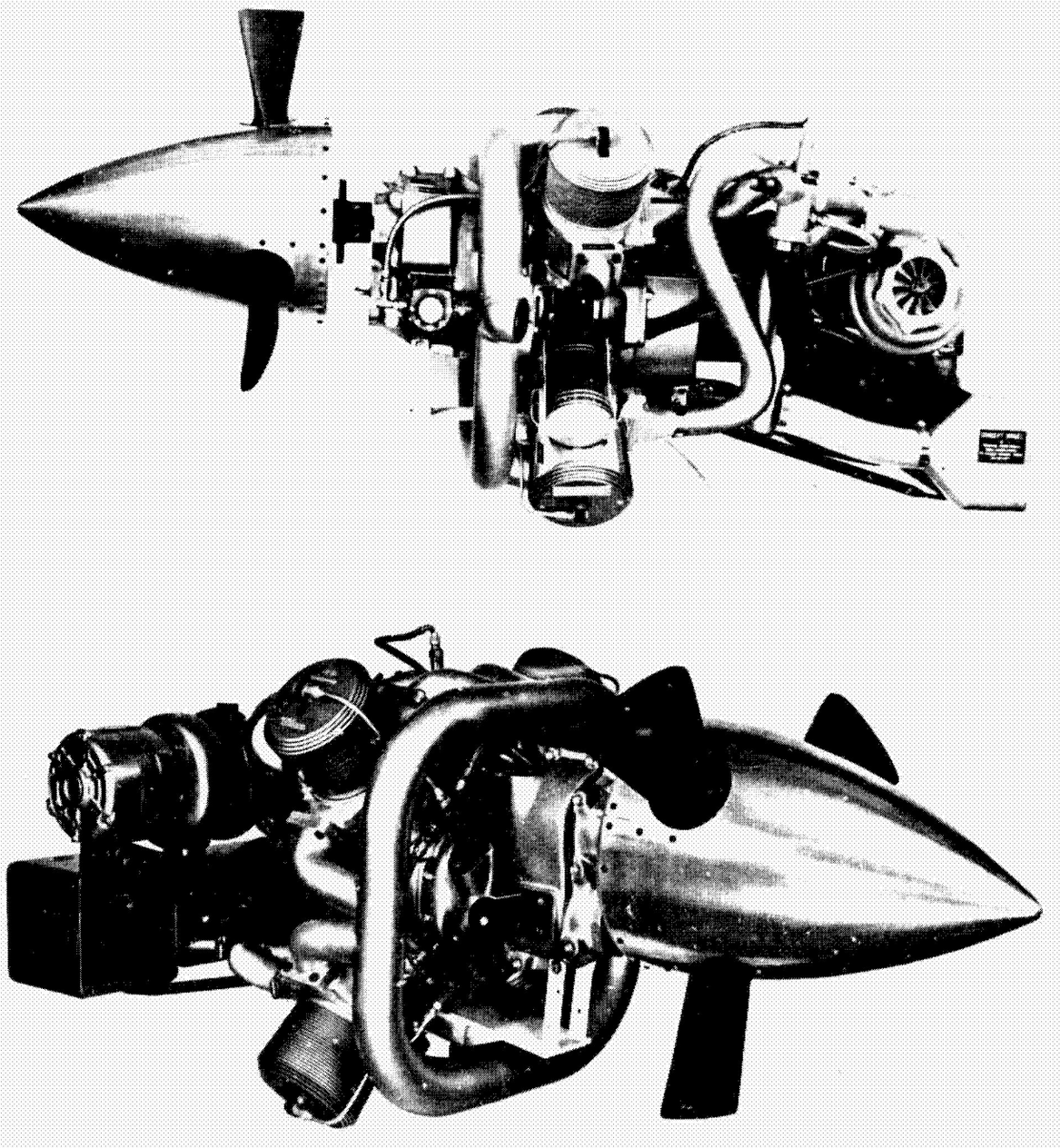

Figure 5.5-1. GTDR-246 Diesel Aircraft Engine (with vertical cylinder) Full-scale Mock-up

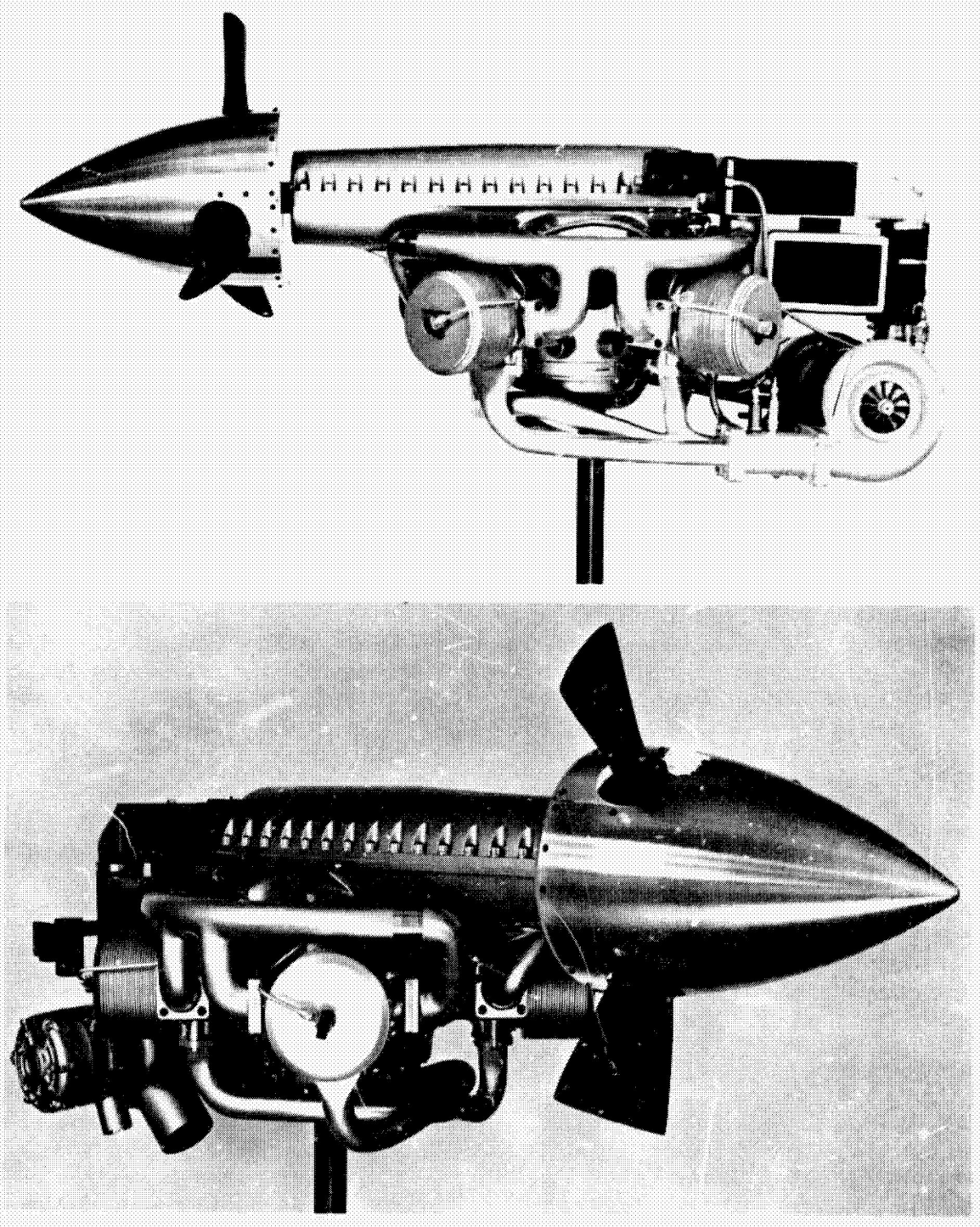

Figure 5.5-2. GTDR-246 Diesel Aircraft Engine (with horizontal cylinder) Full-scale Mock-up